AWARD NUMBER: W81XWH-16-1-0168

TITLE: New podocyte-targeted treatments for focal segmental glomerulosclerosis (FSGS)

PRINCIPAL INVESTIGATOR: Stuart Shankland

CONTRACTING ORGANIZATION: University of Washington

REPORT DATE: January 2020

TYPE OF REPORT: Final Report

PREPARED FOR: U.S. Army Medical Research and Materiel Command
Fort Detrick, Maryland 21702-5012

DISTRIBUTION STATEMENT: Approved for Public Release; Distribution Unlimited

The views, opinions and/or findings contained in this report are those of the author(s) and should not be construed as an official Department of the Army position, policy or decision unless so designated by other documentation.

REPORT DOCUMENTATION PAGE

Form Approved
OMB No. 0704-0188

1. REPORT DATE	2. REPORT TYPE	3. DATES COVERED
Jan 2020	FINAL	09/30/2016 - 09/29/2019

4. TITLE AND SUBTITLE

New podocyte-targeted treatments for focal segmental glomerulosclerosis (FSGS)

5a. CONTRACT NUMBER
W81XWH-16-1-0168

5b. GRANT NUMBER

5c. PROGRAM ELEMENT NUMBER

6. AUTHOR(S)
Stuart Shankland, Suzie Pun

E-Mail: stuartjs@uw.edu, spun@uw.edu

5d. PROJECT NUMBER

5e. TASK NUMBER

5f. WORK UNIT NUMBER

7. PERFORMING ORGANIZATION NAME(S) AND ADDRESS(ES)
University of Washington, 4333 Brooklyn Ave NE, Seattle, WA 98195-9472

8. PERFORMING ORGANIZATION REPORT NUMBER

9. SPONSORING / MONITORING AGENCY NAME(S) AND ADDRESS(ES)

U.S. Army Medical Research and Development Command
Fort Detrick, Maryland 21702-5012

10. SPONSOR/MONITOR'S ACRONYM(S)

11. SPONSOR/MONITOR'S REPORT NUMBER(S)

12. DISTRIBUTION / AVAILABILITY STATEMENT

Approved for Public Release; Distribution Unlimited

13. SUPPLEMENTARY NOTES

14. ABSTRACT
Focal segmental glomerulosclerosis (FSGS), the leading glomerular cause of kidney failure, is characterized by progressive glomerulosclerosis that leads to declining kidney function. The common theme across all FSGS patients is podocyte dysfunction and loss: reduced podocyte number directly underlies glomerulosclerosis, and hereditary FSGS is caused by mutated genes that disrupt the podocyte cytoskeleton. Despite increasing evidence indicating that podocytes are the cells primarily injured in FSGS, the current mainstay in FSGS treatment is immunosuppressant therapy that does not directly target these cells, leading to adverse side effects. Moreover, these drugs do not halt disease progression in all patients. FSGS remains notoriously difficult to treat, highlighting the clinical need for novel, podocyte-targeted treatment strategies to increase therapeutic efficacy and mitigate side effects. Many lines of evidence support targeted podocyte delivery as a viable approach: podocytes are highly endocytotic, many frontline drugs exhibit direct effects on podocytes, and experimental drugs (e.g. Bis-T-23) that protect the podocyte cytoskeleton are effective in animal models of FSGS. However, to date there are no technologies for targeted drug delivery to podocytes.

15. SUBJECT TERMS
focal segmental glomerulosclerosis (FSGS), podocyte targeting, polymer, kidney accumulation

16. SECURITY CLASSIFICATION OF:			17. LIMITATION OF ABSTRACT	18. NUMBER OF PAGES	19a. NAME OF RESPONSIBLE PERSON
a. REPORT	b. ABSTRACT	c. THIS PAGE			USAMRMC
Unclassified	Unclassified	Unclassified	Unclassified	58	19b. TELEPHONE NUMBER *(include area code)*

Table of Contents

1. Introduction:

The leading glomerular cause of chronic kidney disease (CKD), which affects over 25 million Americans, is focal segmental glomerulosclerosis (FSGS). Despite increasing evidence that podocytes are the primary injured cells in FSGS, the current standard of care is immunosuppressant therapy that leads to adverse side effects. The main goal of this work is to develop a podocyte-selective drug delivery system for FSGS by developing a polymeric drug delivery vehicle that is comprised of polymers engineered for maximal kidney accumulation that are functionalized with podocyte-targeting ligands for molecular recognition.

2. Keywords:

focal segmental glomerulosclerosis (FSGS), podocyte targeting, polymer, kidney accumulation

3. Accomplishments:

a. Major Goals (revised with No Cost Extension, PI: Pun)

Specific Aim 1: Develop kidney accumulating polymeric drug carriers

- a. Synthesis of Polymer Panel (Pun)
  - i. Bis-T-23 and monomers. December 2016. 100% complete
  - ii. Synthesis of polymer panel. May 2017. 100% complete
  - iii. Characterization of polymers. May 2017. 100% complete
  - iv. Synthesis of Dex-polymer panel. September 2019. 100% complete.
- b. Drug loading and release studies (Pun)
  - i. Bis-T-23 loading and characterization. June 2017. 100% complete
  - ii. Bis-T-23 release studies and polymer refinement. Sept 2017. 100% complete
  - iii. Dex release studies. Feb 2020 0% complete.
- c. Biodistribution and kidney distribution studies
  - i. Synthesis of labeled polymers. (Pun) Sept 2018. 75% complete.
  - ii. Biodistribution in mice. (Pun and Shankland) March 2018.
  - iii. Kidney distribution studies. (Shankland) June 2018. 100% complete.
  - iv. Synthesis of labeled Dex polymers. March 2020. 0% complete
  - v. Biodistribution of labeled Dex polymers. May 2020. 0% complete.

Specific Aim 2: Identify and characterize a novel podocyte-binding peptide

- a. Cell preparation and characterization (Shankland and Pun)
  - i. Isolation of cultured podocytes and control cell line (Shankland) December 2016 100% complete
- b. Phage display for podocyte-binding peptides (Pun)
  - i. Phage display rounds (Pun) using Nephrin as target Sept 2018 (100% complete)
  - ii. Phage display rounds (Pun) using primary podocytes as target Sept 2018 (100% complete)
  - iii. NGS analysis (Pun) March 2018
- c. Selex for podocyte binding aptamers (Pun)
  - i. Development of SELEX aptamer-particle display for Pun Lab. March 2017. 100% complete
  - ii. Aptamer-particle display screening using nephrin. Aug 2017. 100% complete.
  - iii. NGS Sequencing and analysis. Sept 2017. N/A
- d. Ligand evaluation (Pun and Shankland)
  - i. Synthesis of potential ligands (Pun) Sept 2019
  - ii. In vitro validation (Pun) March 2018 100% complete
  - iii. Ligand biodistribution in mice (Pun and Shankland) July 2018. 50% complete
  - iv. Kidney distribution (Shankland) July 2018 50% complete
  - v. Ligand optimization (Pun) Sept 2018

Specific Aim 3: Evaluate efficacy in a mouse model of FSGS

- a. Synthesis of polymers for efficacy studies (Pun) March 2020 33% complete
- b. Synthesis of polymers for biodistribution studies (Pun) March 2020 33% complete.
- c. Efficacy studies
  - i. Podocyte specificity and efficacy validation in vitro (Pun/Shankland) Nov 2018. 5% complete.
  - ii. Efficacy in FSGS model (Shankland/Pun) July 2020 10% complete.
  - vii. Histological analysis (Shankland) September 2020

b. Accomplishments to date

Specific Aim 1. Develop kidney-accumulating polymeric carriers.
In Years 1 and 2, we (i) synthesized a panel of polymers to determine polymer properties for kidney accumulation and (ii) synthesized polymers reversibly conjugated to Bis-T-23, a drug reported to increase actin polymerization in podocytes, thereby reducing symptoms of FSGS in animal models. We successfully produced anionic polymers that accumulate preferentially in the kidney. However, we were unable to reproduce reports of Bis-T-23 efficacy both in vitro and in vivo. Therefore, in Year 3, we pivoted to evaluate alternative drugs for delivery using our kidney-localizing polymers. One clinically-used drug is dexamethasone, a steroid drug that also has systemic side effects and could therefore benefit from targeted renal delivery.

We first confirmed that dexamethasone treatment to cultured podocytes challenged with puromycin aminonucleoside improves cell viability (Figure 1A). We then designed and synthesized a polymer for podocyte-targeted dexamethasone delivery (Figure 1B). This polymer contains monomer units that impart water solubility (purple), a conjugate site for eventual antibody conjugation to impart podocyte targeting (red) and dexamethasone attached via a reversible hydrazone bond (brown). The hydrazone linkage is broken in acidic conditions that would be present after receptor-mediated internalization into acidic endosome structures. The synthesized polymer has low polydispersity (D= 1.114) and self-assembled into micelle structures with average diameter of 22 nm and anionic surface charge.

We then conjugated the anti-podocyte antibody (see Specific Aim 2) to the polymer and showed that increased internalization was observed in a ligand density-dependent manner (Figure 1C). These results suggest successful targeted-delivery of the polymer-drug conjugate into cells. However, when we tested this polymer in the PAN challenge assay with cultured podocytes, we did not see any improvement in survival with treatment despite extensive optimization in experimental conditions (Figure 1D). Based on these results, we hypothesized that the dexamethasone drug was not being released quickly enough after internalization.

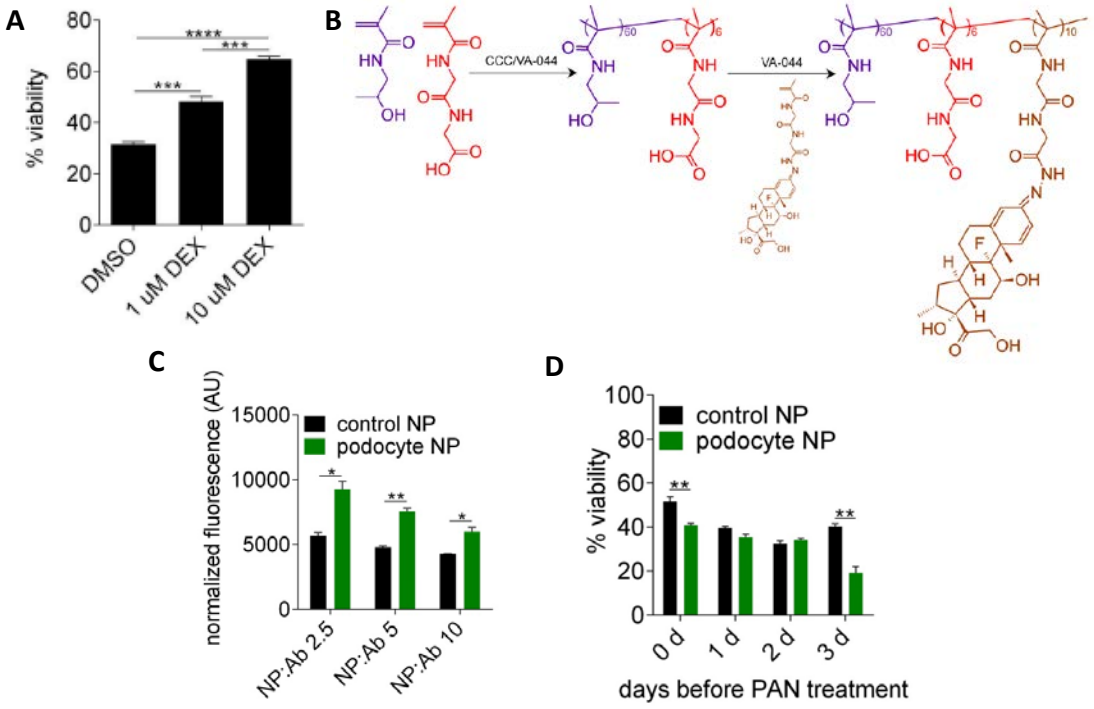

Figure 1. A. Dexamethasone rescues podocytes in an in vitro drug challenge model. B. Structure of dexamethasone-conjugated polymer that contains monomers for water solubility (purple), targeting ligand conjugation (red) and reversibly-loaded drug (brown). C. Internalization study of fluorescently-labeled micelles of dexamethasone-conjugated polymer that are unfunctionalized (control NP) or functionalized with an anti-podocyte antibody (podocyte NP). D. Podocyte-targeted micelles containing dexamethasone via a hydrazone linkage do not rescue podocytes in an in vitro drug challenge model

Based on this study, we synthesized a second polymer that includes a pendant dexamethasone connected via a more labile linkage (Figure 2A). This linkage was previously shown to have much faster release kinetics. This polymer also self-assembles into micelles with diameter around 40 nm, as determined by dynamic light scattering (Figure 2B). We also conjugated anti-podocyte antibodies for targeted uptake and fluorescently-labeled the polymers so we could monitor internalization by flow cytometry. Podocyte-targeted were internalized >13-fold more efficiently than control, untargeted polymers (Figure 2C). Our next step is to test activity of the polymers in cultured podocytes. If efficacy is observed, we will move forward to *in vivo* testing.

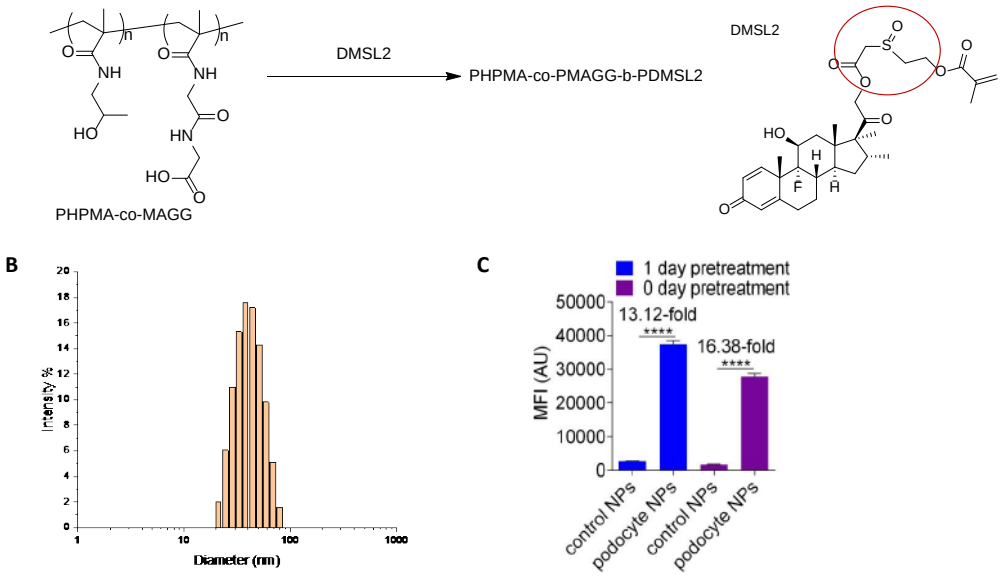

Figure 2. A. Dexamethasone-functionalized polymer with more labile linkage for faster drug release. B. Polymer self-assembles into micelles with average diameter of 40 nm. C. Polymers conjugated with anti-podocyte antibodies are internalized more efficiently by cultured podocytes than control, unfunctionalized polymers.

<u>Specific Aim 2: Identification of a podocyte-targeting ligand.</u>

This aim is completed. We are using an anti-podocyte antibody developed by co-PI Stuart Shankland's group.

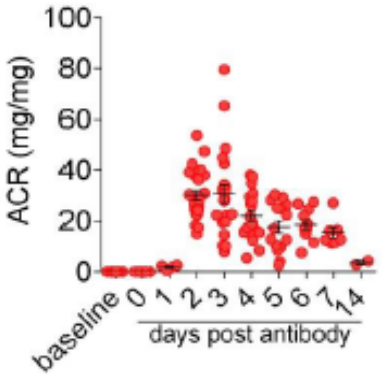

Figure 3. FSGS induction in mice using anti-podocyte antibody.

<u>Specific Aim 3: Efficacy studies.</u>

First, we optimized our antibody-induced FSGS model. Mice were injected with cytotoxic anti-podocyte antibodies on days -1 and 0 and then monitored for proteinuria, a symptom of FSGS, by urine collection and evaluation of albumin to creatinine ratio. We observed proteinuria by two days post-treatment, with gradual resolution by 2 weeks post-disease induction.

Next, we evaluated in vivo targeting using the anti-podocyte-functionalized, dexamethasone-conjugated polymers. Polymers were labeled with Cy5 for imaging. Polymers were labeled with Cy5 for imaging. Polymer accumulation was observed in lung, liver, spleen and kidneys (Fig 4A). Kidneys were harvested and imaged by fluorescence microscopy. Significantly increased fluorescence

was observed in the glomeruli of animals injected with targeted polymer compared to control polymer (Fig 4B). We quantified glomerular association by image analysis of 10 random glomeruli. Significantly higher fluorescence was observed in animals treated with targeted polymer compared to control polymer (Fig 4C). Therefore, the podocyte antibody can be used to increased delivery of polymer-drug conjugates to glomeruli.

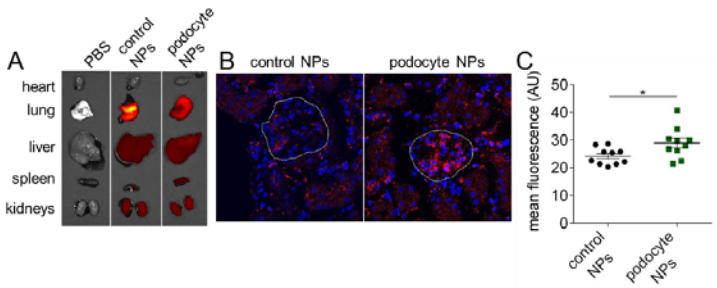

Figure 4. A. Xenogen imaging of organs of mice treated with PBS, control NP and Shampodo-modified NPs (podocyte NP). B. Fluorescence microscopy imaging of kidney sections of mice treated with podocyte NP or control NP. C. Quantification of polymer fluorescence in mice treated with podocyte NP or control NP.

c. Training and Professional Development

Several scientists have been supported on this work. Yilong Cheng, a postdoctoral fellow, developed boronic acid-based polymers for this work. Shixian Lyu, a postdoctoral fellow, developed dexamethasone-conjugated polymers. Alex Prossnitz, a graduate student, has received training in polymer synthesis (from Yilong Cheng) and has synthesized the polymer panel together with Yilong Cheng. Gary Liu, a graduate student, has received training in polymer synthesis (from Postdoc Yilong Cheng) and also contributed toward polymer synthesis. He has also gained experience in drug release studies as well as developed assays for monitoring Bis-T-23 in cultured cells. Gary Liu has also learned animal models of kidney disease (from Scientist Dr. Diana Eng) and podocyte biology (from Drs. Stuart Shankland and Jeffrey Pippin). He has attended the American Society of Nephrology Annual Conference as a STARS recipient for 3 years.

d. Results dissemination:

1. Liu GW, Johnson SL, Jain R, Peeler DJ, Shankland SJ, Pun SH. Optimized nonviral gene delivery for primary urinary renal progenitor cells to enhance cell migration. J Biomed Mater Res A. 2019 Dec;107(12):2718-2725. doi: 10.1002/jbm.a.36775. Epub 2019 Aug 22. PMID: 31404486

2. Lee, D.C., Prossnitz, A.N., Lamm, R.J., Boydston, A.J., and Pun, S.H. (2019) Dual polymerizations: untapped potential for biomaterials. *Adv Healthcare Materials*, 8 (6), 1800861. PMID: 30369103. PMCID: PMC6426662.

3. Liu, G.W.*, Prossnitz, A.N.*, Eng, D.G., Cheng, Y., Subrahmanyam, N., Pippin, J.W., Lamm, R.J., Ngambenjawong, C., Ghandehari, H., Shankland, S.J., and Pun, S.H. (2018) Glomerular disease augments kidney accumulation of synthetic anionic polymers. *Biomaterials,* v178:317-325. PMID: 29891232.

4. Cheng, Y., Liu, G.W., Jain, R., Pippin, J.W., Shankland, S.J., and Pun, S.H. Boronic acid copolymers for direct loading and acid-triggered release of Bis-T-23 in cultured podocytes. ACS Biomaterials Science and Engineering, v4:3968-3973. PMID: 31259236. PMCID: PMC6599616.

e. Plans for next reporting period to accomplish the goals: Nothing to report

4. Impact : Dr. Pun's grant remains in a no-cost extension. At this time, there is nothing to report and we expect that impact will be assessed in her final report.

- **What was the impact on the development of the principal discipline(s) of the project?**
  - *Nothing to Report*
- **What was the impact on other disciplines?**

  Nothing to Report
- **What was the impact on technology transfer?**
  - *Nothing to Report*
- **What was the impact on society beyond science and technology?**
  - *Nothing to Report*

5. Changes: None.

6. Products (total):

Poster presentation at the 2016 NanoDDS Conference.
GW Liu, JW Pippin, SJ Shankland, SH Pun. Bis-T-23 efficacy in *in vitro* models of podocyte injury. *nanoDDS*, Baltimore, MD, 2016. (Poster)

Poster presentation at 2018 Polymers in Medicine and Biology Conference. Prossnitz, A.N., Liu, G.W., Eng, D.G., Cheng, Y., Pippin, J.W., Lamm, R.J., Ngambenjawong, C., Shankland, S., Pun, S.H. (2018) Glomerular disease augments kidney accumulation of synthetic anionic polymers. Polymers in Medicine and Biology. Napa, California.

Poster presentation at American Society of Nephrology Annual Meeting. GW Liu, AN Prossnitz, DG Eng, Y Cheng, JW Pippin, RJ Lamm, C Ngambenjawong, SJ Shankland, SH Pun. Glomerular disease augments kidney accumulation of synthetic polymers. *American Society of Nephrology*, San Diego, CA, 2018. (Poster)

7. Participants and Other Collaborating Organizations

Name: Suzie Pun
Project Role: PI
Researcher Identifier: ORCID ID 0000-0003-1443-4996
Nearest person month worked: 2 (20% effort)
Contribution to project: Project oversight and coordination; reporting

Name: Stuart Shankland
Project Role: Partnering PI
Nearest Person month worked: 2 (20%)
Contribution to project: strategic planning and experimental design

Name: Diana Eng
Project Role: Research Scientist
Nearest Person month worked: 6 (50%)
Contribution to project: Is overseeing all animal work

Name: Natalya Kaverina
Project Role: Research Scientist
Nearest Person month worked: 6 (50%)
Contribution to project: Is responsible for immunostaining and protein detection

Name: Gary Liu
Project Role: Graduate Student
Nearest person month worked: 3 (25% effort)
Contribution to project: Dexamethasone-polymer testing in cultured podocytes and FSGS mouse model.

Name: Shixian Lyu
Project Role: Chemistry postdoc
Nearest person month worked:3 (25% effort)
Contribution to project: Synthesis of dexamethasone-conjugated polymers.

Name: Alex Prossnitz
Project Role: Graduate Student
Nearest person month worked: 4 (33% effort)
Contribution to project: Synthesis of polymers for biodistribution studies.

Changes in Other Support: Not applicable (final report)
What other other organizations were involved as partners?: Nothing to report

8. Special Reporting Requirements: See attached quad chart

9. Appendices – publications

1. Liu GW, Johnson SL, Jain R, Peeler DJ, Shankland SJ, Pun SH. Optimized nonviral gene delivery for primary urinary renal progenitor cells to enhance cell migration. J Biomed Mater Res A. 2019 Dec;107(12):2718-2725. doi: 10.1002/jbm.a.36775. Epub 2019 Aug 22. PMID: 31404486

2. Lee, D.C., Prossnitz, A.N., Lamm, R.J., Boydston, A.J., and Pun, S.H. (2019) Dual polymerizations: untapped potential for biomaterials. *Adv Healthcare Materials*, 8 (6), 1800861. PMID: 30369103. PMCID: PMC6426662.

3. Liu, G.W.*, Prossnitz, A.N.*, Eng, D.G., Cheng, Y., Subrahmanyam, N., Pippin, J.W., Lamm, R.J., Ngambenjawong, C., Ghandehari, H., Shankland, S.J., and Pun, S.H. (2018) Glomerular disease augments kidney accumulation of synthetic anionic polymers. *Biomaterials,* v178:317-325. PMID: 29891232.

4. Cheng, Y., Liu, G.W., Jain, R., Pippin, J.W., Shankland, S.J., and Pun, S.H. Boronic acid copolymers for direct loading and acid-triggered release of Bis-T-23 in cultured podocytes. ACS Biomaterials Science and Engineering, v4:3968-3973. PMID: 31259236. PMCID: PMC6599616.

New podocyte-targeted treatments for focal segmental glomerulosclerosis

PR151175

W81XWH-16-1-0167

PI: Stuart Shankland **Org:** University of Washington **Award Amount:** $1,027,871

Study/Product Aims

- The goal of this work is to demonstrate the therapeutic efficacy of podocyte-selective drug delivery in FSGS. The development of such a platform can transform how FSGS is treated by enabling clinical translation of new classes of small molecule and biologic drugs, and by "rescuing" drug candidates that have failed due to poor solubility or systemic toxicity.
- We hypothesize that podocyte-selective drug delivery *in vivo* will be an effective strategy to halt and reverse experimental FSGS in mice while minimizing systemic toxicity. Accordingly, we will develop a polymeric drug delivery vehicle comprising (*i*) polymers engineered for maximal kidney accumulation, functionalized with (*ii*) podocyte-targeting peptides for molecular recognition, and (*iii*) loaded with Bis-T-23 for podocyte protection.

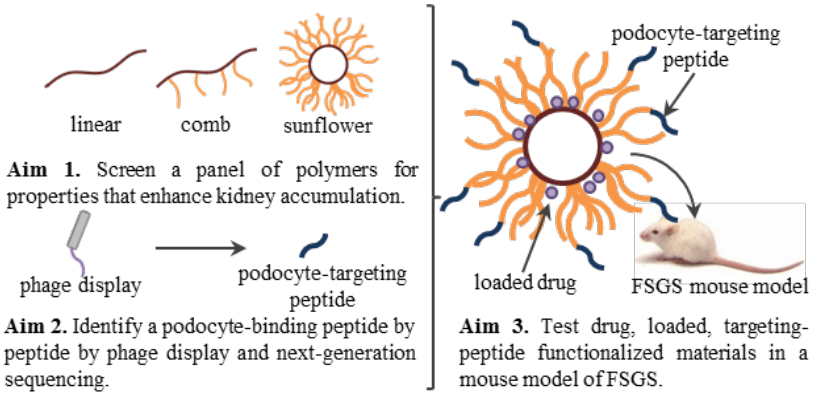

Figure 1. Overview of proposal. In **Aim 1**, a panel of polymers with different structure, charge, and molecular weight will be screened for materials that accumulate in the kidney. At the same time, in **Aim 2** a podocyte-targeting peptide will be identified using phage display and next-generation sequencing. The optimized material from Aim 1, loaded with Bis-T-23 drug and functionalized with targeting peptide from Aim 2, will be tested in a mouse model of FSGS in **Aim 3**.

Timeline and Cost

Activities CY	16	17	18	19
Start-up				
1. Develop kidney-accumulating polymeric drug carriers				
2. Identify and characterize a novel podocyte-binding peptide				
3. Evaluate efficacy of polymer drug formulations in mouse model FSGS				
Estimated Budget ($K)	**$0**	**$333,673**	**$332,095**	**$362,103**

Updated: January 2020

Goals/Milestones (Example) Stuart to complete

CY17 Goal – Develop kidney-accumulating polymeric carriers.

✔ synthesized a panel of polymers to determine polymer properties for kidney accumulation

✔ synthesized polymers reversibly conjugated to Bis-T-23,

CY18 Goals – Identification of a podocyte-targeting ligand.

✔ generated an anti-podocyte antibody

CY19-20 Goal – efficacy studies

✔ Polymers were labeled with Cy5 for imaging. Polymer accumulation was observed in kidneys

Comments/Challenges/Issues/Concerns

- Work continues to optimize drug delivery to podocytes in disease states

Budget Expenditure to Date

Projected Expenditure:	$1,027,871
Actual Expenditure:	$1,027,871

Received: 25 July 2019 | Revised: 31 July 2019 | Accepted: 7 August 2019

DOI: 10.1002/jbm.a.36775

ORIGINAL ARTICLE

Society For Biomaterials | WILEY

Optimized nonviral gene delivery for primary urinary renal progenitor cells to enhance cell migration

Gary W. Liu[1] | Soren L. Johnson[1] | Ritika Jain[1] | David J. Peeler[1] | Stuart J. Shankland[2] | Suzie H. Pun[1]

[1]Department of Bioengineering and Molecular Engineering & Sciences Institute, University of Washington, Seattle, Washington

[2]Department of Medicine, Division of Nephrology, University of Washington School of Medicine, Seattle, Washington

Correspondence
Gary W. Liu and Suzie H. Pun, Department of Bioengineering and Molecular Engineering & Sciences Institute, University of Washington, 3720 15th Ave NE, Seattle, WA 98195.
Email: garywliu@uw.edu (G. W. L.) and spun@uw.edu (S. H. P.)

Funding information
National Institute of Neurological Disorders and Stroke, Grant/Award Number: NIH 2R01NS064404; U.S. Department of Defense, Grant/Award Number: PR151965; National Science Foundation Graduate Research Fellowship Program, Grant/Award Number: DGE-1256082

Abstract

Progressive loss of glomerular podocytes during kidney disease leads to irreversible kidney failure, and is exacerbated by the fact that podocytes are terminally differentiated epithelial cells and unable to proliferate. Regeneration of lost podocytes must therefore derive from nonpodocyte sources. Human urine-derived renal progenitor cells (uRPCs) are attractive podocyte progenitors for cell therapy applications due to their availability from patient urine and ability to migrate to injured glomeruli and differentiate into *de novo* podocytes after intravenous administration. Because gene delivery has emerged as an important strategy to augment the functionality and survival of cell therapies prior to injection, in this work we optimized nonviral gene delivery conditions (cell density, DNA dose, % FBS, and transfection material composition) to primary uRPCs. Using the cationic polymer-peptide conjugate VIPER for gene delivery and the *Sleeping Beauty* transposon/transposase constructs for gene integration, we optimized transfection parameters to achieve efficient transgene expression (up to 55% transfected cells) and stable transgene expression (>65% integration efficiency) lasting up to 10 days. With these methods, we transfected uRPCs to overexpress CXCR4, an important chemokine receptor that mediates uRPC migration to the kidneys after intravenous injection, and demonstrate that CXCR4-uRPCs exhibit enhanced migration compared to mock-transfected cells.

KEYWORDS
gene delivery, glomerular parietal epithelial cell, kidney, nonviral, podocyte, renal progenitor cell

1 | INTRODUCTION

New therapies to arrest chronic kidney disease (CKD) progression and prevent end-stage kidney failure are urgently needed as the cost of treating these patients approaches a staggering $114 billion/year in the United States (Saran et al., 2019). A leading cause of CKD is injury and loss of glomerular podocytes, highly specialized and differentiated epithelial cells that are an integral component of the glomerular filtration barrier (Matsusaka et al., 2005; Wharram et al., 2005). As podocytes are terminally differentiated and unable to proliferate, replenishment of podocyte number during physiological and pathological podocyte loss is entirely dependent on cellular regeneration by nonpodocyte sources (Kaverina, Eng, Schneider, Pippin, & Shankland, 2016; Lasagni, Lazzeri, Shankland, Anders, & Romagnani, 2013; Shankland, Pippin, & Duffield, 2014). During disease conditions when podocyte loss is aggravated (e.g., by circulating factors, autoreactive antibodies, genetic mutations of key podocyte cytoskeletal proteins; Beck et al., 2009; Hahm et al., 2017; Patrakka et al., 2000), the rate of

Gary W. Liu and Soren L. Johnson contributed equally to the study.

podocyte loss overwhelms the regenerative capacity of endogenous podocyte progenitors. Continuous net podocyte depletion leads to focal, then global, glomerulosclerosis that deteriorates kidney filtration (Wharram et al., 2005). Maintaining podocyte number is critical for kidney function, and autologous transfer of podocyte progenitors may be clinically strategic to supplement the endogenous progenitor reservoir and meet the increased regenerative demand during disease.

Renal progenitor cells (RPCs) are an attractive candidate for podocyte cell therapies due to their ease of sourcing from urine and their ability to integrate into injured mouse glomeruli and differentiate into *de novo* podocytes after intravenous administration. Within the nephron, RPCs are a subset of parietal epithelial cells (PECs) that line the Bowman's capsule and are characterized as $CD133^{+}CD24^{+}$ (CD, cluster of differentiation), markers of stem and progenitor cells (Shankland, Smeets, Pippin, & Moeller, 2014). Bowman's capsule RPCs are contiguous with glomerular podocytes and exhibit a gradient in phenotype from multipotent RPCs near the urinary pole to podocyte-committed RPCs near the vascular pole. Clinically, RPCs are shed into urine during active proteinuria (Lazzeri et al., 2015), presenting a noninvasive avenue of collecting and expanding these cells for therapeutic applications. Intravenous infusion of urine-derived RPCs (uRPCs) in an animal model of doxorubicin hydrochloride-induced nephropathy significantly reduced proteinuria, and administered uRPCs integrated into glomeruli and expressed podocyte proteins synaptopodin, nephrin, and podocin, suggesting differentiation into *de novo* podocytes (Lazzeri et al., 2015; Ronconi et al., 2009).

Gene delivery is often applied to cell therapies to augment the functionality and survival of the transferred cells: in cancer immunotherapy, the Food and Drug Administration-approved T-cell therapies Yescarta and Kymriah recognize B-cell leukemias through viral transduction of CD19 chimeric antigen receptors. An interesting candidate for gene delivery to RPCs is the chemokine receptor C-X-C chemokine receptor type 4 (CXCR4), which is expressed on multiple cell types (e.g., hematopoietic stem cells, leukocytes) and mediates cellular migration through binding to its ligand, stromal cell-derived factor-1α (SDF-1α; Kucia et al., 2004), which is often locally upregulated in diseased or injured tissues (Chen et al., 2014; Deng, Xu, & Ren, 2018). CXCR4 mediates RPC migration to the kidneys during disease: blocking CXCR4 on transferred, tissue-derived RPCs with antibodies significantly reduces cell recruitment and efficacy in a mouse model of acute renal failure (Mazzinghi et al., 2008). CXCR4 overexpression through gene delivery has been shown to augment the migration of mesenchymal stem cells (MSCs) to glioblastoma multiforme tumors and the engraftment of human pluripotent stem cell-derived hematopoietic progenitor cells into bone marrow (Jiang, Wang, Fitch, & Yang, 2018; Reid et al., 2018). Similarly, we hypothesize that CXCR4 overexpression via gene delivery methods in transferred uRPCs could enhance cellular homing in response to injured glomeruli and subsequent podocyte regeneration.

Given the clinical potential of uRPCs in regenerating lost podocytes, we developed methods for nonviral gene delivery to uRPCs using a cationic polymer-peptide conjugate, VIPER (virus-inspired polymer for endosomal release), for both transient and stable transgene expression (Cheng, Yumul, & Pun, 2016; Peeler et al., 2019). First, we optimized transfection conditions (cell seeding density, media fetal bovine serum [FBS] content, DNA dose, VIPER composition) to achieve efficient transgene expression (up to 55%) in primary uRPCs. Through co-transfection with *Sleeping Beauty* transposon plasmid and transposase minicircle, we attained long-term (10 day) transgene expression. In translational work, we transfected uRPCs to overexpress CXCR4, and show that transfection significantly increases CXCR4 expression and migration compared to mock-transfected cells.

2 | MATERIALS AND METHODS

2.1 | Plasmids

A tdTomato-T2A-DHFRdm plasmid that carries the T3 SB transposon cassette containing an elongation factor 1-α (EF1α) promoter, tdTomato, *Thosea asigna* virus 2A cleavable peptide (T2A), and a double-mutant of dihydrofolate reductase (DHFRdm) insensitive to methotrexate (MTX) was constructed using the previously reported pMC_T3/mCherry-T2A-DHFRdm construct as a backbone and standard molecular biology cloning techniques (Kacherovsky, Liu, Jensen, & Pun, 2015). A tdTomato-containing plasmid (generous gift from Michael Jensen, Seattle Children's Research Institute) and the NTC9385R-MCS plasmid (Nature Technology; Luke, Carnes, Hodgson, & Williams, 2009) were used as templates for PCR. R6K-RNA-OUT origin of replication and selection gene were amplified with complementary ends and ligated to the transposon. The plasmid was transformed into electrocompetent bacteria according to manufacturer instructions (Nature Technology) and purified using a Plasmid Maxi Kit (Qiagen). SB100× transposase minicircle was described previously (Kacherovsky, Harkey, Blau, Giachelli, & Pun, 2012). pmaxGFP plasmid was purchased from Lonza, and CXCR4 plasmid was a gift from Bryan Roth (Addgene plasmid 66262; Kroeze et al., 2015).

2.2 | VIPER synthesis

The cationic polymer-peptide conjugate VIPER was synthesized and characterized as previously described by reversible addition-fragmentation chain-transfer polymerization (Cheng, Yumul, & Pun, 2016; Peeler et al., 2019). VIPER is a diblock copolymer with the general formula p(OEGMA-*co*-DMAEMA)-*b*-p(DIPAMA-*co*-PDSEMA), where OEGMA is oligo(ethylene glycol) monomethyl ether methacrylate, DMAEMA is 2-(dimethylamino)ethyl methacrylate, DIPAMA is 2-diisopropylaminoethyl methacrylate, and PDSEMA is pyridyl disulfide ethyl methacrylate. After polymerization, copolymers were conjugated with the membrane-lytic peptides melittin, FL-20, CMA-2, C6M3, or MEP-2 as previously described (Peeler et al., 2019).

2.3 | RPC isolation

Human RPCs were isolated from patient urine as previously described with modifications (Lazzeri et al., 2015; Ronconi et al., 2009) and with approval from the University of Washington Institutional Review Board. Briefly, fresh patient urine samples were collected, washed with

phosphate-buffered saline (PBS), and plated with EGM-MV + 20% FBS (Lonza) supplemented with antibiotics on T-75 flasks. Cells were allowed to grow for 6-8 days until confluence. For sorting, cells were lifted with Accutase (Millipore), stained with anti-CD133-allophycocyanin (clone 293C3, Miltenyi Biotec) and anti-CD24-fluorescein isothiocyanate (clone SN3, ThermoFisher Scientific) antibodies, and then sorted for double-positive cells (BD FACSAria III, UW Pathology Flow Cytometry Core). Isotype-stained cells were used to establish gates. Sorted $CD133^{+}CD24^{+}$ cells were plated on T75 flasks and allowed to grow to confluence. Multiple cell stocks were frozen in 5% dimethylsulfoxide/95% FBS or allowed to grow for another passage before freezing.

2.4 | Transfection

In a typical transfection experiment, RPCs were thawed and either plated directly or first allowed to proliferate and then plated in a 24-well plate for experiments. RPCs were transfected after 18-21 hr incubation. For polyplex formulation, VIPER polymer dissolved in 10 μl H_2O at the appropriate nitrogen/phosphate (N/P) mass ratio was added to 1 μg plasmid dissolved in 10 μl H_2O, mixed, and incubated at room temperature for 30 min. Cells were then washed with 500 μl PBS; after PBS was added but before removal, 180 μl media was added to the polyplexes. PBS was then removed from the cells and polyplexes were immediately added. After 4 hr incubation with polyplexes at 37°C, cells were washed with PBS and incubated in fresh media for 24-48 hr.

The tdTomato-T2A-DHFRdm plasmid was co-transfected with SB100× transposase minicircle for genome-integration studies using the methods described above. The total DNA amount was fixed at 1 μg at various transposon:transposase mole ratios (1:0–1:4). Transient and stable tdTomato expression was quantified by flow cytometry on Days 1 and 10, respectively. Percent integration was calculated as the percent tdTomato+ cells on Day 10 divided by the percent tdTomato+ cells on day 1. MTX selection was performed by adding various concentrations of MTX (0-500 nM) to media following co-transfection.

For flow cytometry analysis, cells were washed with PBS, lifted with trypsin for 5 min, resuspended in PBS, stained with Zombie Violet viability dye (BioLegend) according to manufacturer instructions, and resuspended in 1% bovine serum albumin in PBS. Flow cytometry was performed using an Attune NxT flow cytometer (ThermoFisher Scientific), and data were analyzed using the FlowJo software. Statistical analysis was performed using GraphPad Prism 6. To quantify CXCR4 expression, CXCR4-transfected cells were lifted and incubated with mouse anti-CXCR4 monoclonal primary antibody (eBioscience, clone 12G5) for 30 min at 4°C, followed by staining with Alexa Fluor 488-labeled donkey anti-mouse antibody (Jackson ImmunoResearch Laboratories, Inc.) for 30 min at 4°C. Cells were evaluated for CXCR4 protein expression by flow cytometry as described above, using secondary antibody-stained controls to establish negative gates.

2.5 | Migration studies

Renal progenitor cells were transfected as described above with either tdTomato (for mock transfections) or CXCR4 plasmid. At 24-48 hr post-transfection, cells were lifted, resuspended in 200 μl complete media, and then added to the upper chamber of transwell inserts (8-μm pore size, polyester, Corning). Cells were then incubated for 10 min at 37°C to facilitate cell settling. After incubation, 500 μl of 100 ng/ml SDF-1α (PeproTech) in serum-free RPMI was added to the lower chamber, and cells were incubated for 24 hr. Cells were fixed with 4% paraformaldehyde and stained with 4′,6-diamidino-2-phenylindole (DAPI). Image capture and analysis were performed in a blinded manner using a fluorescent microscope (Nikon).

3 | RESULTS

3.1 | Optimization of nonviral gene delivery

Plasmids of minimal size were generated with the short (<500 basepairs) expression and antibiotic-free selection sequence from the Nanoplasmid platform, as transfection efficiency increases with decreasing plasmid size (Levacic, Morys, Kempter, Lachelt, & Wagner, 2017; Suschak, Williams, & Schmaljohn, 2017). To evaluate transient and long-term transfection, plasmids containing the *Sleeping Beauty* transposon system (SBTS) that we have previously reported were generated, but with a tdTomato fluorescent reporter (Kacherovsky et al., 2015). Briefly, the transposon expresses tdTomato and a double-mutant of dihydrofolate reductase (DHFRdm) that confers resistance to methotrexate (MTX) metabolic inhibition. The SBTS is a nonviral gene transfer method currently used in clinical trials for adoptive T-cell therapy (Aronovich, McIvor, & Hackett, 2011). Compared to viral vectors, SBTS is less costly, easier to produce, and exhibits a reduced risk of insertional mutagenesis (Aronovich et al., 2011). Short-term transfection is evaluated by transfection of the plasmid alone, while long-term gene integration is evaluated by co-transfection with transposase, which recognize the inverted terminal repeats flanking the transposon and integrates the transposon into the genome. Subsequent MTX addition could provide an avenue to select for gene-integrated cells for a more homogeneous cell population (Kacherovsky et al., 2015).

The cationic polymer-peptide conjugate, VIPER, was utilized for most of these gene delivery experiments. This block copolymer forms cationic micelles comprised of a positively charged shell that condenses nucleic acid and a reversibly hydrophobic core that hides a membrane-lytic peptide under pH-neutral conditions. After cellular internalization into acidic endosomes and lysosomes, the core of the polymer switches to hydrophilic in nature, reversing micelle assembly and exposing conjugated membrane-lytic melittin peptides that mediate endosomal escape and gene delivery into the cytoplasm (Cheng, Yumul, & Pun, 2016). This delivery technology enables efficient gene delivery *in vitro* and *in vivo*, and in subsequent studies we have developed a panel of VIPER variants with alternative membrane-lytic peptides that exhibit cell type-dependent transfection efficiency (Peeler et al., 2019).

We first screened a panel of the following nonviral transfection reagents: VIPER, Lipofectamine, high-molecular weight branched polyethylenimine, cationic sunflower polymers (Cheng, Wei, et al., 2016), and the TransIT system for delivery of a 4.2 kilo-basepairs plasmid encoding for the reporter gene tdTomato. As VIPER outperformed all other transfection reagents in gene transfer efficiency (Figure S1), VIPER was selected for further optimization. Initial VIPER transfection experiments screened for the effect of cell density, DNA dose, media FBS content, and VIPER composition on transfection efficiency and viability using design of experiments optimization (Olden, Cheng, Yu, & Pun, 2018). First, uRPC density (2.5×10^4 or 5.0×10^4 cells/well) and DNA dose (1 or 2 μg) were optimized. At each of the nitrogen (VIPER tertiary amines) to phosphate (DNA backbone; N/P) ratios tested, transfection with 1 μg DNA resulted in greater viability and number of tdTomato+ cells compared to transfection with 2 μg DNA. Notably, transfections at N/P > 3 with 5.0×10^4 cells/well resulted in greater than double the viability and number of tdTomato+ cells compared to transfections with 2.5×10^4 cells/well (Figure 1a). Therefore, future transfections were performed using 1 μg DNA and 5.0×10^4 cells/well.

Next, media conditions (reduced serum OptiMEM or media containing 10% FBS) were optimized. Generally, the presence of serum improves cell viability, but decreases transfection efficiency. We hypothesized that transfection in media containing 10% FBS would improve transfection efficiency and cell viability at higher N/P ratios. Indeed, at greater N/P, transfections performed in media containing 10% FBS exhibited greater viability and comparable transfection efficiency compared to those performed in OptiMEM (Figure 1b). Accordingly, subsequent transfection experiments were performed in 10% FBS.

A panel of VIPER variants with different membrane-lytic peptides was tested to identify the best-performing VIPER formulation. Cell types exhibit different rates of endosomal acidification and trafficking which may affect the performance of VIPER endosomal escape and plasmid delivery (Olden, Cheng, Cheng, & Pun, 2019; Peeler et al., 2019; Rybak & Murphy, 1998). To account for cellular variances in endosomal dynamics and VIPER performance, a panel of VIPER–peptide conjugates with the following membrane-lytic peptides was screened: melittin, FL-20, CMA-2, C6M3, and MEP-2 (Peeler et al., 2019). These variants capture a range of optimal membrane-lytic activity pH and exhibit robust transfection *in vivo* in the brain after subventricular zone injection (Peeler et al., 2019). Transfection at N/P 10 and 12 with this VIPER panel revealed that VIPER melittin, CMA-2, and MEP-2 variants resulted in a higher number of transfected cells than the other variants (Figure 2). As the original VIPER melittin resulted in the greatest percent transfection and number of transfected cells, this variant was used in subsequent optimization studies.

Having optimized cell density, DNA amount, media conditions, and VIPER peptide, transfection experiments were performed in triplicate for statistical analysis and to optimize VIPER/DNA N/P ratio. Five N/P ratios were tested (Figure 3). Transfection at N/P 12, 14, and 16 resulted in 37, 46, and 49% tdTomato+ cells, respectively. Notably, transfection at N/P 14 resulted in significantly higher transfection efficiency than other ratios without a significant decrease in viability, whereas doubling the N/P ratio from 8 to 16 resulted in a significant decrease in viability from 79.4 ± 10.6% to 45.2 ± 10.9% and no significant increase in transfection efficiency over N/P 14. Therefore, N/P 14 was used for further transfection experiments. Additional experiments using a smaller plasmid, pmaxGFP (3.5 kilo-basepairs),

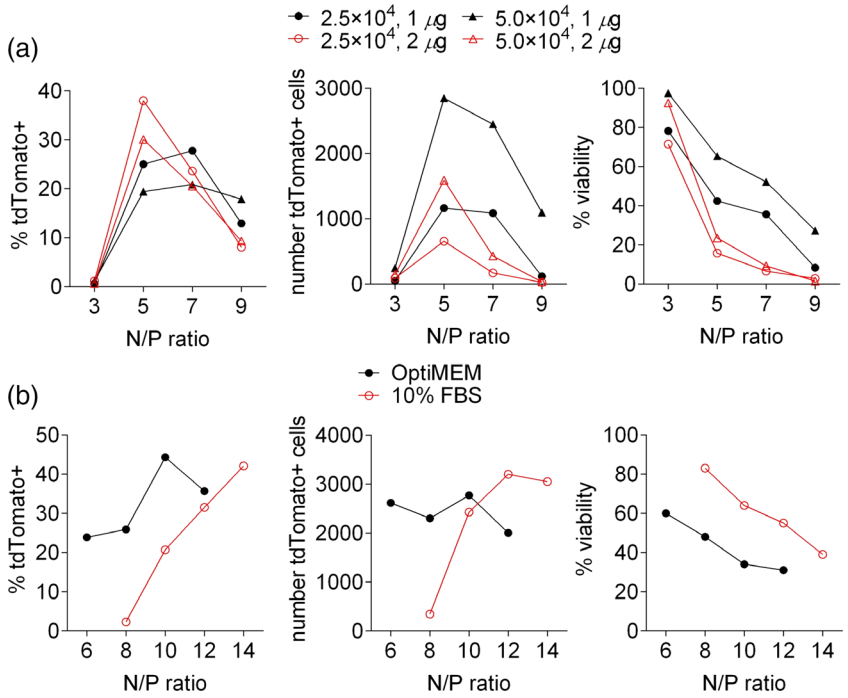

FIGURE 1 Design of experiments optimization of transfection conditions. (a) Effect of cell density and DNA amount on transfection efficiency and cell viability. RPCs (n = 1 each) were transfected with VIPER/DNA polyplexes in OptiMEM at four N/P ratios, 2.5×10^4 or 5.0×10^4 cells/well, and 1 or 2 μg DNA, and then analyzed for % tdTomato+ cells (left), number of tdTomato+ cells (middle), and % viability (right) after 2 days by flow cytometry. (b) Effect of serum on transfection efficiency and cell viability at higher N/P ratios. RPCs (n = 1 each) were transfected with VIPER/DNA polyplexes in OptiMEM or media containing 10% FBS at various N/P ratios, 5.0×10^4 cells/well, and 1 μg DNA, and then analyzed by flow cytometry as described above. FBS, fetal bovine serum; RPC, renal progenitor cell; VIPER, virus-inspired polymer for endosomal release

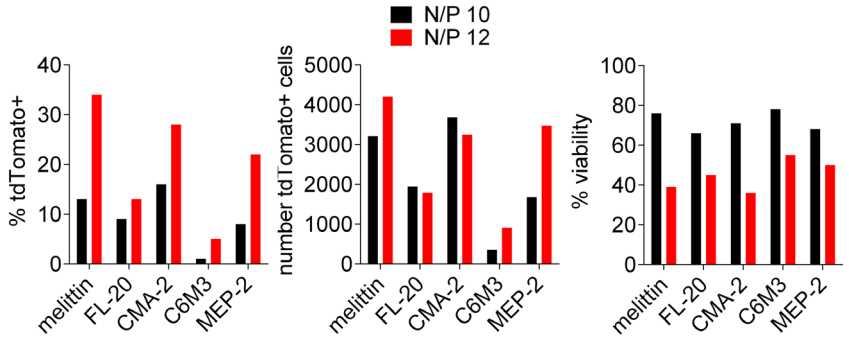

FIGURE 2 Design of experiments optimization of VIPER peptide. RPCs (n = 1 each) were transfected with VIPER/DNA polyplexes in media containing 10% FBS at N/P 10 or 12, 5.0 × 10^4 cells/well, and 1 μg DNA, and then analyzed for % tdTomato+ cells (left), number of tdTomato+ cells (middle), and % viability (right) after 2 days by flow cytometry. FBS, fetal bovine serum; RPC, renal progenitor cell; VIPER, virus-inspired polymer for endosomal release

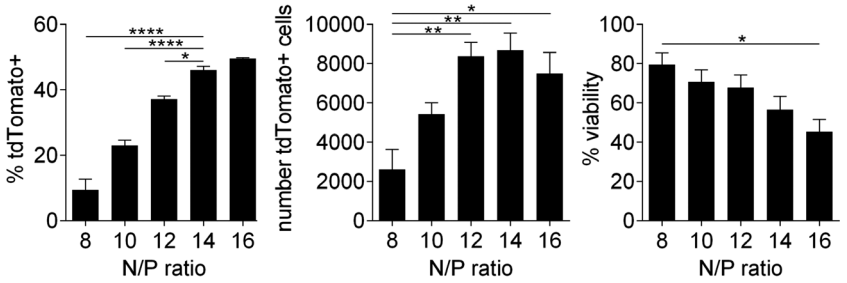

FIGURE 3 Optimization of transfection N/P ratios. RPCs (n = 3 each) were transfected with VIPER/DNA polyplexes in media containing 10% FBS at various N/P ratios, 5.0 × 10^4 cells/well, and 1 μg DNA, and then analyzed for % tdTomato+ cells (left), number of tdTomato+ cells (middle), and % viability (right) after 2 days by flow cytometry. Statistical analysis was performed using a one-way ANOVA with post-hoc Tukey's multiple comparisons test. Select comparisons are shown. Bars represent means ± *SEM*. *p-value < .05, **p-value < .01, ****p-value < .0001. FBS, fetal bovine serum; RPC, renal progenitor cell; VIPER, virus-inspired polymer for endosomal release

yielded 32.7, 55.1, and 44.3% transfection at N/P 10, 15, and 20, respectively (Figure S2).

3.2 | Gene integration

Gene integration efficiency was studied by co-transfecting tdTomato-T2A-DHFRdm transposon plasmid and SB100× transposase minicircle at various mole ratios in a total of 1 μg DNA using the optimized methods. Transient tdTomato expression was analyzed on Day 1, and stable expression was analyzed on Day 10. Notably, in the absence of transposase, minimal tdTomato expression (2.1 ± 0.5%) was observed after 10 days, whereas 12.3 ± 3.5%, 15.9 ± 4.3%, 14.5 ± 1.6%, and 18.6 ± 1.4% expression was observed for transposon:transposase 4:1, 2:1, 1:1, and 1:2, respectively (Figure 4). Integration efficiency was calculated by dividing % expression on day 10 by that of day 1. The highest genome integration (68.0 ± 2.6%) was achieved at transposon: transposase 1:2, which was significantly greater than that of 4:1 (42.3 ± 10.6%) and 1:0 (6.9 ± 1.3%). Therefore, addition of transposase results in stable gene expression. The transposon contains a double-mutant of DHFR, which renders the mutant DHFR 10,000-fold less susceptible to MTX inhibition. Therefore, MTX could be used to enrich uRPCs for those stably transfected with the tdTomato-T2A-DHFRdm transposon construct. However, extended incubation in MTX did not induce robust (>90%) enrichment of stably transfected RPCs (Figure S3). Alternative selection mechanisms, such as puromycin or G418, may improve selection efficiency.

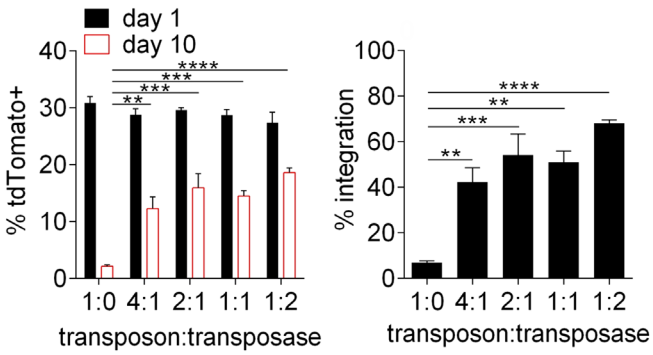

FIGURE 4 *Sleeping Beauty* transposase for stable gene expression. RPCs (n = 3) were transfected with VIPER/DNA polyplexes at five mole ratios of tdTomato-T2A-DHFRdm transposon plasmid to SB100× transposase minicircle. Left: cells were analyzed for transient expression 1 day after transfection (black) and stable expression after 10 days (red). Statistical tests were performed comparing to transposon:transposase 1:0, day 10. Right: percent integration was calculated as the % tdTomato+ after 10 days divided by the % tdTomato+ after 1 day. Statistical analysis was performed using a one-way ANOVA with post-hoc Tukey's multiple comparisons test. Bars represent means ± *SEM*. **p-value < .01, ***p-value < .001, ****p-value < .0001. RPC, renal progenitor cell; VIPER, virus-inspired polymer for endosomal release

3.3 | Overexpression of CXCR4

We then sought to generate CXCR4-overexpressing uRPCs using these optimized nonviral gene delivery methods, as transient CXCR4 expression may be clinically useful to promote the migration of

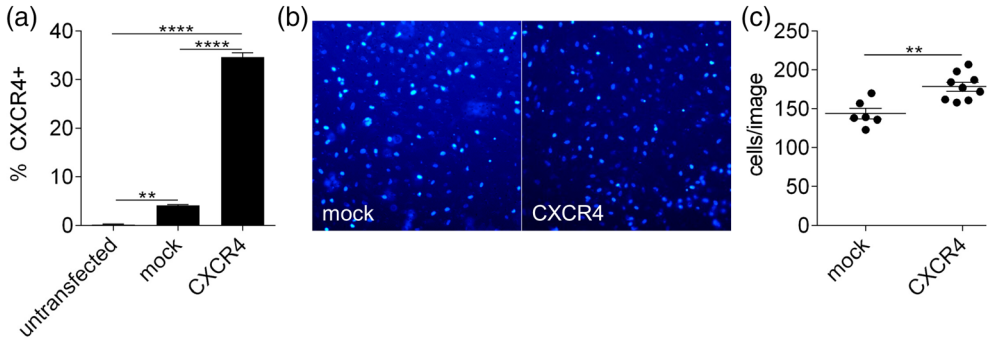

FIGURE 5 CXCR4 expression and migration. (a) RPCs (n = 3) were transfected and analyzed for CXCR4 expression after 24 hr. (b) Representative images of DAPI-stained mock-transfected and CXCR4-transfected RPCs that have migrated in response to SDF-1α through a transwell membrane. (c) Number of migrated mock-transfected or CXCR4-transfected RPCs. Statistical analysis was performed using a one-way ANOVA with post-hoc Tukey's multiple comparisons test or Student's t test. Bars represent means ± *SEM*. **p-value < .01, ****p-value < .0001. DAPI, 4′,6-diamidino-2-phenylindole; RPC, renal progenitor cell

transferred uRPCs onto the glomerular tuft during systemic circulation. To generate CXCR4-uRPCs, cells were transfected with CXCR4 plasmid or tdTomato plasmid as a mock transfection at N/P 14, and analyzed for CXCR4 expression by flow cytometry. Untransfected cells were also analyzed to establish baseline CXCR4 expression. Transfection with CXCR4 plasmid resulted in a greater percentage of CXCR4+ cells (∼35%) compared to mock transfection (∼4%; Figure 5a). CXCR4 expression observed in mock transfection conditions may be due to nonspecific antibody binding rather than true gene expression. Transfected cells were then tested for migration in transwell migration assays. At 24 or 48 hr post-transfection, cells were lifted and placed into the upper chamber of transwell membranes, and the CXCR4 ligand SDF-1α was added to the lower chamber. In two independent, replicate studies, CXCR4-transfected cells exhibited greater migration in response to SDF-1α compared to mock-transfected cells (Figure 5b,c, p-value = 0.0019).

4 | DISCUSSION

The progressive loss of glomerular podocytes during disease overwhelms the regenerative capacity of endogenous podocyte progenitors and directly underlies CKD and end-stage kidney failure. Cell therapies leveraging RPCs, which are capable of engrafting onto injured kidney glomeruli and differentiating into new podocytes after intravenous infusion (Lazzeri et al., 2015; Ronconi et al., 2009), may be clinically strategic in enhancing the rate of endogenous podocyte regeneration and arresting CKD progression. These new therapies will likely utilize gene delivery methods to augment the therapeutic efficacy of the transferred cells. In this work, we optimized nonviral gene delivery conditions to primary RPCs. Nonviral gene delivery presents many advantages compared to viral gene delivery, including unrestricted cargo plasmid size, reduced cost, and reduced risk of immunogenicity (Olden et al., 2018).

We identified uRPC culture conditions and VIPER composition that lead to optimal nonviral gene delivery for both short-term and long-term transgene expression. After 24 hr post-transfection, we observed up to 55% transfected cells, which decreases to <3% over 10 days. Clinically, transient expression may be useful to temporarily confer transferred stem cells with transgenes that promote migration and homing to diseased tissue, but desist after cells adopt differentiated and reparative phenotypes. Given the importance of CXCR4 in mediating RPC migration to the injured kidney (Mazzinghi et al., 2008), we demonstrate that transfected CXCR4-uRPCs exhibit greater CXCR4 expression and cellular migration compared to mock-transfected cells. Nonviral gene delivery has been an important strategy in augmenting stem cell migration and function: microporation of MSCs with CXCR4 minicircle enhances cell migration toward skin injuries (Mun, Shin, Kwon, Lim, & Oh, 2016), and tumor necrosis factor-related apoptosis-inducing ligand (TRAIL)-overexpressing adipose-derived stem cells (Jiang et al., 2016) and MSCs (Han, Hwang, & Na, 2018), mediated by polyplexes, localize to tumors and reduce tumor burden.

Interestingly, a low percentage of untransfected uRPCs expressed CXCR4+ (<1%), whereas Mazzinghi et al.(2008) have reported that RPCs abundantly express CXCR4 at both the protein and mRNA level. This may be due to cell sourcing differences: here, RPCs were collected from urine, while Mazzinghi et al. isolated RPCs from nephrectomized kidney tissue of patients with renal cell carcinoma. A particular subpopulation of RPCs may be more predisposed to be denuded or migrate off of the Bowman's capsule during disease and shed into the urine, resulting in predominantly CXCR4-low-expressing RPCs in the urine. Extended residence in protein-dense urine may also contribute to an altered phenotype (Zhai et al., 2016). Given the importance of CXCR4 in RPC homing, CXCR4 gene delivery methods may be especially important for urinary RPCs with low baseline CXCR4 expression.

Using the SBTS, we also achieved long-term (up to 10 days) gene expression with >65% gene integration efficiency. Here, incorporation of methotrexate selection via a double-mutant of dihydrofolate reductase did not result in significant enrichment of transfected cells. An alternative strategy may be to expand transfected single-cell clones (Lazzeri et al., 2015), although new agents to reverse and prevent cellular senescence after expansion are needed to maintain the function of these cells. Genetic manipulation of RPCs *ex vivo* may present an

avenue to repair genetically caused podocyte dysfunction. Mutations in key podocyte ultrastructure and attachment proteins such as nephrin, podocin, and laminin β2 lead to podocyte dysfunction (Lovric, Ashraf, Tan, & Hildebrandt, 2016) and kidney failure. These patients often fail to respond to frontline steroid therapy, and 50% develop end-stage kidney failure within 15 years (Ha, 2017). While autologous transfer of uRPCs may present an attractive strategy to restore podocyte number, the same genetic mutations would prevent differentiation into functional podocytes. Indeed, Lazzeri et al. (2015) have shown that uRPCs derived from patients with genetic mutations in *NPHS2* differentiate into podocytes with severe cytoskeletal F-actin defects and disruption of nephrin and podocin protein expression. The methods developed here could enable genomic integration of wild-type gene variants or clustered regularly interspaced short palindromic repeats (CRISPR)/Cas9 delivery that correct genetic mutations in uRPCs and therefore lead to differentiation into functional podocytes *in vivo*.

Recent work by the Romagnani group has revealed the different effects of SDF-1α on endogenous and transferred RPCs. Within the glomerulus, podocytes are the main producer of SDF-1α, which under normal and disease conditions maintains quiescence of and inhibits podocyte differentiation by RPCs on the Bowman's capsule (Romoli et al., 2018; Sayyed et al., 2009). Interestingly, systemic blockade of SDF-1α in animals reduces proteinuria and increases podocyte regeneration by PECs during doxorubicin hydrochloride-induced nephropathy compared to untreated animals, likely due to disruption of SDF-1α-mediated PEC quiescence (Romoli et al., 2018). While blockade of intraglomerular SDF-1α may promote podocyte differentiation by endogenous PECs, the CXCR4-SDF-1α axis is still critical in mediating glomerular engraftment of exogenous, transferred RPCs (Mazzinghi et al., 2008).

We report efficient nonviral gene delivery methods (up to 55% transfected cells) to primary uRPCs through optimizing cell density, DNA dose, media FBS content, and VIPER transfection reagent composition. While co-transfection with transposase minicircle resulted in >65% integration efficiency, we did not observe significant enrichment of integrated cells with MTX selection. Transfection with CXCR4 plasmid resulted in greater CXCR4 expression and cellular migration in response to SDF-1α compared to control transfections. Future work will assess migration and therapeutic efficacy of transfected RPCs in animal models of podocyte loss. Given the clinical potential of uRPCs as a cell therapy to regenerate glomerular podocytes, the methods reported here may be useful in future manufacturing applications to augment the survival and differentiation ability of uRPCs. Such gene delivery to uRPCs may also be clinically strategic in regenerating functional podocytes in patients with genetic causes of podocyte dysfunction.

ACKNOWLEDGMENTS

This work was supported by the Office of the Assistant Secretary of Defense for Health Affairs through the Peer Reviewed Medical Research Program under Award Number PR151965, NIH 2R01NS064404, and by the National Science Foundation Graduate Research Fellowship Program under Grant No. DGE-1256082 to G.W.L. S.J.S. was supported by NIH/NIA 5R01AG046231, DOD W81XWH-16-1-0168, NIH/NIDDK R01 DK097598, and UG3/UH3 TR002158. Opinions, interpretations, conclusions, and recommendations are those of the authors and are not necessarily endorsed by the Department of Defense, National Institutes of Health, or the National Science Foundation. We would like to thank Ian Blumenthal and Michael Jensen for their generous gift of tdTomato-containing plasmid, Meilyn Sylvestre for assistance in blinding experimental treatments, and Donna Prunkard and Ngoc-Han Thi Nguyen (UW Pathology) for assistance with cell sorting.

CONFLICT OF INTEREST

The authors declare no potential conflict of interest.

REFERENCES

Aronovich, E. L., McIvor, R. S., & Hackett, P. B. (2011). The sleeping beauty transposon system: A non-viral vector for gene therapy. *Human Molecular Genetics*, *20*, R14–R20.

Beck, L. H., Bonegio, R. G., Lambeau, G., Beck, D. M., Powell, D. W., Cummins, T. D., … Salant, D. J. (2009). M-type phospholipase A2 receptor as target antigen in idiopathic membranous nephropathy. *New England Journal of Medicine*, *361*, 11–21.

Chen, L. H., Advani, S. L., Thai, K., Kabir, M. G., Sood, M. M., Gibson, I. W., … Advani, A. (2014). SDF-1/CXCR4 signaling preserves microvascular integrity and renal function in chronic kidney disease. *PLoS ONE*, *9*, e92227.

Cheng, Y., Wei, H., Tan, J. K. Y., Peeler, D. J., Maris, D. O., Sellers, D. L., … Pun, S. H. (2016). Nano-sized sunflower polycations as effective gene transfer vehicles. *Small*, *12*, 2750–2758.

Cheng, Y., Yumul, R. C., & Pun, S. H. (2016). Virus-inspired polymer for efficient in vitro and in vivo gene delivery. *Angewandte Chemie (International Ed. in English)*, *55*, 12013–12017.

Deng, Q. J., Xu, X. F., & Ren, J. (2018). Effects of SDF-1/CXCR4 on the repair of traumatic brain injury in rats by mediating bone marrow derived Mesenchymal stem cells. *Cellular and Molecular Neurobiology*, *38*, 467–477.

Ha, T. S. (2017). Genetics of hereditary nephrotic syndrome: A clinical review. *Korean Journal of Pediatrics*, *60*, 55–63.

Hahm, E., Wei, C., Fernandez, I., Li, J., Tardi, N. J., Tracy, M., … Reiser, J. (2017). Bone marrow-derived immature myeloid cells are a main source of circulating suPAR contributing to proteinuric kidney disease. *Nature Medicine*, *23*, 100–106.

Han, J., Hwang, H. S., & Na, K. (2018). TRAIL-secreting human mesenchymal stem cells engineered by a non-viral vector and photochemical internalization for pancreatic cancer gene therapy. *Biomaterials*, *182*, 259–268.

Jiang, X., Fitch, S., Wang, C., Wilson, C., Li, J., Grant, G. A., & Yang, F. (2016). Nanoparticle engineered TRAIL-overexpressing adipose-derived stem cells target and eradicate glioblastoma via intracranial delivery. *Proceedings of the National Academy of Sciences of the United States of America*, *113*, 13857–13862.

Jiang, X., Wang, C., Fitch, S., & Yang, F. (2018). Targeting tumor hypoxia using nanoparticle-engineered CXCR4-overexpressing adipose-derived stem cells. *Theranostics*, *8*, 1350–1360.

Kacherovsky, N., Harkey, M. A., Blau, C. A., Giachelli, C. M., & Pun, S. H. (2012). Combination of sleeping beauty transposition and chemically induced dimerization selection for robust production of engineered cells. *Nucleic Acids Research*, *40*, e85.

Kacherovsky, N., Liu, G. W., Jensen, M. C., & Pun, S. H. (2015). Multiplexed gene transfer to a human T-cell line by combining sleeping beauty transposon system with methotrexate selection. *Biotechnology and Bioengineering*, *112*, 1429–1436.

Kaverina, N. V., Eng, D. G., Schneider, R. R., Pippin, J. W., & Shankland, S. J. (2016). Partial podocyte replenishment in experimental FSGS derives from nonpodocyte sources. *American Journal of Physiology. Renal Physiology*, *310*, F1397–F1413.

Kroeze, W. K., Sassano, M. F., Huang, X. P., Lansu, K., JD, M. C., Giguère, P. M., … Roth, B. L. (2015). PRESTO-tango as an open-source resource for interrogation of the druggable human GPCRome. *Nature Structural & Molecular Biology*, *22*, 362.

Kucia, M., Jankowski, K., Reca, R., Wysoczynski, M., Bandura, L., Allendorf, D. J., … Ratajczak, M. Z. (2004). CXCR4-SDF-1 signalling, locomotion, chemotaxis and adhesion. *Journal of Molecular Histology*, *35*, 233–245.

Lasagni, L., Lazzeri, E., Shankland, S. J., Anders, H. J., & Romagnani, P. (2013). Podocyte mitosis—A catastrophe. *Current Molecular Medicine*, *13*, 13–23.

Lazzeri, E., Ronconi, E., Angelotti, M. L., Peired, A., Mazzinghi, B., Becherucci, F., … Romagnani, P. (2015). Human urine-derived renal progenitors for personalized modeling of genetic kidney disorders. *Journal of the American Society of Nephrology*, *26*, 1961–1974.

Levacic, A. K., Morys, S., Kempter, S., Lachelt, U., & Wagner, E. (2017). Minicircle versus plasmid DNA delivery by receptor-targeted polyplexes. *Human Gene Therapy*, *28*, 862–874.

Lovric, S., Ashraf, S., Tan, W., & Hildebrandt, F. (2016). Genetic testing in steroid-resistant nephrotic syndrome: When and how? *Nephrology, Dialysis, Transplantation*, *31*, 1802–1813.

Luke, J., Carnes, A. E., Hodgson, C. P., & Williams, J. A. (2009). Improved antibiotic-free DNA vaccine vectors utilizing a novel RNA based plasmid selection system. *Vaccine*, *27*, 6454–6459.

Matsusaka, T., Xin, J., Niwa, S., Kobayashi, K., Akatsuka, A., Hashizume, H., … Ichikawa, I. (2005). Genetic engineering of glomerular sclerosis in the mouse via control of onset and severity of podocyte-specific injury. *Journal of the American Society of Nephrology*, *16*, 1013–1023.

Mazzinghi, B., Ronconi, E., Lazzeri, E., Sagrinati, C., Ballerini, L., Angelotti, M. L., … Romagnani, P. (2008). Essential but differential role for CXCR4 and CXCR7 in the therapeutic homing of human renal progenitor cells. *The Journal of Experimental Medicine*, *205*, 479–490.

Mun, J.-Y., Shin, K. K., Kwon, O., Lim, Y. T., & Oh, D.-B. (2016). Minicircle microporation-based non-viral gene delivery improved the targeting of mesenchymal stem cells to an injury site. *Biomaterials*, *101*, 310–320.

Olden, B. R., Cheng, E., Cheng, Y., & Pun, S. H. (2019). Identifying key barriers in cationic polymer gene delivery to human T cells. *Biomaterials Science*, *7*, 789–797.

Olden, B. R., Cheng, Y., Yu, J. L., & Pun, S. H. (2018). Cationic polymers for non-viral gene delivery to human T cells. *Journal of Controlled Release*, *282*, 140–147.

Patrakka, J., Kestilä, M., Wartiovaara, J., Ruotsalainen, V., Tissari, P., Lenkkeri, U., … Jalanko, H. (2000). Congenital nephrotic syndrome (NPHS1): Features resulting from different mutations in Finnish patients. *Kidney International*, *58*, 972–980.

Peeler, D. J., Thai, S. N., Cheng, Y., Horner, P. J., Sellers, D. L., & Pun, S. H. (2019). pH-sensitive polymer micelles provide selective and potentiated lytic capacity to venom peptides for effective intracellular delivery. *Biomaterials*, *192*, 235–244.

Reid, J. C., Tanasijevic, B., Golubeva, D., Boyd, A. L., Porras, D. P., Collins, T. J., & Bhatia, M. (2018). CXCL12/CXCR4 signaling enhances human PSC-derived hematopoietic progenitor function and overcomes early in vivo transplantation failure. *Stem Cell Reports*, *10*, 1625–1641.

Romoli, S., Angelotti, M. L., Antonelli, G., Kumar VR, S., Mulay, S. R., Desai, J., … Romagnani, P. (2018). CXCL12 blockade preferentially regenerates lost podocytes in cortical nephrons by targeting an intrinsic podocyte-progenitor feedback mechanism. *Kidney International*, *94*, 1111–1126.

Ronconi, E., Sagrinati, C., Angelotti, M. L., Lazzeri, E., Mazzinghi, B., Ballerini, L., … Romagnani, P. (2009). Regeneration of glomerular podocytes by human renal progenitors. *Journal of the American Society of Nephrology*, *20*, 322–332.

Rybak, S. L., & Murphy, R. F. (1998). Primary cell cultures from murine kidney and heart differ in endosomal pH. *Journal of Cellular Physiology*, *176*, 216–222.

Saran, R., Robinson, B., Abbott, K. C., Agodoa, L. Y. C., Bragg-Gresham, J., Balkrishnan, R., … Shahinian, V. (2019). US renal data system 2018 annual data report: Epidemiology of kidney disease in the United States. *American Journal of Kidney Diseases*, *73*, A7–A8.

Sayyed, S. G., Hägele, H., Kulkarni, O. P., Endlich, K., Segerer, S., Eulberg, D., … Anders, H. J. (2009). Podocytes produce homeostatic chemokine stromal cell-derived factor-1/CXCL12, which contributes to glomerulosclerosis, podocyte loss and albuminuria in a mouse model of type 2 diabetes. *Diabetologia*, *52*, 2445–2454.

Shankland, S. J., Pippin, J. W., & Duffield, J. S. (2014). Progenitor cells and podocyte regeneration. *Seminars in Nephrology*, *34*, 418–428.

Shankland, S. J., Smeets, B., Pippin, J. W., & Moeller, M. J. (2014). The emergence of the glomerular parietal epithelial cell. *Nature Reviews. Nephrology*, *10*, 158–173.

Suschak, J. J., Williams, J. A., & Schmaljohn, C. S. (2017). Advancements in DNA vaccine vectors, non-mechanical delivery methods, and molecular adjuvants to increase immunogenicity. *Human Vaccines & Immunotherapeutics*, *13*, 2837–2848.

Wharram, B. L., Goyal, M., Wiggins, J. E., Sanden, S. K., Hussain, S., Filipiak, W. E., … Wiggins, R. C. (2005). Podocyte depletion causes glomerulosclerosis: Diphtheria toxin-induced podocyte depletion in rats expressing human diphtheria toxin receptor transgene. *Journal of the American Society of Nephrology*, *16*, 2941–2952.

Zhai, T., Furuta, I., Akaishi, R., Ishikawa, S., Morikawa, M., Yamada, T., … Minakami, H. (2016). Alteration of podocyte phenotype in the urine of women with preeclampsia. *Scientific Reports*, *6*, 24258.

SUPPORTING INFORMATION

Additional supporting information may be found online in the Supporting Information section at the end of this article.

How to cite this article: Liu GW, Johnson SL, Jain R, Peeler DJ, Shankland SJ, Pun SH. Optimized nonviral gene delivery for primary urinary renal progenitor cells to enhance cell migration. *J Biomed Mater Res*. 2019;107A:2718–2725. https://doi.org/10.1002/jbm.a.36775

ADVANCED HEALTHCARE MATERIALS
www.advhealthmat.de

Dual Polymerizations: Untapped Potential for Biomaterials

*Daniel C. Lee, Robert J. Lamm, Alex N. Prossnitz, Andrew J. Boydston, and Suzie H. Pun**

Block copolymers with unique architectures and those that can self-assemble into supramolecular structures are used in medicine as biomaterial scaffolds and delivery vehicles for cells, therapeutics, and imaging agents. To date, much of the work relies on controlling polymer behavior by varying the monomer side chains to add functionality and tune hydrophobicity. Although varying the side chains is an efficient strategy to control polymer behavior, changing the polymer backbone can also be a powerful approach to modulate polymer self-assembly, rigidity, reactivity, and biodegradability for biomedical applications. There are many developments in the syntheses of polymers with segmented backbones, but these developments are not widely adopted as strategies to address the unique constraints and requirements of polymers for biomedical applications. This review highlights dual polymerization strategies for the synthesis of backbone-segmented block copolymers to facilitate their adoption for biomedical applications.

1. Introduction

Recent advancements in polymerization techniques have afforded the ability to control, with unprecedented precision, the composition, sequence, molecular weight, size distribution, and mechanical and chemical properties of polymers. In turn, the precision synthesis of polymers has enabled the development of highly tunable materials for use in tissue engineering, drug delivery, and biomaterial implants. As of 2017, there were 8 polymeric micelle systems in clinical trials for evaluation as cancer treatments.[1] Polymeric systems are also used in Food and Drug Administration (FDA) approved platforms for prolonged drug delivery.[2] While there has been tremendous progress in both basic polymer science and translation into biomedical applications, there remain many unsolved challenges that can potentially be addressed with new monomers, sequences, or polymeric architectures. Block copolymers (BCPs), polymers with distinct repeat units connected by covalent bonds, are particularly interesting as their behaviors differ from a physical blend of the homopolymers.

The development of reversible-deactivation radical polymerization (RDRP) and other polymerizations such as ring-opening metathesis polymerization (ROMP) with "living" characteristics have enabled chemists to synthesize BCPs using a single polymerization by sequential addition of monomer to a growing polymer chain end. These advancements in polymer synthesis have vastly expanded the potential for polymer structures.[3] Polymer with unique architectures such as block, star, comb, brush, knot, and cyclic polymers (**Figure 1**, upper) have been shown to affect the mechanical properties of biomaterials and affect administration route, biodistribution, and cargo loading of polymeric drug delivery systems.[4–10] Star polymers with internal hydrophobic blocks are used to encapsulate poorly soluble drugs, followed by hydrophilic blocks that ensure hydration and prevent aggregation.[11] Star polymers have also been used for imaging and diagnosis.[12] Comb and brush polymers have been designed to contain hydrophobic regions to encapsulate and deliver paclitaxel,[13] doxorubicin,[14] and imaging agents, or to incorporate cationic monomers to complex with nucleic acids for gene delivery applications.[15,16] Cyclic polymers have longer circulation times compared to their linear analogs[7,17] and have been used as a multi-macroinitiator in the synthesis of sunflower polymers for drug and nucleic acid delivery.[8,18] Other single-molecule polymeric structures, such as hyperbranched polymers and dendrimers, have made an impact in tumor targeting.[5,9]

Some of these polymeric architectures, as well as linear amphiphilic polymers, allow for self-assembly into supramolecular structures.[19,20] These supramolecular structures (Figure 1, lower) contain regions of hydrophobicity and regions of hydrophilicity with controlled sizes that can be designed by the user to sequester drugs, protect proteins from the immune system, adsorb to surfaces in the presence of a stimulus, and perform many tasks not possible with prior tools. Micelles that contain a hydrophobic core have been used to store hydrophobic cargo such as chemotherapeutics, hormones, and imaging agents in both academic and clinical settings.[1,21] Micellar structures can also utilize stimulus-responsive bonds to improve the stability of drug–micelle complexes,[22] or crosslinked cores to prolong stability in

D. C. Lee
Molecular Engineering and Sciences Institute
University of Washington
3946 W Stevens Way NE, Seattle, WA 98105, USA
R. J. Lamm, A. N. Prossnitz, Prof. S. H. Pun
Department of Bioengineering
University of Washington
3720 15th Ave NE, Seattle, WA 98105, USA
E-mail: spun@uw.edu
Prof. A. J. Boydston
Department of Chemistry
University of Washington
4000 15th Ave NE, Seattle, WA 98195, USA
The ORCID identification number(s) for the author(s) of this article can be found under https://doi.org/10.1002/adhm.201800861.

DOI: 10.1002/adhm.201800861

vivo.[23] Polymeric micelles have medical applications beyond drug delivery, and have been studied extensively as diagnostic agents.[24,25]

Polymersomes, bilayer vesicles consisting of polymer building blocks,[26] have also been used to deliver diagnostic agents,[27] hydrophobic chemotherapeutics such as doxorubicin and paclitaxel,[28] and hydrophilic molecules such as genes[29] and proteins.[30] Polymersomes exhibit prolonged circulation in the body due to diminished opsonization compared to liposomes and slower kinetics of disassembly below the critical micelle concentration (CMC) due to the greater molecular weight of the building blocks.[26,31,32] Stimuli-responsive polymersomes have been developed to increase the precision of drug release. For example, reduction-sensitive polymersomes are used for intracellular delivery of cargo in response to higher intracellular concentrations of reducing agents such as glutathione compared to the extracellular environment.[33] There are multiple excellent reviews on stimuli-responsive polymersomes with potential stimuli including pH, temperature, redox potential, light, and others.[34–36]

Gels made with polymers with side chains that promote gelation at varied temperatures such as hydroxyethyl methacrylate (HEMA) or *n*-isopropylacrylamide (NIPAM) can be made to be sensitive to temperature and pH.[37] Notably, temperature-sensitive BCPs with lower critical solution temperature (LCST) between room temperature and physiological temperature have been used as injectable materials since they are liquid upon injection, but can gel within the body.[38] This form of polymeric system is used in a FDA-approved platform for sustained drug delivery.[2] Additionally, self-assembled structures can be aggregated to form larger, irregular structures. One such example is that of micellar agglomerates which start as a multimodal population of nanoscale micelles, but after an increase in temperature, undergo a phase transition forming macroscale gels.[39]

In these applications, the polymer behavior is often manipulated by modifying the polymer side chains and not the polymer backbone. While the monomer side chains of BCPs heavily dictate the behavior and properties of BCPs, the polymer backbone can also be used to impart biodegradability, reactivity,[40] as well as other behaviors and properties that cannot be achieved by changing the monomer side chains. For example, the polymer backbone of guanidinum side chain containing polymers has been shown to affect the cellular uptake of small interfering RNA (siRNA) and proteins differently.[41] Additionally, some approaches to synthesize backbone-segmented BCPs allow for the inclusion of stimuli-responsive moieties between polymer blocks.[42,43]

The ability to segment the BCP backbone into different repeats is a powerful tool to further engineer the behavior and properties of polymeric materials. Because a polymerization is multiple turnovers of the same reaction, it results in a repetitive backbone structure. For example, radical polymerization of vinyl groups results in an aliphatic backbone and ring opening polymerization of cyclic electrophilic monomers results in a backbone with electrophilic repeats.

One effective approach to achieve BCPs with segmented backbone structures is to employ more than one polymerization. To date, there have been many developments in these dual polymerization approaches, but these developments have not been widely adopted as strategies to address the unique constraints and requirements of polymers used in biomedical applications. For this review, dual polymerizations include any approaches that use more than one unique polymerization, even if the polymer is isolated between polymerizations. We highlight useful synthetic strategies to facilitate the exploration of backbone-segmented BCPs in biomedical applications. Eventually, further developments in polymer synthesis will enable more feasible permutations of backbones and side chains,

Daniel C. Lee is a Ph.D. student at the Molecular Engineering and Sciences Institute at the University of Washington. He graduated from the Cornell University with a B.S. degree in Chemistry and Psychology and then worked in the energy industry for a few years. Daniel started his Ph.D. in 2016 and his research focuses on developing polymers for biomaterials and drug delivery applications.

Andrew J. Boydston conducted his doctoral research at the University of Texas at Austin and was co-advised by Prof. Christopher W. Bielawski and Prof. C. Grant Willson. After graduating, he took a NIH postdoctoral position at the California Institute of Technology with Prof. Robert H. Grubbs. In 2010, he started as an Assistant Professor of Chemistry at the University of Washington. In 2018, he moved to the University of Wisconsin as the Yamamoto Family Professor of Chemistry. His research group focuses on photoredox catalysis, polymer synthesis, mechanochemical transduction, and additive manufacturing (3D printing).

Suzie Hwang Pun is the Robert F. Rushmer Professor of Bioengineering at the University of Washington. Her group develops polymeric biomaterials for applications in drug, gene, and cell therapy. She received her Ph.D. in chemical engineering from the California Institute of Technology under the supervision of Prof. Mark E. Davis.

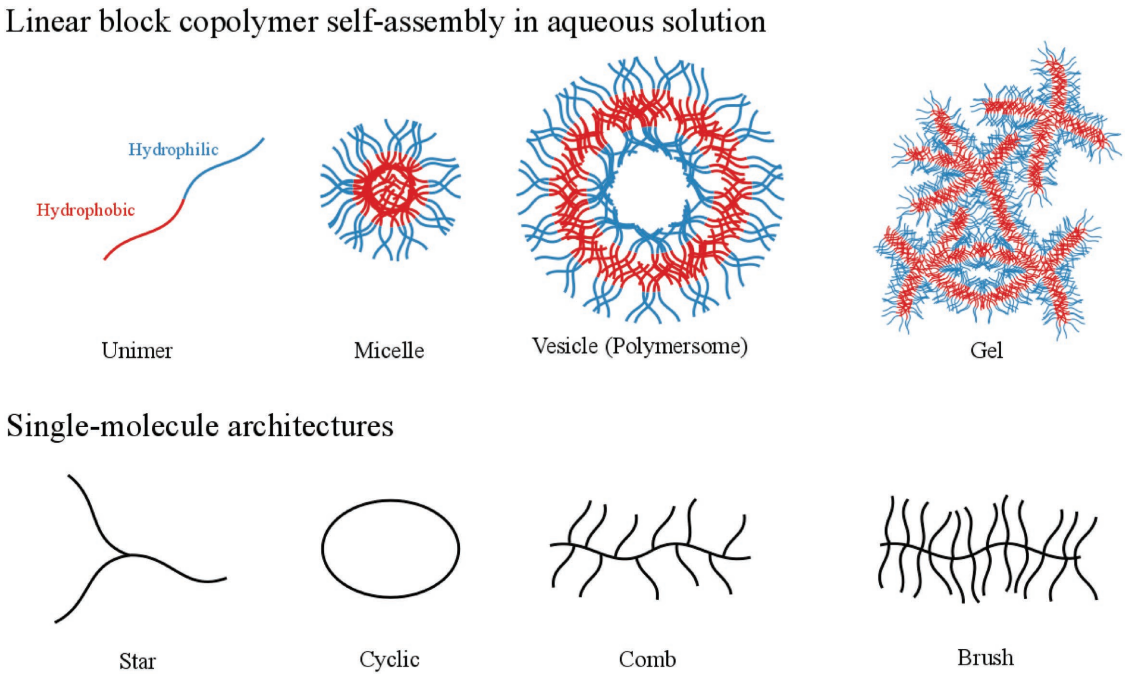

Figure 1. Diagrams of polymer structures often used for biological applications. Above, amphipathic polymers are capable of forming supramolecular structures including spherical micelles, vesicles, and gels. Below, single-molecule structures including stars with various numbers of arms, cyclic polymers, comb polymers, and brush polymers have been used with success for the delivery of therapeutics and diagnostics. More complex structures can be achieved, for example, comb polymers with cyclic backbones or micelles formed from star polymers, by combining multiple structures in the design of a biomaterial.

expanding the potential repertoire of highly engineerable materials for biomedical applications.

In this review, we focus on syntheses of backbone-segmented polymers by the use two or more polymerization systems. We start with a description of BCPs and their applications, followed by an overview of each polymerization method individually, and then a survey of different polymerizations that have been combined in the synthesis of unique BCPs. Although viable options for synthesizing BCPs, polymer–polymer couplings and conjugation with poly(ethylene glycol) exceed the scope of this review.

2. Controlled Polymerizations

A brief summary of the monomer scope and advantages of each polymerization is provided in **Figure 2**.

2.1. Atom Transfer Radical Polymerization (ATRP)

ATRP is a proven strategy for the precision synthesis of polymers for biomaterials.[44] ATRP is a RDRP technique pioneered by Wang and Matyjaszewski in 1995 that utilizes a transition metal complex to reduce the number of active chain ends in solution.[45] ATRP is well studied and developed for broad monomer scope and tunable kinetics,[46] and results in a non-biodegradable polymer backbone whose behavior can be dictated by the monomer side chains. Many functionalized methacrylates and acrylates compatible with ATRP are commercially available. Additionally, methacryloyl chloride and related compounds are also commercially available, allowing for in-house synthesis of custom monomers. For example, cyclodextrin-functionalized methacrylates have been made for ATRP.[47] Commercially available compounds such as α-bromoisobutyryl bromide allow for synthesis of custom initiators.

ATRP has three potential drawbacks for biomedical applications. One drawback is that ATRP has limited functional group tolerance. Vinyl monomers with charged side groups are difficult to polymerize by ATRP. ATRP can be successful in water, but must be carefully designed to control initiation and minimize catalyst degradation.[48,49] Another drawback is that the aliphatic polymer backbone is not biodegradable. One final drawback is that the residual levels of copper in polymers made by ATRP may be toxic at concentrations as low as 5 ppb.[50] To mitigate this last drawback, there have been many advances over the past 20 years minimizing the use of copper in ATRP including reverse ATRP, activators regenerated by electron transfer (AGET) ATRP, initiators for continuous activator regeneration (ICAR) ATRP, supplemental activators and reducing agents (SARA) ATRP, electrochemical ATRP (eATRP), photoinduced electron transfer ATRP, organocatalyzed ATRP, and sonication-induced ATRP.[44,51] Reverse ATRP and eATRP are mentioned later in this review. Unlike conventional ATRP, in which Cu(I) is introduced to initiate the polymerization, in reverse ATRP and eATRP, Cu(II) is reduced in situ to produce Cu(I). In reverse ATRP, a thermal radical initiator is used to reduce Cu(II) to Cu(I); in eATRP, electrodes can be used to reduce the copper, resulting in the active species.

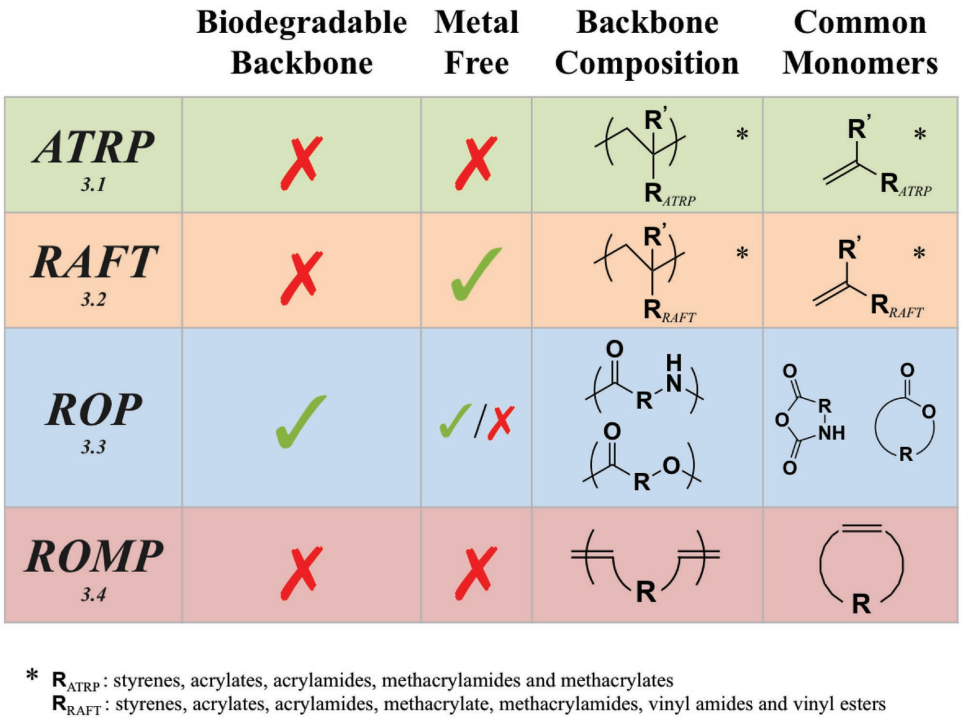

* R_{ATRP}: styrenes, acrylates, acrylamides, methacrylamides and methacrylates
R_{RAFT}: styrenes, acrylates, acrylamides, methacrylate, methacrylamides, vinyl amides and vinyl esters

Figure 2. Brief summary of the properties and composition of polymers synthesized by ATRP, RAFT, ROP, and ROMP.

2.2. Reversible Addition–Fragmentation Chain Transfer (RAFT)

RAFT is a robust polymerization strategy for a wide variety of vinyl monomers. RAFT maintains a low concentration of active chain end species by degenerative transfer onto a chain transfer agent (CTA).[52] Since its introduction by Chiefari et al. in 1998,[53] RAFT has been widely adopted for the synthesis of polymers for biomedical applications due to its wide functional group tolerance, tunable kinetics, and ease of use. Similar to ATRP, RAFT results in a non-biodegradable polymer backbone whose behavior can be dictated by the monomer side chains. RAFT can be used to polymerize methacrylates, acrylates, methacrylamides, acrylamides, vinyl esters, and vinyl amides.[54] Methacryloyl chloride and related compounds are commercially available starting materials for the synthesis of custom RAFT monomers. Additionally, many CTAs are commercially available. A variety of polymer structures can be obtained by RAFT polymerization[55] and RAFT polymers have been used in biomedical applications.[56]

Of the three drawbacks mentioned for ATRP, RAFT overcomes both the limited functional group tolerance and the use of a copper catalyst. Due to the broad functional group compatibility of RAFT, monomers with polar side chains can be polymerized in aqueous and organic solvents. RAFT has been used to polymerize monomers with pendant biomolecules.[57–59] RAFT polymerization has been performed on the surface of biologics, including living cells,[60] and has been shown to work in complex solvents like wine.[61] Additionally, RAFT polymerizations do not use a metal catalyst, eliminating the need for metal removal and further purification.

While the use of RAFT CTAs over ATRP has its advantages, it comes with its own limitations. RAFT CTAs are expensive to purchase and difficult to synthesize. Additionally, some CTAs are hydrolytically unstable.[62]

2.3. Ring Opening Polymerization (ROP)

ROP is a diverse class of polymerizations for cyclic electrophilic monomers such as *N*-carboxyanhydrides (NCAs), lactides, lactams, polycarbonates, and related compounds. Aside from water-sensitive condensation reactions, ROP is the most common way to synthesize polymers with biodegradable polyester or polyamide backbones. Biodegradability, and the subsequent potential for biocompatibility has led to the use of ROP-synthesized polymers in many biomedical applications.[63]

The synthetic approaches to ROP are more varied than the previously mentioned polymerizations. ROP can be catalyzed by acids, bases, organometallic complexes, and enzymes.[64–70] Because alcohol and amine groups are common nucleophiles used to initiate ROP, drugs with these heteroatoms can be used to initiate ROP. For example, regioselective activation of a hydroxyl group in paclitaxel can be used to initiate ROP of lactide.[71] Polylactones, polylactides, and poly-NCAs/polypeptides are common in biomedical applications due to their biocompatibility and biodegradability. Blocks of ROP polymers are commonly used to make up the core of self-assembled structures since high molecular weight polyesters are hydrophobic.

However, ROPs have limited functional group tolerance. Because ROPs require a nucleophile to open the ring of the electrophilic cyclic monomers, other heteroatoms like water or free alcohols can interfere with the polymerization, making polymerization difficult in some laboratory conditions. This sensitivity also makes functionalizing ROP monomers difficult;

it is more common to functionalize the side chains postpolymerization, however specific chemistries are required to affect efficient functionalization of ROP polymer side chains.[72]

2.4. ROMP

ROMP of strained cyclic monomers is a useful strategy for the synthesis of functionalized polymers. Many different transitional metal metathesis catalysts have been developed, each with its own advantages, but it was the commercial production of ruthenium-based metathesis catalysts that made ROMP feasible for bioapplications due to its functional group tolerance.[73,74] ROMP backbones are olefinic and often hydrophobic, but the olefins can be further reacted to make the polymers biodegradable; for example, the olefins in the ROMP backbone of poly(oxanobornene) were reacted to make alginic acid mimics.[40] ROMP has broad functional group tolerance and has been used to make polymers with peptides, imaging agents, and therapeutics.[75–79]

Due to use of Ru catalysts for ring closing metathesis in commercial pharmaceutical synthesis, there has been extensive work in modifying Grubbs' ruthenium-based catalysts for metatheses in aqueous and organic solvents.[80–82] Additionally, there are many commercially available ROMP monomers and catalysts. Custom ROMP monomers can also be synthesized by thermally cracking commercially available dicyclopentadiene, and reacting cyclopentadiene with functionalized alkenes, resulting in a functionalized norbornene molecule. Ru ROMP catalysts are often extremely active and can be used to polymerize macromonomers with both synthetic polymers and large bioactive molecules as side chains.[74,83]

There are two main disadvantages to ROMP. First is that Ru transition metal complexes are toxic, and thus the International Conference on Harmonization guidelines limit permissible ruthenium exposure.[84] While there has been recent advances in ruthenium purification, these strategies are energy intensive.[80–82] Another drawback is that commercially available catalysts for ROMP are expensive. This problem is compounded by the fact that unlike the ring closing metathesis commonly used by the pharmaceutical industry, in ROMP, the [Ru] species acts as the initiator and is thus attached to the polymer chain, preventing it from being easily recycled in a catalytic cycle.

3. Strategies for Dual Polymerizations

Developments in RDRPs and other living polymerizations have made sequence-controlled synthesis of BCPs easier by allowing one-pot techniques such as sequential monomer addition. Employing multiple polymerizations for the synthesis of segmented backbone polymers offers an additional level of control over polymer behavior and characteristics. For example, combining hydrophobic biodegradable poly(lactic acid) with hydrophilic non-biodegradable poly(HEMA) may confer new pharmacokinetic properties to the polymer. This section reviews works that use two or more different polymerizations in the synthesis of a single material and is organized by three main approaches: 1) the use of orthogonal polymerizations (often in a single pot); 2) postpolymerization functionalization with a new initiator motif; 3) postpolymerization functionalization with a new monomer motif.

Figure 3 has a schematic road map for using dual polymerizations to synthesize BCPs with different architectures.

3.1. Orthogonal Polymerizations in One Pot

One approach to the synthesis of BCPs is the use of two or more orthogonal polymerizations. A successful pairing of two orthogonal polymerizations for the synthesis of BCPs allows a one-pot polymerization and removes the need for intermediate deprotection or purification. However, orthogonal polymerization systems must be carefully selected as the reagents and conditions necessary for one polymerization may interfere

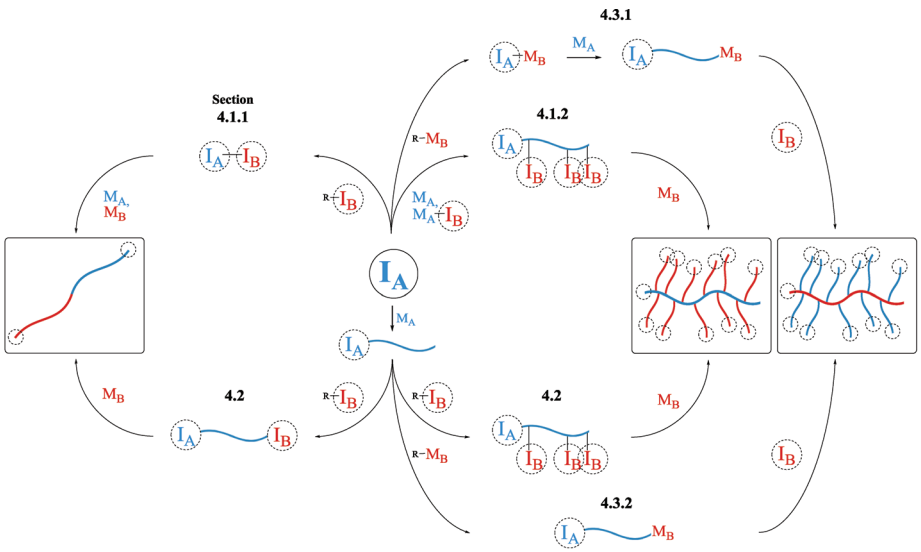

Figure 3. Schematic road map for using dual polymerizations to synthesize BCPs with different architectures.

with or initiate the second polymerization, resulting in loss of polymerization control. For example, small levels of acrylates can undergo chain transfer with the ROMP catalyst;[85] some CTA_{RAFT} are susceptible to aminolysis and may be incompatible with the use of strong bases or substituted amines, both of which are commonly used for ROP and the latter of which are used as ligands in ATRP.[62]

The use of orthogonal polymerizations can be further broken down into two approaches. The first approach involves the use of a single difunctional initiator I_A–I_B in which I_A only reacts in polymerization system A and I_B only reacts in polymerization system B. As there is a thorough review on this topic published in 2006, this section focuses on developments in this approach since 2006.[86]

The second approach involves the polymerization of an inimer M_A–I_B, a monomer that contains both the monomer motif for polymerization A (M_A) and an initiator motif for polymerization B (I_B); initiator I_B does not polymerize monomer M_A and only polymerizes monomer M_B in a subsequent polymerization.

3.1.1. The Use of a Single Difunctional Initiator I_A–I_B

ROP–RAFT Initiator–Chain Transfer Agent I_{ROP}–CTA_{RAFT} (Inifers): Combining ROP with radical polymerizations is useful for biomedical applications. ROP can be used to make biodegradable blocks, while the radical polymerization can be used to make stable blocks for prolonged circulation. Many difunctional ROP–RAFT inifers (I_{ROP}–CTA_{RAFT}) in which one end contains an alcohol or amine (I_{ROP}) and the other contains a trithiocarbonate, dithiobenzoate, or xanthogenate (CTA_{RAFT}) have been used to make block copolymers. These inifers have been used to copolymerize a variety of vinyl monomers with many cyclic ester monomers with dispersities lower than 1.1.[87–91] These polymerizations can be done in one pot, simultaneously or sequentially, suggesting that the polymerizations are orthogonal. The incorporation efficiency of RAFT monomer and ROP monomer into the final polymer can be adjusted by changing the monomer feed ratio or catalyst loading. Additionally, this strategy has been used to incorporate thiols in the RAFT chain and subsequently attach biologically relevant molecules for cell adhesion or metal chelators for imaging applications.[89]

Due to the relatively low reactivity of the alcohols and the mild conditions for RAFT, water and free alcohols do not significantly hydrolyze CTA_{RAFT} within the timeframe of the polymerization. In fact, some common RAFT monomers have pendant alcohol groups. Unlike alcohols, however, primary and secondary amines must be protected as they are reactive enough to aminolyze the CTA under common polymerization conditions, leading to early irreversible termination of the RAFT chain end and poor control over molecular weight distribution.[62] Zhang and co-workers used an inifer (I_{ROP}–CTA_{RAFT}) for amine-initiated ROP of *N*-carboxyanhydride and RAFT of NIPAM and found their polymerization resulted in block copolymers of lower dispersity if the ROP-initiating amine was protected during RAFT.[92]

ROP–ATRP Difunctional Initiators I_{ROP}–I_{ATRP}: Many difunctional ROP–ATRP initiators (I_{ROP}–I_{ATRP}) in which one end contains an alcohol or amine (I_{ROP}) and the other contains a substituted halide (I_{ATRP}) have been used to make block copolymers.[93–96] These polymerizations can be done simultaneously or sequentially in a single pot, making it an attractive option in the synthesis of block copolymers. This combination is robust and synthetically accessible as α-bromoisobutyryl bromide and related compounds are commercially available and can be reacted with multivalent alcohols to synthesize I_{ROP}–I_{ATRP}. Because these conjugation reactions can be carried out under mild conditions, stimuli-responsive linkages can also be incorporated. For example, I_{ROP}–I_{ATRP} connected by a disulfide linkage was synthesized by coupling chemistry and used to grow p(lactic acid)-*block*-p(oligo(ethylene glycol) methacrylate) (p(LA)-*b*-p(OEGMA) (**Figure 4**).[97] The amphiphilic polymers were used to make micelles which were found to be nontoxic to HeLa cervical cancer cells and, upon introduction of dithiothreitol, cleave at the disulfide linkage that covalently bound the hydrophobic and hydrophilic blocks, resulting in disassembly of the micelle.

One interesting application of I_{ROP}–I_{ATRP} is the incorporation of a radical generator in the middle of a difunctional initiator. Chang and co-workers showed simultaneous ROP and reverse ATRP by the use of an I_{ROP}–azo-I_{ROP} initiator in which the azo bond disassociates upon heating and produces two active radical chains.[98] The addition of Cu(II) allowed the control of the radical chain end via reverse ATRP and resulted in polymers with lower dispersity when compared to the polymerization done without Cu(II). When the reaction is heated to 90 °C, only the reverse ATRP polymerization proceeds. But heating the polymerization to >110 °C in the presence of the $Sn(oct)_2$ resulted in simultaneous ROP and reverse ATRP.

As mentioned in the ROP–RAFT section, there are potential concerns of reagents in one polymerization negatively affecting the second polymerization. However, it is also possible to use a single nonmonomer reagent for both the polymerizations. We found this to be common for the ROP–ATRP combination. For example, a tin species can be used both as a catalyst for ROP and a reductant for copper in reverse ATRP;[99] a substituted amine can be used both as a catalyst for ROP and a ligand for copper in ATRP.[100,101] The use of shared substituted amines between ROP and ATRP has also been demonstrated when the ROP was mediated by lipase Novozym 435.[102] *N*,*N*,*N*′,*N*″,*N*″-pentamethyldiethylenetriamine (PMDETA) and 4,4′-dinonyl-2,2′-dipyridyl (dNbpy), common copper ligands in ATRP, can also be used to coordinate metal ions in solution which would otherwise coordinate to the histidine in the lipase active site and prevent the enzyme-catalyzed ROP.

In a particularly interesting use of enzyme-mediated ROP, Meijer and co-workers used Novozym 435 to make an enantiomerically rich p((S)-4-methyl-caprolactone).[103] (S)-caprolactone was found to be more active toward polymerization by Novoyzm 435; to prevent the (R) enantiomer from polymerizing at low concentrations of (S)-caprolactone, a Ni species was intentionally introduced into the polymerization to deactivate the lipase to prevent polymerization of the less active enantiomer once most of the (S)-caprolactone was polymerized. The Ni species also acted as a reductant for subsequent ATRP.

ATRP–RAFT Inifers I_{ATRP}–CTA_{RAFT}: Difunctional ATRP–RAFT inifers have been synthesized and used to perform

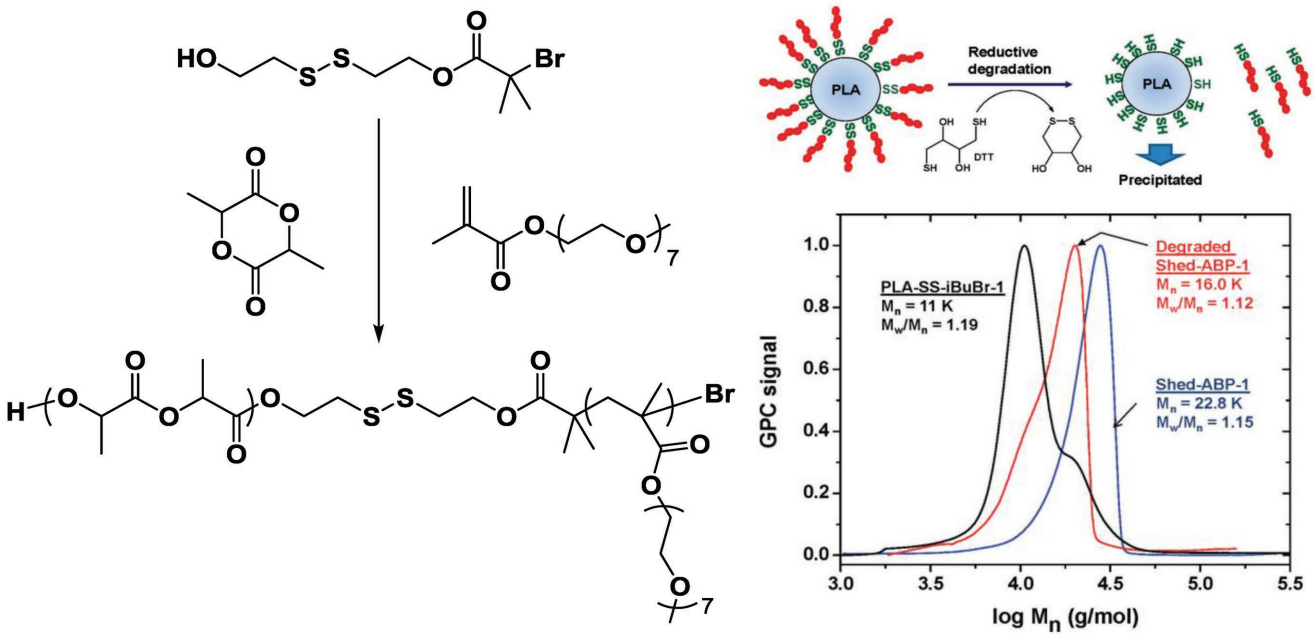

Figure 4. ROP/RAFT from a single difunctional initiator. The polymer has been used to make stimuli-responsive micelles. Reproduced with permission.[97] Copyright 2011, American Chemical Society.

simultaneous and sequential ATRP and RAFT. These difunctional inifers have been made with a stimuli-responsive linker which upon application of the specified stimulus can result in cleavage of the diblock copolymer. Thiol/redox sensitive difunctional inifers connected by a disulfide linkage have been used to make polymeric micelles with sheddable coronas; these polymers have been used for more efficient gene transfection of neurons when decorated with the Tet1 peptide.[42] Acid-cleavable diblock copolymers have also been made with the potential for application in nanofabrication and stimuli-responsive micelles.[43]

Because ATRP and RAFT both require the generation of a radical active chain end which is often mediated by a third species, there is significant potential for overlap; the use of a single organic photocatalyst for photoinduced electron transfer RAFT (PET–RAFT) and organocatalyzed ATRP (O-ATRP) has recently been published.[104,105] The RAFT/ATRP combination has even been used to polymerize the same monomer.[104] Despite their similarities, however, difunctional I_{ATRP}–CTA_{RAFT} inifers can be used to polymerize different monomers on their respective chain ends. For example, pairs such as acrylate/styrene and methacrylate/acrylate have been used to make BCPs with ATRP and RAFT.[42,43,104–107]

ROMP–ATRP I_{ROMP}–I_{ATRP}: The main consideration when employing ROMP–ATRP is the difference in polymerization kinetics between the two approaches. Because ROMP is generally much faster than any other living polymerization, ROMP must be slowed down in dual polymerizations by the addition of bulky monomers or low ring strain monomers. An active ROMP chain end with no ROMP monomer available can result in chain transfer which results in sequence scrambling and high dispersities. If this condition is met, it is possible to do dual ROMP–ATRP. In one example, a modified Grubbs catalyst (I_{ROMP}–I_{ATRP}) was used to synthesize poly(butadiene)-*block*-poly(methyl methacrylate).[108]

3.1.2. Polymerizing an Initiator Monomer M_A–I_B (Inimer)

In this section, we review the use of an inimer (M_A–I_B) in which a single molecule has a monomer motif polymerizable in polymerization A (M_A) and an orthogonal initiator motif that does not react in the first polymerization (I_B). These pendant initiators (I_B) can be used to initiate subsequent polymerizations. This approach often results in a polymer with many initiating side chains, making it an attractive method to synthesize polymers with unique architectures. In all the examples described, while the first polymerization used for inimer M_A varied, the pendant initiator (I_B) was almost always I_{ATRP}.[14,109–114] This may be because I_{ATRP}-functionalized monomers are easy to synthesize for the reasons described previously. To our knowledge, there are no examples of a monomer containing a pendant CTA_{RAFT} for subsequent RAFT, perhaps due to the relative cost and synthetic complexity of CTA_{RAFT} compared to I_{ATRP}.

The inimer approach has been used to make dendritic nanoparticles. Guan and co-workers synthesized a hydrophobic core which was first synthesized by chain walking polymerization of ethene and a vinyl-functionalized ATRP initiator.[110] ATRP was then used to grow a hydrophilic block with OEGMA which was terminated with a *N*-hydroxysuccinimide (NHS) ester–functionalized acrylate. The terminal NHS was used to conjugate fluorescein and ovalbumin to demonstrate bioconjugation and the potential for this system in biomedical applications such as protein delivery and imaging.

Bottlebrush polymers with high grafting densities can also be synthesized by the inimer approach. In one example, RAFT was used to copolymerize a styrene and a maleimide-containing monomer, the latter of which was functionalized with both I_{ROP} and I_{ATRP} for their respective polymerizations.[14] In a different approach, a norbornene monomer functionalized with an I_{ROP} and an I_{ATRP} were polymerized by ROMP and

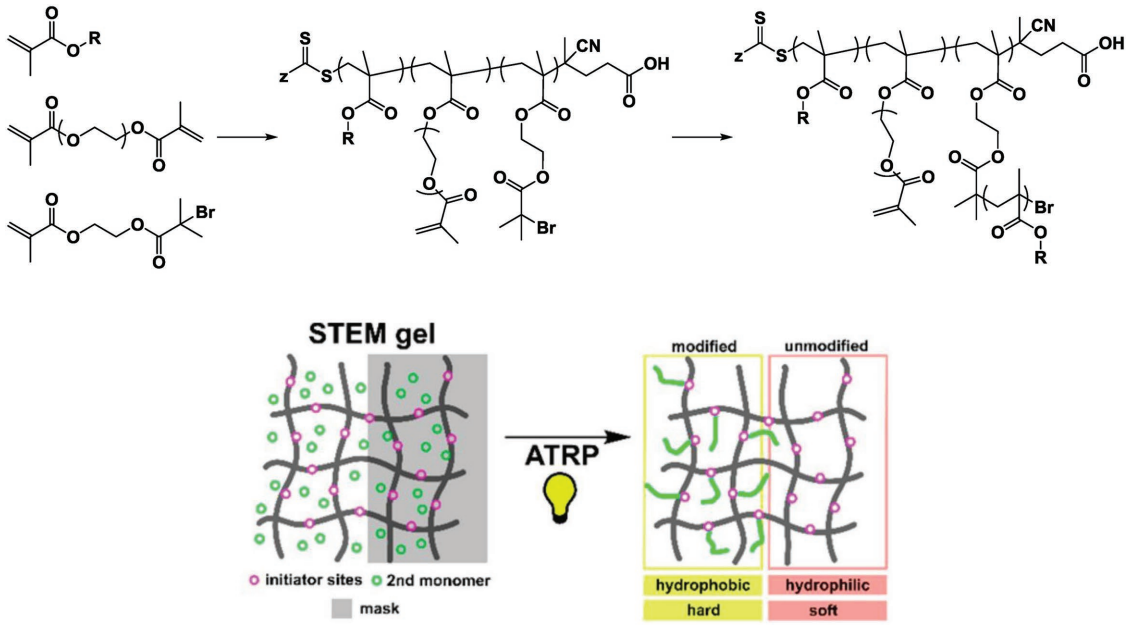

Figure 5. RAFT/ATRP combination by polymerizing an inimer. This approach has been used to reinforce gels with a second polymerization. Reproduced with permission.[112] Copyright 2018, American Chemical Society.

then ROP and ATRP were subsequently initiated off the side chains.[109] The order of polymerization using this inimer can also be switched.[111]

The inimer approach has also been used to make structurally tailored and engineered macromolecular gels whose material properties can be modified by the application of a site-specific stimulus.[112] Matyjaszewski and co-workers copolymerized an acrylate, a diacrylate, and an acrylate inimer M_{RAFT}–I_{ATRP} by RAFT, resulting in an initial gel. The gel was then dried and subsequently soaked in a dimethylformamide solution of copper and ATRP monomer. The gel was then irradiated to initiate ATRP from the pendant I_{ATRP}. A wide variety of monomers were used and yielded segmented materials with hard and soft regions with different hydrophobic character, depending on which sections were irradiated for ATRP (**Figure 5**).

In another example, three different controlled radical polymerization mechanisms were combined by the inimer approach. A (2,2,6,6-tetramethylpiperidin-1-yl)oxyl (TEMPO)functionalized acrylate and an I_{ATRP}-functionalized acrylate were polymerized by RAFT. The pendant initiators were then subsequently initiated, forming bottlebrush structures.[113]

3.2. Postpolymerization Modification with I_B

Polymers can be further modified postpolymerization by conjugating a new initiator (I_B) to the polymer chain end or on monomer side chains. If a new initiator were conjugated onto the chain end, a block copolymer could be synthesized; if a new initiator were conjugated onto a monomer side chain, a comb or bottlebrush polymer could be synthesized. In this section, we review works that use postpolymerization functionalization of a polymer with a new initiator motif or use secondary reactions to activate a latent initiator into an active one.

3.2.1. Postpolymerization Functionalization/Activation with New I_B

Postpolymerization Functionalization with I_{ATRP}: Pendant alcohols on monomer side chains or chain ends can be easily functionalized to form an I_{ATRP}.[8,115–120] Commercially available α-bromoisobutyryl bromide can be reacted with the pendant alcohols of a polymer at room temperature for a few hours with excess triethylamine with good conversion. One limitation of postpolymerization functionalization by this method is that a hydrophilic polymer may not be soluble in suitable organic solvents like tetrahydrofuran or dichloromethane. In this case, an inimer as discussed in the previous section is a suitable alternative.

Pendant I_{ATRP} has been used to make block copolymers and bottlebrush polymers with low dispersities. In one example,[119] beta-cyclodextrin alcohols were used to initiate ROP of caprolactone. The hydrophobic polycaprolactone block was capped with an ATRP initiator to polymerize a second, amine containing cationic block (**Figure 6**). These cationic cyclodextrin-based star polymers could deliver nucleic acids to R264.7 cells, a macrophage cell line, with similar efficiencies as commercial agent Lipofectamine with comparable or decreased toxicity. A similar strategy of conjugating I_{ATRP} to chain ends was used to develop triblock materials which form gels at physiological temperature for potential injectable administration.[120]

Another approach is to functionalize a ROMP polymer chain end with an I_{ATRP} by terminating ROMP with a symmetric *cis*-alkene with an I_{ATRP}.[121] Additionally, an asymmetric vinyl ether functionalized with an I_{ATRP} can be used to cap the polymer; however, it was found that this is not as efficient because there is a probability that the chain end is functionalized with the vinyl ether group as opposed to the I_{ATRP}.

Postpolymerization Functionalization with a CTA_{RAFT}: The RDRP of a monomer that also contains a pendant CTA_{RAFT}

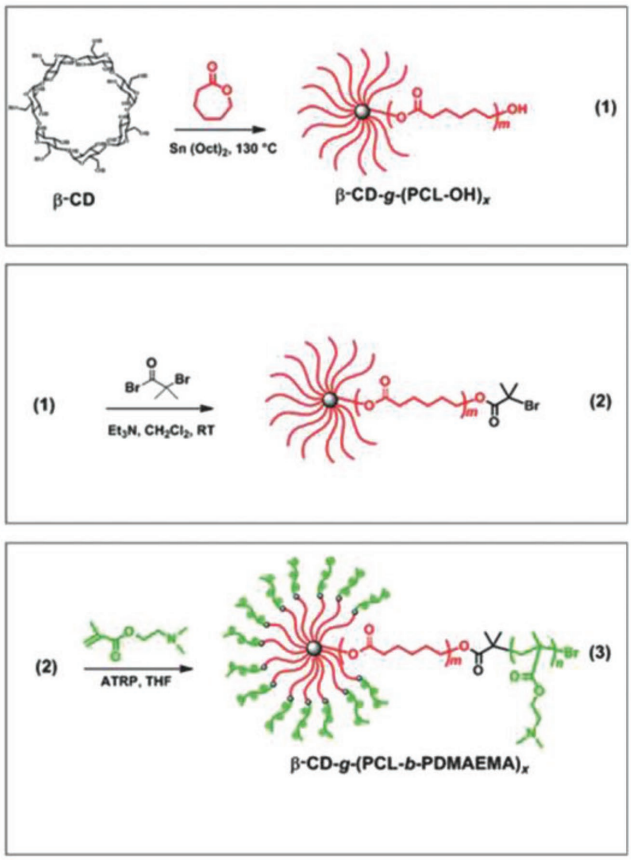

Figure 6. ROP/ATRP by end capping a polymer with a new initiator. This approach has been used to make carriers for gene delivery. Adapted with permission.[119] Copyright 2018, Wiley-VCH.

risks generating a hyperbranched structure and thus is difficult to use in the synthesis of block copolymers. However, it is possible to functionalize the polymer side chains and chain ends with CTA_{RAFT} after the initial polymerization. In one example, Bolton and Rzayev use RAFT to copolymerize a methacrylate with a pendant I_{ATRP} and a methacrylate with a protected alcohol.[114] After I_{ATRP} was used to grow some side chain polymers, the protected alcohol was deprotected postpolymerization and used to conjugate on CTA_{RAFT} for subsequent RAFT.

Postpolymerization Functionalization/Activation with/of I_{ROP}: One common approach to the synthesis of polypeptides is the ROP of NCA initiated by a primary amine. There is a more detailed review specifically on the synthesis of biohybrid block copolymers,[122] but this section highlights the use of dual polymerization for the synthesis of peptide–polymer copolymers. Due to the high heteroatom content of NCAs which may be incompatible with other polymerization methods, it is common to use other polymerizations first, followed by terminal functionalization with an amine for subsequent ROP of NCA monomers. This strategy was utilized in the development of nontoxic pH-responsive micelles which release prednisone more quickly at low pH.[123]

There are many ways to functionalize different polymer chain ends with amines.[123,124] Specifically for polymers synthesized by ATRP, the halide on the polymer chain end can be a useful reactive site for the introduction of amines. One approach is to replace the halogen chain end of ATRP with an amine and use that to directly initiate ROP of NCA. The use of a multivalent amine allows for the synthesis of miktoarm star polymers.[125,126] Brzezinska and Deming further reacted their amine terminated polymer to incorporate a nickelacycle end group which was then used to initiate a ROP of NCA.[127]

A difunctional initiator that contains a protected amine may also be used. After the first polymerization, the amine is deprotected and used to initiate ROP of NCA. As discussed above, an unprotected amine can result in higher polymer dispersities due to RAFT CTA aminolysis,[92,128] or act as a ligand for Cu and will interfere with ATRP.

Postpolymerization Functionalization/Activation with/of I_{ROMP}: While it is more common to perform ROMP before other polymerizations, it is also possible to conjugate on an I_{ROMP} for subsequent ROMP via cross metathesis.[129] Metal-free ROMP (MF-ROMP), an organic photoinduced method for ROMP, has also been shown to be amenable to subsequent polymerization. Because MF-ROMP can be initiated by vinyl ethers, latent vinyl ethers such as allyl ethers can be easily isomerized postpolymerization to yield the new active initiator. In one example, styrene was copolymerized with allyl ether-functionalized styrene by ATRP.[130] After polymerization, the halide chain end was removed and the allyl ether was isomerized to the active vinyl ether form and used to initiate MF-ROMP.

3.2.2. In Situ Modification of Latent I_B

In Situ Modification of a Polymerization to Prevent Chain Transfer: ROMP and ROP result in the ring open form of the monomers which have similar reactivities to their starting monomers and thus chain transfer can be a common problem. Chain transfer results in scrambling of the polymer sequence and makes synthesis of block copolymers difficult. For ROMP, unfunctionalized norbornene is never used in the synthesis of block copolymers due to high rates of chain transfer. Living polymerizations with ROMP typically use norbornenes with pendant maleimides or other groups that have been shown to be too bulky or electron deficient for chain transfer.

With regards to ROP, polymerizations of cyclic monomers exist in some ring-chain equilibrium, high thermodynamic drive for the linear ring open form is necessary to prevent intramolecular chain transfer or macrocyclization. One approach to polymerize low ring strain macrolactones is to use extremely strong bases to compensate for the lack of enthalpic drive to open the ring. However, this poses a problem for the synthesis of block copolymers as strong bases also catalyze intra- and intermolecular chain transfer via transesterification, scrambling the polymer sequence. One strategy that has eliminated transesterification-induced sequence scrambling when copolymerizing low and high ring strain lactones is to first polymerize low ring strain macrolactones with a strong base, quench the active chain, and subsequently reinitiate the polymerization of a higher ring strain monomer with a weaker base.[131] The weaker base could be used to polymerize higher ring strain lactones but did not induce transesterification and the block copolymer sequence was preserved.

In Situ Modification of a Polymerization to React New Monomers: Some polymerization systems such as RAFT have monomers of such disparate reactivities that a single chain end cannot be used to polymerize both the monomers. For example, the same CTA_{RAFT} cannot be used to polymerize electron deficient vinyl acetates with more electron rich methacrylates. Although these differences in monomer reactivity may limit the ability to synthesize statistical copolymers, they can be exploited to synthesize block copolymers. Thang and co-workers developed a switchable CTA_{RAFT} that can polymerize either methacrylates or vinyl acetates depending on its charge. A protonated pyridinyl dithiocarbamate, which polymerizes electron rich methacrylates, can then be deprotonated by dimethylaminopyridine (DMAP) to polymerize electron deficient vinyl acetates. While control of these polymerizations varied, some copolymerizations achieved dispersities as low as 1.1 in a single pot.[132]

In situ modification of ROPs has been used to make well-defined block copolymers. In situ modification of a ROP iron catalyst allows for orthogonal ROP of epoxides and lactides. By switching the oxidation state of the Lewis acid catalyst either chemically[133] or electrochemically,[134] poly(cyclohexane oxide)-*block*-polylactide was synthesized in a single pot. In situ modification of a ROP chain end can be used to synthesize block copolymers of different cyclic ester monomers. The different reactivities of carbonates, lactones, and lactides in ROP prevent the use of a single active chain end for copolymerization. Guo and co-workers developed a combination of different acids and bases to controllably switch the chain end and monomer reactivities to catalyze the ROP of different cyclic ester monomers.[135] In one system, Guo and co-workers combined the use of their pH-switchable ROP and the work by Thang and co-workers with pH-switchable RAFT CTAs.[136] With this system, these one-pot polymerizations can be taken to nearly quantitative conversion in the synthesis of tetrablock copolymers with well-defined blocks of low dispersities.

The Use of Light-Controlled Orthogonal Polymerizations: Light-controlled polymerizations allow activation and deactivation of a polymerization with temporal and spatial control. Often, these systems pair an initiating motif with an appropriate photocatalyst which generates an acid or radical to initiate the polymerization upon excitation by light.[137] Because of the many permutations of unique photocatalyst/initiator pairs, the use of different wavelengths to initiate different polymerizations can be a powerful technique in dual orthogonal polymerizations. However, despite this potential, there have been few examples of this to date, perhaps due to limitations such as functional group incompatibility, limited mutual solubility, or poor control over molecular weight.

One approach is the use of a single switchable catalyst that behaves differentially in response to different wavelengths of light. The use of a one-pot sequential polymerization of two monomers has also been explored with cationic-RAFT polymerization.[138,139] In one particularly interesting example, Fors and co-workers were able to use different wavelengths of light to switch between pyrylium-catalyzed cationic polymerization of vinyl ether or $Ir(ppy)_3$-catalyzed polymerization of methyl acrylate in a single pot.[140] In another example, 550–750 nm light was used for the polymerization of methyl methacrylate and 350–380 nm light was used for photoacid generation for ROP.[141]

3.3. Postpolymerization Modification with a New Monomer Motif M_B

This approach polymerizes a macromonomer, a polymer functionalized with a monomer motif M_B that only reacts in a subsequent polymerization (P_A–M_B). This "graft-through" approach results in a bottlebrush polymer. There are two general strategies to synthesize a macromonomer. One approach is to polymerize M_A from an inimer I_A–M_B, resulting in P_A–M_B. Another strategy is to conjugate M_B onto the polymer chain end or a monomer side chain postpolymerization.

Because of the high enthalpic drive toward norbornene polymerization and the high activity and functional group tolerance of the Grubbs metathesis catalysts, "graft-through" ROMP is a powerful strategy in the synthesis of bottlebrush polymers. Grubbs' catalyst has been shown to graft-through macromonomers as large as 8.7 kDa; smaller macromonomers with molecular weights of 2.2 kDa can be polymerized with degrees of polymerization (DPs) reaching upward of 4000.[142,143] ROMP has been used to polymerize branched macromonomers with two pendants polymers, forming bottlebrush polymers.[144,145] ATRP of methacrylate-capped poly(ethylene oxide) macromonomers has also been shown to result in polymers with DPs as high as 400.[146]

3.3.1. Macromonomer Synthesis Starting from I_A–M_B

Macromonomer synthesis from an inimer starts similarly to the examples in Section 3.1.2. However, instead of first polymerizing the monomer and then growing a second polymer off the pendant initiator, the order is reversed. In this approach, a polymer is first grown off the initiator I_A and then a second polymerization is used to "graft through" the pendant monomer (M_B).

There are many papers that use a CTA_{RAFT}–M_{ROMP} to make bottlebrush polymers, some of which are done in a single pot.[85,145,147–150] In these papers, RAFT is first used to make linear macromonomers (P_{RAFT}–M_{ROMP}). The norbornene moiety (M_B) is then used to "graft through" with ROMP (**Figure 7**). However, one limitation with a one-pot approach to RAFT–ROMP polymerization is that it is important to purify away residual acrylates, as the cross metathesis of the active ROMP chain end with the acrylate results in early irreversible termination.[85] These findings have been corroborated and in fact used to functionalize ROMP polymer chain ends with acrylates.[121,151] Modified Grubbs metathesis catalysts have also been used in cyclopolymerizations of 1,6-heptadiene macromonomers with polycaprolactone tails.[152]

In a similar approach, alcohol-functionalized norbornene (I_{ROP}–M_{ROMP}) was first used for ROP of lactides and the resulting macromonomer was "grafted through" with ROMP.[153]

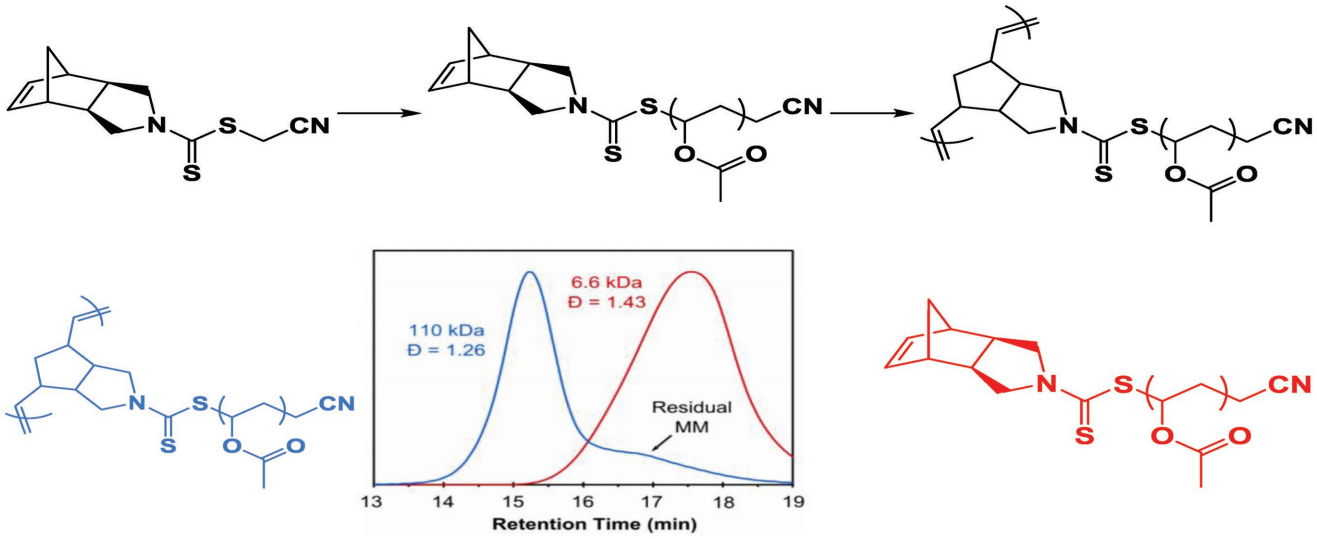

Figure 7. RAFT/ROMP by polymerizing a macromonomer. Reproduced with permission.[147] Copyright 2015, Elsevier Ltd.

3.3.2. Macromonomer Synthesis by Postpolymerization Functionalization of Polymer

Instead of starting with an inimer (I_A–M_B), the monomer motif can be functionalized onto the polymer postpolymerization. In one example, azide–alkyne click chemistry was used to conjugate M_{ROMP} onto a polymer and then ROMP was used to "graft through" to create bottle brush polymers with dispersities of <1.1.[144,153] Other high efficiency reactions, such as NHS ester transesterification, have been used to conjugate M_{ROMP} onto a polymer chain end.[154] This strategy was used in the development of a delivery system for doxorubicin, a small molecule chemotherapeutic.

For an example with a condensation polymerization, Alizadeh et al. exploited the same mechanism of their polymerization to cap their polymer with a reactive end group. Poly(*p*-benzamides) were synthesized by polycondensation. The phenols of the phenyl esters are good leaving groups and the aromatic amines can substitute them even at temperatures as low as −70 °C. While this paper shows chain end functionalization with I_{ROP} alcohol, I_{ROP} amine, an ATRP initiator, and even a click chemistry–compatible alkyne, we wanted to highlight the chain end functionalization with norbornene for subsequent ROMP.[155]

4. Conclusion

Major advances in polymer chemistry in the last quarter century have changed the way we conceptualize and synthesize materials. Specifically, advances in RDRP and other controlled polymerizations with "living" characteristics have unlocked many advances in biology and medicine: BCPs of novel architectures or BCPs assembled into supramolecular structures can be used for targeted delivery of therapeutics and imaging agents, and for the development of new biomaterials. We surveyed different strategies employed to synthesized BCPs via dual polymerizations, categorized into i) use of orthogonal polymerizations (often in a single pot), ii) postpolymerization functionalization with a new monomer motif. With this review, we hope to highlight useful synthetic strategies for the synthesis of BCPs with segmented backbones to facilitate their use in biomedical applications. As the field of polymer science and engineering grows, we expect even more creative ways to synthesize highly engineered BCPs with any permutations of backbones and side chains for biomedical applications.

There are many considerations for deciding which polymerization to use in the synthesis of a particular block. To briefly summarize a few important points: ROP can be used to synthesize polymers with biodegradable backbones but these polymerizations are sensitive to nucleophilic heteroatoms; ROMP has broad functional group tolerance and can introduce unique reactivity into the backbone but fewer ROMP monomers are commercially compared to those of other polymerization systems. Both ATRP and RAFT produce polymers with nondegradable backbones but there are advantages unique to each. ATRP initiators are more stable toward aminolysis than CTA_{RAFT} and are easier to functionalize onto a chain end but RAFT does not require removal of the metal species used in ATRP

Combining multiple polymerization systems further expands the repertoire of potential materials by increasing diversity in the available polymer backbones but the drawbacks of each polymerization determine the optimal sequence of these polymerizations. For example, because free amines can aminolyze CTA_{RAFT}, the RAFT block is usually synthesized before amine-initiated ROP.[62] Because ROMP can react with residual acrylates, ATRP/RAFT blocks are usually done after ROMP.[85] We have included some experimental considerations for dual polymerization in their respective sections. As each polymerization system is investigated and improved, more limitations will be addressed, allowing more of them to be performed in a single pot.

Of the emerging polymerization techniques, we suspect that the use of light-controlled polymerizations holds many unexplored synergies with existing strategies for dual

polymerizations. Because these light-controlled polymerizations can be spatially and temporally controlled, they confer new degrees of tunability in polymer synthesis with the potential to expand the complex structures available for use. New materials with varied monomer characteristics, varied backbone characteristics via multiple polymerization techniques, and varied structural characteristics via temporal and spatial control of polymerizations will enable polymers to meet the expanding material needs in medicine.

Acknowledgements

The work was supported by the NIH Grant Nos. 2R01NS064404, 1R01CA177272, and 1R01HL139007 and the DOD Grant Nos. PR151175 and SC130249. R.J.L. and A.N.P. were both supported by the NSF Graduate Fellowships, Grant Nos. 2013163249 and 2016226159, respectively.

Conflict of Interest

The authors declare no conflict of interest.

Keywords

biomaterials, block copolymers, dual polymerizations, orthogonal polymerizations, tandem polymerizations

Received: July 22, 2018
Revised: September 5, 2018
Published online: October 21, 2018

[1] A. Varela-Moreira, Y. Shi, M. H. A. M. Fens, T. Lammers, W. E. Hennink, R. M. Schiffelers, *Mater. Chem. Front.* **2017**, *1*, 1485.
[2] R. Voelker, *JAMA, J. Am. Med. Assoc.* **2018**, *319*, 220.
[3] F. S. Bates, G. H. Fredrickson, *Annu. Rev. Phys. Chem.* **1990**, *41*, 525.
[4] M. Trollsås, J. L. Hedrick, *J. Am. Chem. Soc.* **1998**, *120*, 4644.
[5] C. E. Wang, P. S. Stayton, S. H. Pun, A. J. Convertine, *J. Controlled Release* **2015**, *219*, 345.
[6] L. Y. Qiu, Y. H. Bae, *Pharm. Res.* **2006**, *23*, 1.
[7] N. Nasongkla, B. Chen, N. Macaraeg, M. E. Fox, J. M. J. Fréchet, F. C. Szoka, *J. Am. Chem. Soc.* **2009**, *131*, 3842.
[8] H. Wei, C. E. Wang, N. Tan, A. J. Boydston, S. H. Pun, *ACS Macro Lett.* **2015**, *4*, 938.
[9] P. Kesharwani, A. K. Iyer, *Drug Discovery Today* **2015**, *20*, 536.
[10] T. Zhao, Y. Zheng, J. Poly, W. Wang, *Nat. Commun.* **2013**, *4*, 1873.
[11] F. Wang, T. K. Bronich, A. V. Kabanov, R. D. Rauh, J. Roovers, *Bioconjugate Chem.* **2005**, *16*, 397.
[12] X. Jin, P. Sun, G. Tong, X. Zhu, *Biomaterials* **2018**, *178*, 738.
[13] J. Zou, Y. Yu, Y. Li, W. Ji, C.-K. Chen, W.-C. Law, P. N. Prasad, C. Cheng, *Biomater. Sci.* **2015**, *3*, 1078.
[14] W. Wu, W. Dai, X. Zhao, J. Zhang, Y. Zhao, *Polym. Chem.* **2018**, *9*, 1947.
[15] J. M. Benns, J. S. Choi, R. I. Mahato, J. S. Park, Sung Wan Kim, *Bioconjugate Chem.* **2000**, *11*, 637.
[16] D. S. H. Chu, J. G. Schellinger, J. Shi, A. J. Convertine, P. S. Stayton, S. H. Pun, *Acc. Chem. Res.* **2012**, *45*, 1089.
[17] C. E. Wang, H. Wei, N. Tan, A. J. Boydston, S. H. Pun, *Biomacromolecules* **2016**, *17*, 69.
[18] Y. Cheng, H. Wei, J. K. Y. Tan, D. J. Peeler, D. O. Maris, D. L. Sellers, P. J. Horner, S. H. Pun, *Small* **2016**, *12*, 2750.
[19] H. Wei, X. Zhang, C. Cheng, S. X. Cheng, R. X. Zhuo, *Biomaterials* **2007**, *28*, 99.
[20] M. R. Nabid, S. J. Tabatabaei Rezaei, R. Sedghi, H. Niknejad, A. A. Entezami, H. A. Oskooie, M. M. Heravi, *Polymer* **2011**, *52*, 2799.
[21] K. Kataoka, A. Harada, Y. Nagasaki, *Adv. Drug Delivery Rev.* **2001**, *47*, 113.
[22] M. Harada, I. Bobe, H. Saito, N. Shibata, R. Tanaka, T. Hayashi, Y. Kato, *Cancer Sci.* **2011**, *102*, 192.
[23] C. J. Rijcken, C. J. Snel, R. M. Schiffelers, C. F. van Nostrum, W. E. Hennink, *Biomaterials* **2007**, *28*, 5581.
[24] V. S. Trubetskoy, *Adv. Drug Delivery Rev.* **1999**, *37*, 81.
[25] J. Park, G. Von Maltzahn, E. Ruoslahti, S. N. Bhatia, M. J. Sailor, *Angew. Chem.* **2008**, *120*, 7394.
[26] B. M. Discher, Y. Won, D. S. Ege, J. C. Lee, F. S. Bates, D. E. Discher, D. A. Hammer, *Adv. Sci.* **2012**, *284*, 1143.
[27] J. Leong, J. Y. Teo, V. K. Aakalu, Y. Y. Yang, H. Kong, *Adv. Healthcare Mater.* **2018**, *7*, 1701276.
[28] F. Ahmed, R. I. Pakunlu, A. Brannan, F. Bates, T. Minko, D. E. Discher, *J. Controlled Release* **2006**, *116*, 150.
[29] H. Lomas, I. Canton, S. MacNeil, J. Du, S. P. Armes, A. J. Ryan, A. L. Lewis, G. Battaglia, *Adv. Mater.* **2007**, *19*, 4238.
[30] Y. Wang, L. Wang, B. Li, Y. Cheng, D. Zhou, X. Chen, X. Jing, Y. Huang, *ACS Macro Lett.* **2017**, *6*, 1186.
[31] N. Maurer, D. B. Fenske, P. R. Cullis, *Expert Opin. Biol. Ther.* **2001**, *1*, 923.
[32] D. E. Discher, F. Ahmed, *Annu. Rev. Biomed. Eng.* **2006**, *8*, 323.
[33] K. M. Park, D. W. Lee, B. Sarkar, H. Jung, J. Kim, Y. H. Ko, K. E. Lee, H. Jeon, K. Kim, *Small* **2010**, *6*, 1430.
[34] F. Meng, Z. Zhong, J. Feijen, *Biomacromolecules* **2009**, *10*, 197.
[35] R. Cheng, F. Feng, F. Meng, C. Deng, J. Feijen, Z. Zhong, *J. Controlled Release* **2011**, *152*, 2.
[36] R. Cheng, F. Meng, C. Deng, H. A. Klok, Z. Zhong, *Biomaterials* **2013**, *34*, 3647.
[37] W. S. Shim, J. S. Yoo, Y. H. Bae, D. S. Lee, *Biomacromolecules* **2005**, *6*, 2930.
[38] B. Jeong, Y. H. Bae, D. S. Lee, S. W. Kim, *Nature* **1997**, *388*, 860.
[39] A. Bose, S. Jana, A. Saha, T. K. Mandal, *Polymer* **2017**, *110*, 12.
[40] M. Wathier, S. S. Stoddart, M. J. Sheehy, M. W. Grinstaff, *J. Am. Chem. Soc.* **2010**, *132*, 15887.
[41] J. M. Sarapas, C. M. Backlund, B. M. deRonde, L. M. Minter, G. N. Tew, *Chem. - Eur. J.* **2017**, *23*, 6858.
[42] H. Wei, J. G. Schellinger, D. S. H. Chu, S. H. Pun, *J. Am. Chem. Soc.* **2012**, *134*, 16554.
[43] X. Sui, Z. Zhang, S. Guan, Y. Xu, C. Li, Y. Lv, A. Chen, L. Yang, L. Gao, *Polym. Chem.* **2015**, *6*, 2777.
[44] C. Boyer, N. A. Corrigan, K. Jung, D. Nguyen, T. K. Nguyen, N. N. M. Adnan, S. Oliver, S. Shanmugam, J. Yeow, *Chem. Rev.* **2016**, *116*, 1803.
[45] J. S. Wang, K. Matyjaszewski, *J. Am. Chem. Soc.* **1995**, *117*, 5614.
[46] K. Matyjaszewski, *Macromolecules* **2012**, *45*, 4015.
[47] M. Zhang, Q. Xiong, W. Shen, Q. Zhang, *RSC Adv.* **2014**, *4*, 30566.
[48] M. Fantin, A. A. Isse, A. Gennaro, K. Matyjaszewski, *Macromolecules* **2015**, *48*, 6862.
[49] M. Fantin, A. A. Isse, A. Venzo, A. Gennaro, K. Matyjaszewski, *J. Am. Chem. Soc.* **2016**, *138*, 7216.
[50] P. Z. Elias, G. W. Liu, H. Wei, M. C. Jensen, P. J. Horner, S. H. Pun, *J. Controlled Release* **2015**, *208*, 76.
[51] X. Pan, M. Fantin, F. Yuan, K. Matyjaszewski, *Chem. Soc. Rev.* **2018**, *47*, 5457.

[52] M. R. Hill, R. N. Carmean, B. S. Sumerlin, *Macromolecules* **2015**, *48*, 5459.
[53] J. Chiefari, Y. K. B. Chong, F. Ercole, J. Krstina, J. Jeffery, T. P. T. Le, R. T. A. Mayadunne, G. F. Meijs, C. L. Moad, G. Moad, E. Rizzardo, S. H. Thang, *Macromolecules* **1998**, *31*, 5559.
[54] S. Perrier, *Macromolecules* **2017**, *50*, 7433.
[55] A. Gregory, M. H. Stenzel, *Prog. Polym. Sci.* **2012**, *37*, 38.
[56] B. D. Fairbanks, P. A. Gunatillake, L. Meagher, *Adv. Drug Delivery Rev.* **2015**, *91*, 141.
[57] B. Apostolovic, S. P. E. Deacon, R. Duncan, H.-A. Klok, *Biomacromolecules* **2010**, *11*, 1187.
[58] R. N. Johnson, R. S. Burke, A. J. Convertine, A. S. Hoffman, P. S. Stayton, S. H. Pun, *Biomacromolecules* **2010**, *11*, 3007.
[59] D. S. H. Chu, J. G. Schellinger, M. J. Bocek, R. N. Johnson, S. H. Pun, *Biomaterials* **2013**, *34*, 9632.
[60] J. Niu, D. J. Lunn, A. Pusuluri, J. I. Yoo, M. A. O'Malley, S. Mitragotri, H. T. Soh, C. J. Hawker, *Nat. Chem.* **2017**, *9*, 537.
[61] D. K. Schneiderman, J. M. Ting, A. A. Purchel, R. Miranda, M. V. Tirrell, T. M. Reineke, S. J. Rowan, *ACS Macro Lett.* **2018**, *7*, 406.
[62] D. B. Thomas, A. J. Convertine, R. D. Hester, A. B. Lowe, C. L. Mccormick, *Macromolecules* **2004**, *37*, 1735.
[63] A.-C. Albertsson, I. K. Varma, *Biomacromolecules* **2003**, *4*, 1466.
[64] O. Dechy-cabaret, B. Martin-Vaca, D. Bourissou, *Chem. Rev.* **2004**, *104*, 6147.
[65] N. Hadjichristidis, H. Iatrou, M. Pitsikalis, G. Sakellariou, *Chem. Rev.* **2009**, *109*, 5528.
[66] K. Makiguchi, T. Satoh, T. Kakuchi, *Macromolecules* **2011**, *44*, 1999.
[67] N. E. Kamber, W. Jeong, R. M. Waymouth, R. C. Pratt, B. G. G. Lohmeijer, J. L. Hedrick, *Chem. Rev.* **2007**, *107*, 5813.
[68] H. R. Kricheldorf, *Angew. Chem., Int. Ed.* **2006**, *45*, 5752.
[69] J. Cheng, T. J. Deming, in *Synthesis of Polypeptides by Ring-Opening Polymerization of α-Amino Acid N-Carboxyanhydrides* (Ed: T. Deming), Peptide-Based Materials. Topics in Current Chemistry, Vol. *310*, Springer, Berlin, Heidelberg **2011**, pp. 1–26.
[70] S. Kobayashi, S. Kobayashi, H. Uyama, H. Uyama, S. Kimura, S. Kimura, *Chem. Rev.* **2001**, *101*, 3793.
[71] R. Tong, J. Cheng, *Macromolecules* **2012**, *45*, 2225.
[72] S. Lv, Y. Wu, J. Dang, Z. Tang, Z. Song, S. Ma, X. Wang, X. Chen, J. Cheng, L. Yin, *Polym. Chem.* **2017**, *8*, 1872.
[73] C. W. Bielawski, R. H. Grubbs, *Prog. Polym. Sci.* **2007**, *32*, 1.
[74] C. W. Bielawski, R. H. Grubbs, in *Controlled and Living Polymerizations: From Mechanisms to Applications* (Eds: A. H. E. Müller, K. Matyjaszewski), WILEY-VCH Verlag GmbH & Co. KGaA, Weinheim **2010**, pp. 297–342, https://onlinelibrary.wiley.com/doi/10.1002/9783527629091.ch6.
[75] E. K. Riga, D. Boschert, M. Vöhringer, V. T. Widyaya, M. Kurowska, W. Hartleb, K. Lienkamp, *Macromol. Chem. Phys.* **2017**, *218*, 1700273.
[76] A. E. Madkour, A. H. R. Koch, K. Lienkamp, G. N. Tew, *Macromolecules* **2010**, *43*, 4557.
[77] R. M. Conrad, R. H. Grubbs, *Angew. Chem., Int. Ed.* **2009**, *48*, 8328.
[78] J. K. Kammeyer, A. P. Blum, L. Adamiak, M. E. Hahn, N. C. Gianneschi, *Polym. Chem.* **2013**, *4*, 3929.
[79] D. C. Church, S. Nourian, C.-U. Lee, N. A. Yakelis, J. P. Toscano, A. J. Boydston, *ACS Macro Lett.* **2017**, *6*, 46.
[80] *Olefin Metathesis: Theory and Practice* (Ed: K. Grela), Wiley, Hoboken, NJ, USA **2014**, https://www-wiley-com.offcampus.lib.washington.edu/en-us/Olefin+Metathesis%3A+Theory+and+Practice-p-9781118207949.
[81] C. S. Higman, J. A. M. Lummiss, D. E. Fogg, *Angew. Chem., Int. Ed.* **2016**, *55*, 3552.
[82] P. Wheeler, J. H. Phillips, R. L. Pederson, *Org. Process Res. Dev.* **2016**, *20*, 1182.
[83] R. Verduzco, X. Li, S. L. Pesek, G. E. Stein, *Chem. Soc. Rev.* **2015**, *44*, 2405.
[84] *Int. Conf. on Harmonization, Guideline for Elemental Impurities Q3D*, ICH, Geneva, Switzerland **2014**, https://www.ich.org/fileadmin/Public_Web_Site/ICH_Products/Guidelines/Quality/Q3D/Q3D_Step_4.pdf.
[85] A. Li, J. Ma, G. Sun, Z. Li, S. Cho, C. Clark, K. L. Wooley, *J. Polym. Sci., Part A: Polym. Chem.* **2012**, *50*, 1681.
[86] K. V Bernaerts, F. E. Du Prez, *Prog. Polym. Sci.* **2006**, *31*, 671.
[87] H. U. Kang, Y. C. Yu, S. J. Shin, J. H. Youk, *J. Polym. Sci., Part A: Polym. Chem.* **2013**, *51*, 774.
[88] S. Jin Shin, Y. Chang Yu, J. Deok Seo, S. Ju Cho, J. Ho Youk, C. to, J. H. Youk, *J. Polym. Sci., Part A: Polym. Chem.* **2014**, *52*, 1607.
[89] E. Themistou, G. Battaglia, S. P. Armes, *Polym. Chem.* **2014**, *5*, 1405.
[90] Y. Zheng, W. Turner, M. Zong, D. J. Irvine, S. M. Howdle, K. J. Thurecht, *Macromolecules* **2011**, *44*, 1347.
[91] T. Oztürk, M. Göktas, B. Hazer, *J. Appl. Polym. Sci.* **2010**, *117*, 1638.
[92] X. Zhang, J. Li, W. Li, A. Zhang, *Biomacromolecules* **2007**, *8*, 3557.
[93] V. A. Piunova, H. W. Horn, G. O. Jones, J. E. Rice, R. D. Miller, *J. Polym. Sci., Part A: Polym. Chem.* **2016**, *54*, 563.
[94] C. Aydogan, C. Kutahya, A. Allushi, G. Yilmaz, Y. Yagci, *Polym. Chem.* **2017**, *8*, 2899.
[95] Z. Tong, Y. Li, H. Xu, H. Chen, W. Yu, W. Zhuo, R. Zhang, G. Jiang, *ACS Macro Lett.* **2016**, *5*, 867.
[96] J. Zhou, H. Xu, Z. Tong, Y. Yang, G. Jiang, *Mater. Sci. Eng., C* **2018**, *89*, 237.
[97] B. K. Sourkohi, A. Cunningham, Q. Zhang, J. K. Oh, B. Khorsand Sourkohi, A. Cunningham, Q. Zhang, J. K. Oh, *Biomacromolecules* **2011**, *12*, 3819.
[98] C.-F. Huang, S.-W. Kuo, H.-F. Lee, F.-C. Chang, *Polymer* **2005**, *46*, 1561.
[99] W. Jakubowski, K. Matyjaszewski, *Macromolecules* **2005**, *38*, 4139.
[100] L. Lei, F. Li, H. Zhao, Y. Wang, *J. Polym. Sci., Part A: Polym. Chem.* **2018**, *56*, 699.
[101] J. Song, J. Xu, S. Pispas, G. Zhang, *RSC Adv.* **2015**, *5*, 38243.
[102] M. De Geus, L. Schormans, A. R. A. Palmans, C. E. Koning, A. Heise, *J. Polym. Sci., Part A: Polym. Chem.* **2006**, *44*, 4290.
[103] J. Peeters, A. R. A. Palmans, M. Veld, F. Scheijen, A. Heise, E. W. Meijer, *Biomacromolecules* **2004**, *5*, 1862.
[104] Y. Wang, M. Fantin, K. Matyjaszewski, Y. Wang, M. Fantin, K. Matyjaszewski, *Macromol. Rapid Commun.* **2018**, *39*, 1800221.
[105] J. C. Theriot, G. M. Miyake, C. A. Boyer, *ACS Macro Lett.* **2018**, *7*, 662.
[106] C.-F. Huang, Y.-A. Hsieh, S.-C. Hsu, K. Matyjaszewski, *Polymer* **2014**, *55*, 6051.
[107] C.-F. Huang, R. Nicolay, Y. Kwak, F.-C. Chang, K. Matyjaszewski, *Macromolecules* **2009**, *42*, 8198.
[108] C. W. Bielawski, J. Louie, R. H. Grubbs, M. Beckman, C. W. Bielawski, A. Janis Louie, R. H. Grubbs, *J. Am. Chem. Soc.* **2000**, *122*, 12872.
[109] M. B. Runge, S. Dutta, N. B. Bowden, *Macromolecules* **2006**, *39*, 498.
[110] G. Chen, D. Huynh, P. L. Felgner, Z. Guan, *J. Am. Chem. Soc.* **2006**, *128*, 4298.
[111] M. Xie, J. Dang, H. Han, W. Wang, J. Liu, X. He, Y. Zhang, *Macromolecules* **2008**, *41*, 9004.
[112] J. Cuthbert, A. Beziau, E. Gottlieb, L. Fu, R. Yuan, A. C. Balazs, T. Kowalewski, K. Matyjaszewski, *Macromolecules* **2018**, *51*, 3808.
[113] D. Zehm, A. E. Laschewsky, H. Liang, J. Urgen, P. Rabe, J. P. Rabe, *Macromolecules* **2011**, *44*, 9635.
[114] J. Bolton, J. Rzayev, *ACS Macro Lett.* **2012**, *1*, 15.
[115] S. Boisse, M. A. Kryuchkov, N.-D. Tien, C. G. Bazuin, R. E. Prud'homme, *Macromolecules* **2016**, *49*, 6973.
[116] M. A. Kryuchkov, C. Detrembleur, R. J. Jerome, R. E. Prud'homme, C. G. Bazuin, *Macromolecules* **2011**, *44*, 5209.
[117] M. Spasova, L. Mespouille, O. Coulembier, D. Paneva, N. Manolova, I. Rashkov, P. Dubois, *Biomacromolecules* **2009**, *10*, 1217.
[118] X. Cao, W. Mao, Y. Mai, L. Han, S. Che, *Macromolecules* **2018**, *51*, 4381.

[119] H. Cheng, X. Fan, C. Wu, X. Wang, L.-J. Wang, X. J. Loh, Z. Li, Y.-L. Wu, *Macromol. Rapid Commun.* **2018**, *1800207*, 1.
[120] W. Zhu, A. Nese, K. Matyjaszewski, *J. Polym. Sci., Part A: Polym. Chem.* **2011**, *49*, 1942.
[121] J. B. Matson, R. H. Grubbs, *Macromolecules* **2008**, *41*, 5626.
[122] G. Fuks, R. M. Talom, F. Gauffre, *Chem. Soc. Rev.* **2011**, *40*, 2475.
[123] L. Wang, R. Zeng, C. Li, R. Qiao, *Colloids Surf., B* **2009**, *74*, 284.
[124] H. Kukula, H. Schlaad, M. Antonietti, S. Fö, *J. Am. Chem. Soc.* **2002**, *124*, 1658.
[125] J. Babin, C. Leroy, S. Lecommandoux, R. Borsali, Y. Gnanou, D. Taton, *Chem. Commun.* **2005**, 1993.
[126] J. Babin, D. Taton, M. Brinkmann, S. Lecommandoux, *Macromolecules* **2008**, *41*, 1384.
[127] K. R. Brzezinska, T. J. Deming, *Macromol. Biosci.* **2004**, *4*, 566.
[128] C.-J. Huang, F.-C. Chang, *Macromolecules* **2008**, *41*, 7041.
[129] T. C. Castle, E. Khosravi, L. R. Hutchings, *Macromolecules* **2006**, *39*, 5639.
[130] P. Lu, N. M. Alrashdi, A. J. Boydston, *J. Polym. Sci., Part A: Polym. Chem.* **2017**, *55*, 2977.
[131] V. Ladelta, J. D. Kim, P. Bilalis, Y. Gnanou, N. Hadjichristidis, *Macromolecules* **2018**, *51*, 2428.
[132] M. Benaglia, J. Chiefari, Y. K. Chong, G. Moad, E. Rizzardo, S. H. Thang, *J. Am. Chem. Soc.* **2009**, *131*, 6914.
[133] A. B. Biernesser, K. R. D. Chiaie, J. B. Curley, J. A. Byers, *Angew. Chem., Int. Ed.* **2016**, *55*, 5251.
[134] M. Qi, Q. Dong, D. Wang, J. A. Byers, *J. Am. Chem. Soc.* **2018**, *140*, 48.
[135] P. Zhenjiang Li, K. Guo, X. Wang, J. Liu, S. Xu, J. Xu, X. Pan, J. Liu, S. Cui, Z. Li, *Polym. Chem.* **2016**, *7*, 6281.
[136] H. Dong, Y. Zhu, Z. Li, J. Xu, J. Liu, S. Xu, H. Wang, Y. Gao, K. Guo, *Macromolecules* **2017**, *50*, 9295.
[137] A. J. Teator, D. N. Lastovickova, C. W. Bielawski, *Chem. Rev.* **2016**, *116*, 1969.
[138] Q. Michaudel, V. Kottisch, B. P. Fors, *Angew. Chem., Int. Ed.* **2017**, *56*, 9670.
[139] K. Satoh, H. Hashimoto, S. Kumagai, H. Aoshima, M. Uchiyama, R. Ishibashi, Y. Fujiki, M. Kamigaito, *Polym. Chem.* **2017**, *8*, 5002.
[140] V. Kottisch, Q. Michaudel, B. P. Fors, *J. Am. Chem. Soc.* **2017**, *139*, 10665.
[141] A. Ohtsuki, L. Lei, M. Tanishima, A. Goto, H. Kaji, *J. Am. Chem. Soc.* **2015**, *137*, 5610.
[142] Y. Xia, J. A. Kornfield, R. H. Grubbs, *Macromolecules* **2009**, *42*, 3761.
[143] Y. Xia, A. J. Boydston, R. H. Grubbs, *Angew. Chem., Int. Ed.* **2011**, *50*, 5882.
[144] K. Kawamoto, M. Zhong, K. R. Gadelrab, L.-C. Cheng, C. A. Ross, A. Alexander-Katz, J. A. Johnson, *J. Am. Chem. Soc.* **2016**, *138*, 11501.
[145] Y. Li, E. Themistou, J. Zou, B. P. Das, M. Tsianou, C. Cheng, *ACS Macro Lett.* **2012**, *1*, 52.
[146] D. Neugebauer, Y. Zhang, T. Pakula, S. S. Sheiko, K. Matyjaszewski, *Macromolecules* **2003**, *36*, 6746.
[147] J. C. Foster, S. C. Radzinski, S. E. Lewis, M. B. Slutzker, J. B. Matson, *Polymer (Guildf)* **2015**, *79*, 205.
[148] S. L. Pesek, X. Li, B. Hammouda, K. Hong, R. Verduzco, *Macromolecules* **2013**, *46*, 6998.
[149] Z. Li, J. Ma, N. S. Lee, K. L. Wooley, *J. Am. Chem. Soc.* **2011**, *133*, 1228.
[150] H. Zhou, J. A. Johnson, *Angew. Chem., Int. Ed.* **2013**, *52*, 2235.
[151] C. Lexer, R. Saf, C. Slugovc, *J. Polym. Sci., Part A: Polym. Chem.* **2009**, *47*, 299.
[152] E.-H. Kang, I.-H. Lee, T.-L. Choi, *ACS Macro Lett.* **2012**, *1*, 1098.
[153] Y. Xia, B. D. Olsen, J. A. Kornfield, R. H. Grubbs, *J. Am. Chem. Soc.* **2009**, *131*, 18525.
[154] J. A. Johnson, Y. Y. Lu, A. O. Burts, Y.-H. Lim, M. G. Finn, J. T. Koberstein, N. J. Turro, D. A. Tirrell, R. H. Grubbs, *J. Am. Chem. Soc.* **2011**, *133*, 559.
[155] M. Alizadeh, A. F. M. Kilbinger, *Macromolecules* **2018**, *51*, 4363.

Biomaterials 178 (2018) 317–325

Contents lists available at ScienceDirect

Biomaterials

journal homepage: www.elsevier.com/locate/biomaterials

Glomerular disease augments kidney accumulation of synthetic anionic polymers

Gary W. Liu [a, 1], Alexander N. Prossnitz [a, 1], Diana G. Eng [b], Yilong Cheng [a, f], Nithya Subrahmanyam [c, e], Jeffrey W. Pippin [b], Robert J. Lamm [a], Chayanon Ngambenjawong [a], Hamidreza Ghandehari [c, d, e], Stuart J. Shankland [b], Suzie H. Pun [a, *]

[a] Department of Bioengineering and Molecular Engineering & Sciences Institute, University of Washington, Seattle, WA, USA
[b] Department of Medicine, Division of Nephrology, University of Washington School of Medicine, Seattle, WA, USA
[c] Department of Pharmaceutics and Pharmaceutical Chemistry, University of Utah, Salt Lake City, UT, USA
[d] Department of Bioengineering, University of Utah, Salt Lake City, UT, USA
[e] Utah Center for Nanomedicine, Nano Institute of Utah, University of Utah, Salt Lake City, UT, USA
[f] Department of Applied Chemistry, School of Science, Xi'an Jiaotong University, Xi'an, PR China

ARTICLE INFO

Article history:
Received 7 March 2018
Received in revised form
31 May 2018
Accepted 2 June 2018
Available online 2 June 2018

Keywords:
Biodistribution
Kidney targeting
Proximal tubule cells
Polymer
Anionic
Glomerular disease

ABSTRACT

Polymeric drug carriers can alter the pharmacokinetics of their drug cargoes, thereby improving drug therapeutic index and reducing side effects. Understanding and controlling polymer properties that drive tissue-specific accumulation is critical in engineering targeted drug delivery systems. For kidney disease applications, targeted drug delivery to renal cells that reside beyond the charge- and size-selective glomerular filtration barrier could have clinical potential. However, there are limited reports on polymer properties that might enhance kidney accumulation. Here, we studied the effects of molecular weight and charge on the *in vivo* kidney accumulation of polymers in health and disease. We synthesized a panel of well-defined polymers by atom transfer radical polymerization to answer several questions. First, the biodistribution of low molecular weight (23–27 kDa) polymers composed of various ratios of neutral:anionic monomers (1:0, 1:1, 1:4) in normal mice was determined. Then, highly anionic (1:4 monomer ratio) low molecular and high molecular weight (47 kDa) polymers were tested in both normal and experimental focal segmental glomerulosclerosis (FSGS) mice, a model that results in loss of glomerular filtration selectivity. Through these studies, we observed that kidney-specific polymer accumulation increases with anionic monomer content, but not molecular weight; experimental FSGS increases kidney accumulation of anionic polymers; and anionic polymers accumulate predominantly in proximal tubule cells, with some distribution in kidney glomeruli. These findings can be applied to the design of polymeric drug carriers to enhance or mitigate kidney accumulation.

1. Introduction

Polymeric carriers have been applied in drug delivery to improve circulation time, alter biodistribution, reduce metabolism, and facilitate cellular internalization of drug cargo [1–5]. The pharmacokinetics of polymeric carriers and their cargo depend on polymer properties including molecular weight, dispersity, charge, functionalization, and self-assembled size and shape [6–9]. Studies investigating polymer structure and resulting biodistribution have mainly focused on exploiting the enhanced permeability and retention effect for cancer applications [10–12]. However, polymeric carriers for kidney diseases remain relatively understudied despite the clinical potential of such technologies. For example, targeted drug delivery to glomerular podocytes could improve the standard of therapy for common glomerular diseases such as minimal change disease and focal segmental glomerulosclerosis (FSGS), and drug delivery to tubular epithelial cells may be strategic for acute kidney injury and polycystic kidney disease treatment [13,14]. The major challenge is that these cell populations reside

* Corresponding author.
E-mail addresses: spun@uw.edu, spun@u.washington.edu (S.H. Pun).
[1] Equally contributing authors.

https://doi.org/10.1016/j.biomaterials.2018.06.001
0142-9612/

beyond the multi-layered glomerular filtration barrier, which comprises the innermost endothelial cells, a middle glomerular basement membrane, and the outer podocytes.

Given that the glomerular filtration barrier is both size- and charge-selective, these two parameters are likely critical when designing drug carriers to target cells past the barrier. Nanoparticle studies by the Davis group have revealed that gold nanoparticles of size ~75 nm target the kidney mesangium [15], and polycation-siRNA polymeric nanoparticles accumulate and disassemble in the anionic glomerular basement membrane [16]. However, the polymer physical properties required to cross this barrier for kidney targeting applications remain to be critically defined. Kamada et al. observed that hydrolyzed poly(vinylpyrrolidone-*co*-dimethyl maleic anhydride) copolymers of molecular weight approximately 10 kDa were anionic and distributed in kidneys up to 4 days after administration, with uptake primarily in proximal tubule cells [17]. Similarly, Borgman et al. reported that *N*-(2-hydroxypropyl)methacrylamide (HPMA) copolymers, functionalized with cyclo(RGDfK) targeting peptides and anionic penta-carboxylic acid residues, distributed preferentially in the kidneys compared to the designed target, tumors, and were retained up to 10 days after administration [18]. Recently, Bruni et al. reported on a panel of poly-ε-caprolactone and poly(ethylene glycol) methyl ether methacrylate star co-polymers (10–27 kDa), which exhibited evidence of kidney clearance *in vivo* [19]. While these reports have revealed in broad strokes that polymers with anionic charge and molecular weight less than 50 kDa accumulate in the kidneys, a rigorous evaluation of the individual and combined effects of polymer molecular weight and charge has yet to be reported.

Advances in controlled radical polymerization techniques have enabled polymer synthesis with precise control over molecular weight, dispersity, architecture, and chemical composition [20]. In this work, we used atom transfer radical polymerization (ATRP) to synthesize a panel of polymers to examine the effect of anionic charge density and molecular weight on kidney accumulation and distribution in mice. We first tested the effect of charge using a panel of low molecular weight (LMW) polymers, and then examined the effect of molecular weight in normal mice and mice with experimental FSGS, a model that results in loss of filtration size-selectivity and proteinuria [21]. Here, we report that highly anionic, LMW polymers preferentially accumulate in the kidneys and are internalized into proximal tubule cells. Conditions of experimental FSGS enhance accumulation of anionic LMW polymers.

2. Results

2.1. Polymer panel synthesis and characterization

We synthesized a panel of copolymers with varying ratios of anionic and neutral monomers by ATRP, with different degrees of polymerization (Table 1). Importantly, this approach yields well-defined polymers with tailored anion densities and molecular weights while keeping other properties constant. The hydrophilic, small molecular weight (~300 Da) monomer oligo(ethylene glycol) methyl ether methacrylate (OEGMA) was selected, as OEGMA-based polymers have been shown to exhibit favorable circulation times, low protein-binding properties, and reduced immunogenicity due to shorter ethylene glycol repeats [22–25]. The second monomer, *tert*-butyl methacrylate (tBuMA), yields methacrylic acids (MAA, anionic in charge) after deprotection. The monomer tBuMA was selected as an alternative to direct MAA polymerization, as MAA is insoluble in many organic solvents. Organic ATRP presents several advantages over aqueous ATRP, and results in polymerizations with less synthetic complexity and higher quality materials.

By varying the ratio of the two monomers and the polymerization time, p(OEGMA-*co*-MAA) copolymers with defined OEGMA:MAA ratios and molecular weights were synthesized (Table 1 and Fig. 1). Polymers with fixed molecular weight but varying anionic MAA content (0%, 50%, and 80%) were prepared to test the effect of charge on biodistribution. Two target molecular weight ranges were synthesized: low molecular weight (LMW) polymers of 20–25 kDa, and high molecular weight (HMW) polymers of 45–50 kDa. These two molecular weight regimes, which are either below or approximately at the renal filtration cutoff of ~50 kDa [26], respectively, were utilized to investigate the effect polymer molecular weight on kidney distribution. For biodistribution and tissue distribution analyses, polymers were fluorescently labeled with Cy3 fluorophore via a stable thioether bond by reduction of the disulfide bond of the pyridyl disulfide-terminated ATRP initiator and subsequent reaction with Cy3-maleimide (Fig. 1).

LMW polymers ranged in number average molecular weight (M_n) from 23 to 27 kDa, and HMW polymers had M_n of 47 kDa, as determined by gel permeation chromatography (GPC). All polymers exhibited dispersity ($Đ$) < 1.5. Within a molecular weight regime, the MAA monomer fraction during polymerization was varied at 0%, 50%, and 80%, resulting in polymer OEGMA:MAA ratios of 1:0 (homopolymer pOEGMA), 1:1, and 1:4, respectively. Monomer ratios within the copolymers, as determined by ^{1}H nuclear magnetic resonance spectroscopy (NMR), were in good agreement with the feed ratios and suggest similar reactivity of the two co-monomers under the polymerization conditions used (Table 1 and Fig. S1).

2.2. Biodistribution of LMW polymers in normal mice

The effect of polymer charge on kidney accumulation was first determined by evaluating the biodistribution of LMW 1:0, 1:1, and 1:4 copolymers 7 days post intravenous injection. This time point is significantly past the circulation half-life of similarly sized polymers (generally $t_{1/2} < 24$ h) [27,28] and was intentionally selected to measure organ accumulation. Fluorescence intensities of the three polymers prior to injection were comparable (Fig. S2). Polymer distribution to major organs (heart, lungs, liver, spleen, kidneys) was determined by whole organ fluorescence imaging after perfusion.

The LMW polymers exhibited a statistically significant increasing linear trend (p-value < 0.0001) in both kidney and liver

Table 1
Summary of p(OEGMA-*co*-MAA) copolymers. Number average molecular weight (M_n) and dispersity ($Đ$) values were determined by gel permeation chromatography. Polymer compositions were determined by ^{1}H NMR. PDS, pyridyl disulfide-functionalized ATRP initiator.

Polymer	Composition	OEGMA:tBuMA feed ratios	OEGMA:tBuMA measured ratios	M_n (Da)	$Đ$
LMW 1:0	p($OEGMA_{76}$)-PDS	100:0	N/A	23,000	1.125
LMW 1:1	p($OEGMA_{70}$-*co*-MAA_{70})-PDS	50:50	1:1.1	27,000	1.140
LMW 1:4	p($OEGMA_{39}$-*co*-MAA_{157})-PDS	20:80	1:3.5	25,000	1.370
HMW 1:4	p($OEGMA_{74}$-*co*-MAA_{296})-PDS	20:80	1:5.4	47,000	1.400

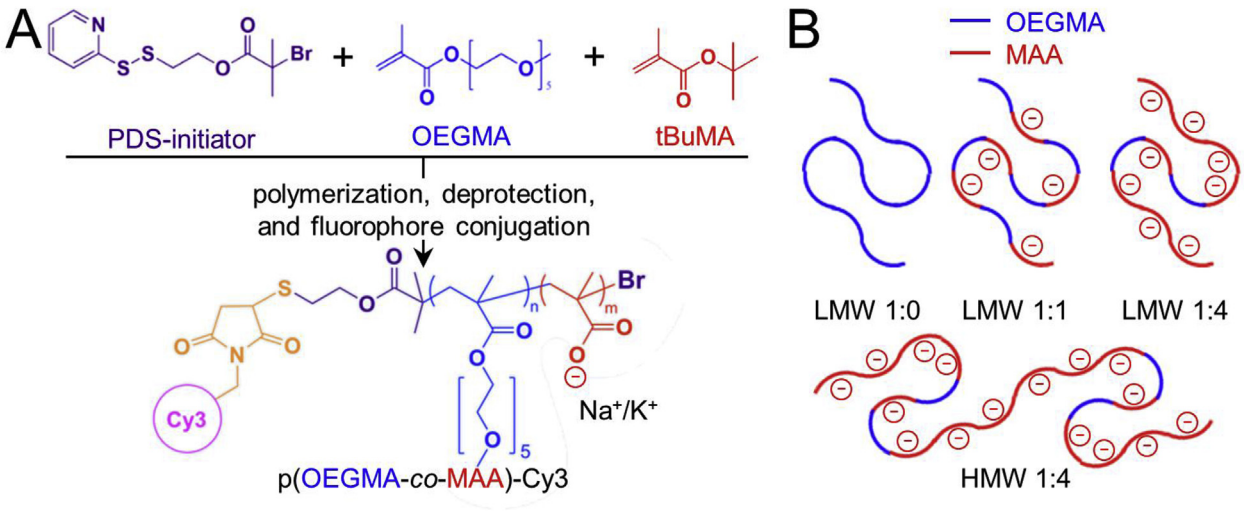

Fig. 1. Schematics of polymer synthesis and composition. A. Concise synthesis scheme of polymers. Polymerization was performed with a pyridyl disulfide (PDS)-terminated ATRP initiator and OEGMA and tBuMA monomers. Deprotection and fluorophore conjugation of polymers yield p(OEGMA-*co*-MAA)-Cy3. **B.** Cartoon schematic of the tested polymers. Polymers were named based on molecular weight and monomer composition. LMW, low molecular weight; HMW, high molecular weight; 1:0, polymer comprising 100% OEGMA monomer; 1:1, polymer comprising 50%/50% of OEGMA and MAA, respectively; 1:4, polymer comprising 20%/80% of OEGMA and MAA, respectively. Blue lines represent OEGMA monomer, and red lines represent MAA monomer. (For interpretation of the references to colour in this figure legend, the reader is referred to the Web version of this article.)

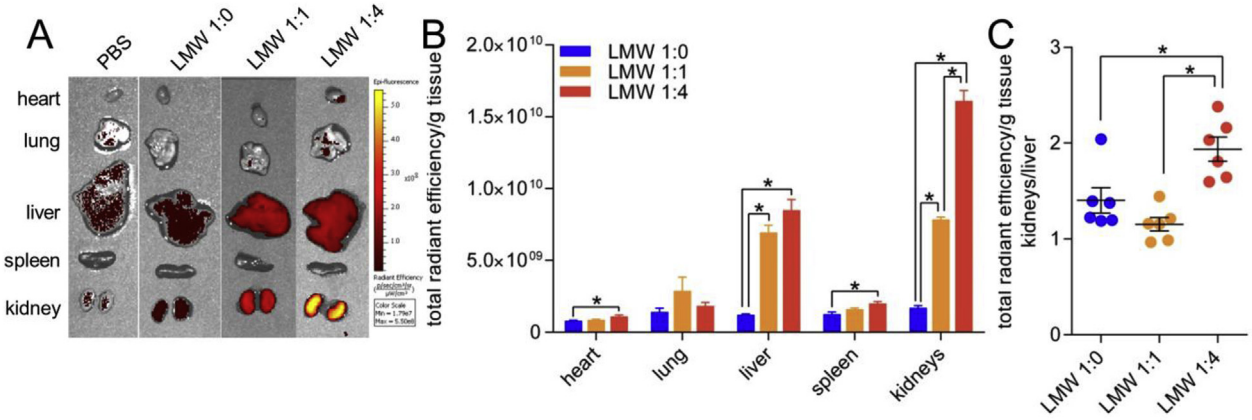

Fig. 2. Organ distribution of low molecular weight (23–27 kDa) polymers in normal mice. A. Representative fluorescent images of major organs 7 days after intravenous administration of PBS or fluorescent polymers. **B.** Region of interest quantification of tissue fluorescence normalized by tissue weight. All treatments were $n = 6$. **C.** Kidney/liver normalized fluorescent signal ratio. Statistical analysis was performed using a one-way ANOVA with post-hoc Tukey's multiple comparisons test, and a post-hoc linear trend test. Bars represent means ± SEM. *p-value < 0.05.

fluorescence trending with MAA content (anionic charge), with LMW 1:4 > 1:1 > 1:0 (Fig. 2A and B). Preferential kidney accumulation was quantified by normalizing the fluorescent signal in the kidneys by that in the liver. LMW 1:4 exhibited the greatest kidney/liver fluorescence ratio compared to other treatments (Fig. 2C). The distribution of labeled polymers in the kidney was determined by confocal microscopy. Fluorescence was primarily detected in the kidney cortex, intracellularly in proximal tubule cells as identified by morphology and proximity to glomeruli structures (Fig. 3). LMW 1:4 copolymers exhibited the most fluorescent staining as well as deposition in kidney glomeruli. In further confirmation of the role of anionic charge on kidney accumulation, *N*-(2-hydroxypropyl) methacrylamide (HPMA) copolymers modified with anionic diethylenetriaminepentaacetic acid chelator (DTPA) exhibited greater kidney/liver fluorescence compared to HPMA control polymers (Fig. S3).

2.3. Biodistribution of HMW and LMW polymers in normal and experimental FSGS mice

We hypothesized that glomerular kidney disease may alter the polymer accumulation in this organ due to loss of filtration selectivity. As highly anionic LMW 1:4 (80% MAA content) copolymers exhibited the most fluorescence in the kidneys, HMW 1:4 ($M_n = 47$ kDa) and LMW 1:4 ($M_n = 25$ kDa) copolymers were tested to determine the effect of molecular weight on biodistribution in normal mice and mice with experimental FSGS. To induce FSGS, a cytotoxic anti-podocyte antibody that causes podocyte loss was administered to mice [21]. Damage to glomeruli and disruption of the glomerular filtration barrier was confirmed histologically (Fig. S4) and by proteinuria, which peaked on day 7 (Fig. 4A) and persisted up to day 14. Polymers were injected on day 7 at peak proteinuria, and polymer distribution assessed 7 days post-

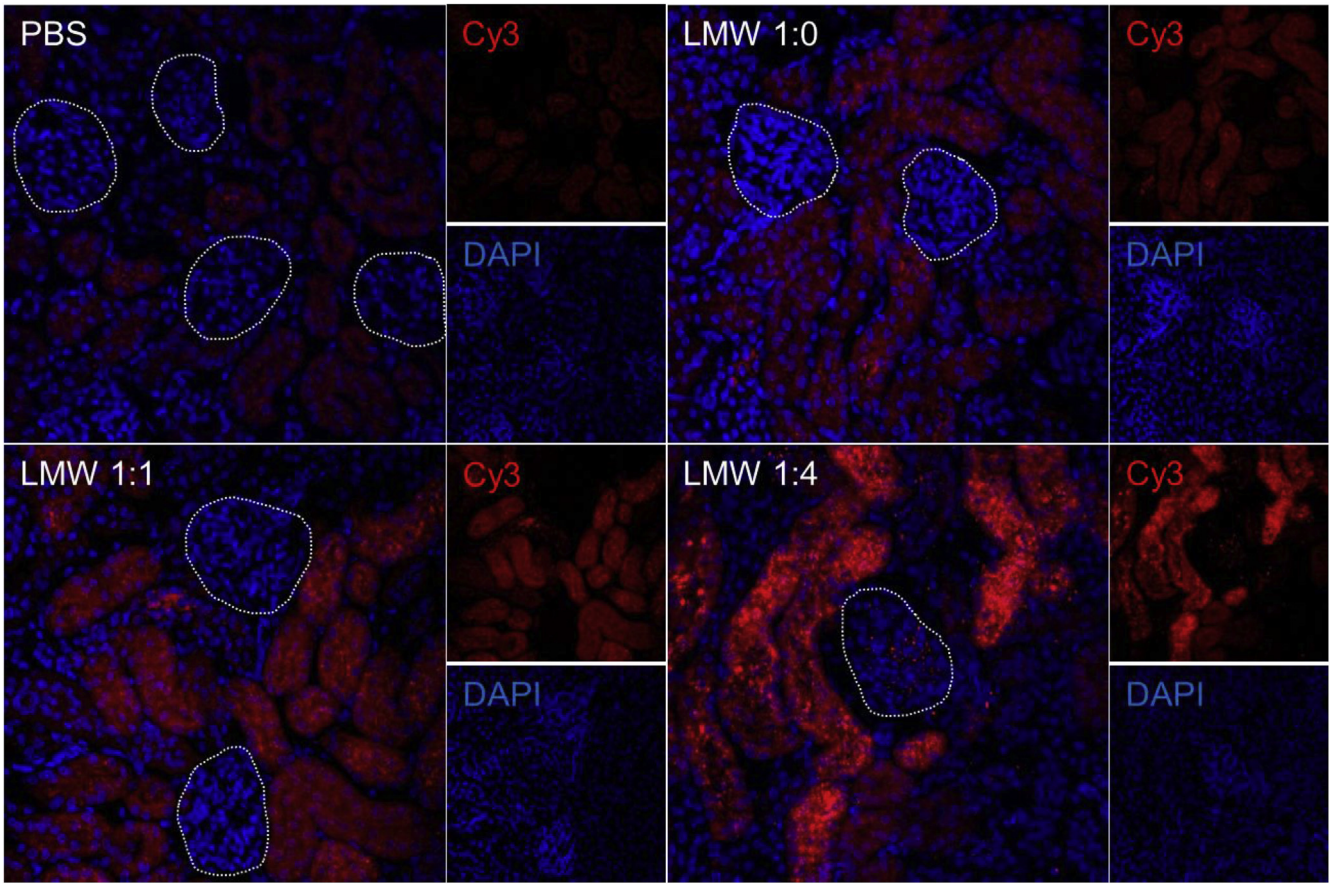

Fig. 3. Kidney distribution of low molecular weight (23–27 kDa) polymers in normal mice. Representative fluorescent images of kidneys 7 days after intravenous administration of PBS or fluorescent polymers obtained by confocal microscopy. Kidney glomeruli are denoted by dashed white lines. Blue, DAPI; red, Cy3-labeled polymers. Individual DAPI and Cy3 channels are shown to the right of their respective images. (For interpretation of the references to colour in this figure legend, the reader is referred to the Web version of this article.)

polymer administration (Fig. 4A).

In normal animals, LMW 1:4 copolymers exhibited greater fluorescence in the kidneys than HMW 1:4 copolymers (Fig. 4B and C). Experimental FSGS increased kidney and liver fluorescence of LMW 1:4 copolymers, but not HMW 1:4 copolymers (Fig. 4C). Generally, LMW 1:4 copolymers exhibited greater kidney/liver fluorescence ratios compared to HMW 1:4 polymers in normal and experimental FSGS conditions (Fig. 4D). Kidney tissue distribution patterns were similar to the initial LMW polymer panel, with no remarkable differences noted in mice with experimental FSGS (data not shown).

2.4. *In vitro characterization of polymers in proximal tubule cells*

The LMW 1:4 polymer was then characterized for internalization, cytotoxicity, and uptake mechanism using an immortalized human proximal tubule cell line, HK-2, which exhibits key features of primary proximal tubule cells [29]. By confocal microscopy, polymer-treated cells exhibited punctate polymer fluorescence within the cell body (Fig. 5A). Treatment of HK-2 cells with 1 μM polymer for up to 7 days did not cause significant differences in viability compared to untreated cells, as determined by MTS/PMS assay (Fig. 5B). To investigate the mechanism of polymer internalization, polymer uptake was measured after incubation in either 37 °C or 4 °C using flow cytometry, as reduced temperature is known to effectively inhibit active endocytosis [17,30]. Incubation of cells on ice (4 °C) significantly reduced polymer fluorescence (p-value < 0.0001) compared to cells maintained at 37 °C (Fig. 5C). Moreover, in a competition uptake experiment with anionic dextran sulfate (500 kDa), incubation of polymer in an excess of dextran sulfate significantly reduced polymer fluorescence intensity to ~46% compared to control (p-value < 0.0001, Fig. 5D).

3. Discussion

In engineering intravenous polymeric drug carriers for targeted drug delivery applications, careful consideration of polymer properties must be taken to understand and control “passive targeting” effects, inadvertent or intentional [20]. Ideally, materials are designed with properties that enhance accumulation at target tissue, and avoid characteristics that enhance accumulation in off-target tissues. This is especially true when considering the kidneys, which filter up to 180 liters of blood per day, and are a major clearance organ with intimate contact with the circulatory system. However, polymer design guidelines to either enhance or avoid kidney targeting have been limited.

Here, we systematically interrogated the effect of polymer anionic charge density and molecular weight, as well as glomerular filtration barrier integrity, on polymer accumulation in the kidneys. Polymers were synthesized by living radical polymerization to control composition and molecular weight. By using a pyridyl disulfide-terminated initiator, polymer chains were fluorescently labeled with a single Cy3-maleimide resulting in ~1:1 dye:polymer ratio, enabling direct comparison of fluorescent signals for the

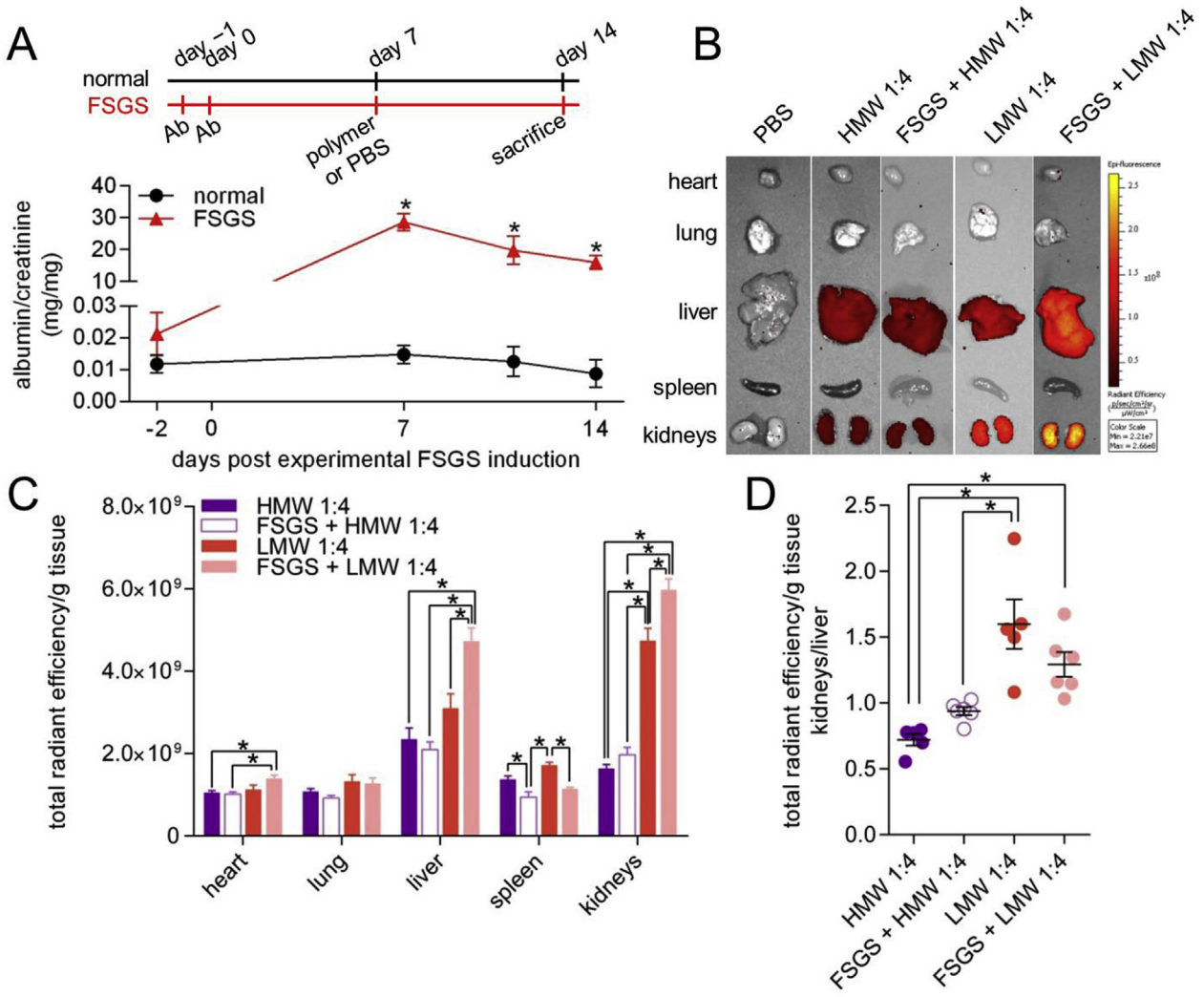

Fig. 4. Organ distribution of polymers in normal and experimental FSGS mice. A. Top: treatment schedule of normal and experimental FSGS mice. FSGS mice were administered a cytotoxic anti-podocyte antibody on days −1 and 0. Both normal and FSGS mice were administered PBS or fluorescent polymers on day 7 and sacrificed on day 14 for analysis. Bottom: urine albumin/creatinine ratios of animals administered the cytotoxic anti-podocyte antibody (red, FSGS, $n = 5$) or not (black, normal, $n = 4$). All mice were administered PBS on day 7. Statistical analysis was performed using a two-tailed Student's *t*-test compared to normal animals. **B.** Representative fluorescent images of major organs analyzed on day 14. **C.** Region of interest quantification of tissue fluorescence normalized by tissue weight. All antibody treatments were $n = 6$; otherwise $n = 5$. **D.** Kidney/liver normalized fluorescent signal ratio. Statistical analysis was performed using a one-way ANOVA with post-hoc Tukey's multiple comparisons test. Bars represent means ± SEM. *p-value < 0.05. (For interpretation of the references to colour in this figure legend, the reader is referred to the Web version of this article.)

polymers tested. Thioether linkages have been reported in a variety of *in vivo* applications, including cellular nanoparticle "backpack" conjugation [31] and antibody-drug conjugates [32]. Whole-organ fluorescence imaging was selected due to ease of fluorophore conjugation and throughput. While this method presents limitations to accurate quantification due to tissue light-scattering [33,34], it still provides a semi-quantitative means of evaluating biodistribution.

In an initial panel, polymers with fixed molecular weights (23–27 kDa), but varying anionic charge, were examined in normal mice. Cationic polymers were not tested due to the toxicity of these materials [35]. The molecular weights were well below the renal filtration cutoff of 50 kDa, allowing passage of these polymers through the glomerular filtration barrier via filtration. A polymer with M_n 25 kDa and high (80%) anionic monomer content localized the most in the kidneys, and was internalized specifically in proximal tubule cells. This was a surprising result, as both the glomerular endothelial cells and the glomerular basement membrane of the filtration barrier are highly negatively charged due to a glycocalyx and anionic heparan sulfate proteoglycans, respectively, and presumably repel the polymers [36]. Other uptake mechanisms, such as secretion and reabsorption, may also result in polymer uptake. Moreover, HPMA polymers containing anionic DTPA also exhibited kidney-specific accumulation, indicating that the observed biodistribution is not unique to MAA monomer and likely generalizable to other anionic monomers.

We utilized a cytotoxic anti-podocyte antibody to induce experimental FSGS. This antibody method is well-reported and specifically causes apoptosis of glomerular podocytes [21,37–47], leading to albuminuria, a clinical signature of a dysfunctional glomerular filtration barrier and loss of size-selective filtration [48]. This model was used to test the effects of polymer molecular weight with fixed anionic charge density (80%). Experimental FSGS increased the kidney fluorescence of LMW 1:4 polymer (25 kDa) but not HMW 1:4 polymer (47 kDa), providing some evidence that LMW 1:4 polymer kidney distribution is driven partly by filtration while HMW 1:4 is not. Moreover, these findings suggest that there is an optimal molecular weight for kidney delivery applications.

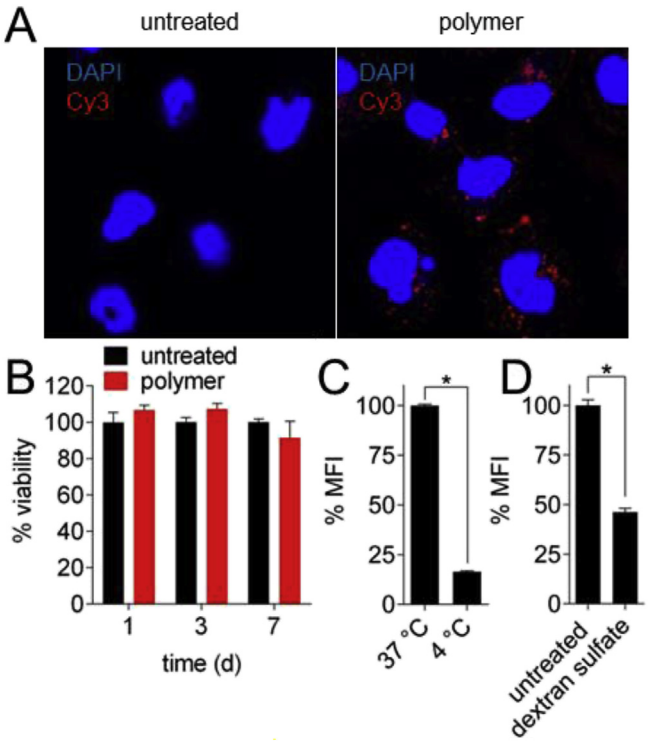

Fig. 5. *In vitro* LMW 1:4 polymer characterization. A. Representative fluorescent images of HK-2 cells after incubation with fluorescent polymer. Cells were incubated with polymers for 2 h prior to imaging. Blue, DAPI; red, Cy3-labeled polymers. **B.** HK-2 cell viability after polymer treatment at various days ($n = 5$). **C.** Polymer uptake, measured by mean fluorescence intensity (MFI), after 1 h incubation with polymer at 37 or 4 °C ($n = 4$). **D.** Polymer uptake, measured by mean fluorescence intensity (MFI), after 1 h incubation with polymer in media or in the presence of dextran sulfate ($n = 3$). Bars represent means ± SEM. Statistical analysis was performed using a two-tailed Student's *t*-test. *p-value < 0.05. (For interpretation of the references to colour in this figure legend, the reader is referred to the Web version of this article.)

Our observation that experimental FSGS enhanced LMW 1:4 polymer distribution suggests that disease conditions resulting in loss of filtration size-selectivity may be exploited to enhance material targeting to the kidneys, similar to the enhanced permeability and retention effect observed in animal models of tumors [20].

These two size regimes, low-molecular weight (~25 kDa) and high-molecular weight (~50 kDa), were selected to test the kidney distribution behavior of polymers below and near the filtration cutoff for linear polymers (~50 kDa). Many reports have shown that circulation half-life increases significantly for linear polymers of size ~50 kDa compared to those of size 20 kDa [49,50], indicating that the filtration cutoff is near 50 kDa. Our study corroborates these findings. Given that the polymer backbones studied here are non-degradable and the clinical importance of eliminating nondegradable materials [51], we therefore studied these molecular weights as an intrinsic control point for elimination rate.

The immortalized human proximal tubule cell line, HK-2, was used to study polymer features *in vitro*, as these cells exhibit similar phenotype, function, and toxicity responses compared to primary cells [29]. LMW 1:4 polymers were internalized into punctate structures as early as 2 h after polymer treatment, and polymer treatment (1 μM) did not inflict significant toxicity, even at extended exposure times (7 d). Notably, this concentration and timescale is significantly higher and longer than what would be encountered *in vivo*, as the injected polymer concentration (40 μM) should be rapidly diluted and cleared after intravenous injection and tissue distribution. In subsequent experiments, polymer internalization was found to be significantly reduced at 4 °C and in the presence of excess anionic dextran sulfate, a known competitor of scavenger receptors, indicating that uptake is driven primarily by active endocytosis and/or non-specific scavenger receptors [17,52]. Proximal tubule reabsorption of macromolecules such as albumin and IgG is well-reported, with multi-ligand scavenger receptors megalin and cubilin responsible for uptake [53,54]. Indeed, various studies have shown that knockdown of megalin and/or cubilin results in reduced kidney uptake of synthetic peptides [55], albumin [56], and nanoparticles [57]. These receptors may mediate uptake of the polymers in the kidneys. Polymer uptake correlating with increasing anionic charge was also observed for the liver, albeit to a lesser degree compared to the kidneys. Liver endothelial and Kupffer cells express scavenger receptors SR-AI and SR-AII that broadly recognize polyanionic ligands [58–60]. These non-specific scavenger receptors may mediate liver uptake of the polymers studied in this work.

While the polymers studied here did not exhibit significant podocyte uptake in the context of glomerular disease, these findings may still be useful for glomerular disease applications. As these polymers seem to be filtered, functionalization of these polymers with ligands that recognize podocyte receptors may enable cellular binding and internalization as these polymers travel through the glomerular filtration barrier. Moreover, targeted drug delivery to proximal tubule cells during glomerular disease may improve renal health. Proteinuria causes tubular cell atrophy and fibrosis due to protein overload, which contributes to worsening chronic kidney disease [61]. Therefore, delivery of pro-survival molecules may be a strategic method of halting tubular necrosis.

4. Conclusions

By examining a panel of synthetic polymers, we have determined that polymers with molecular weight ~25 kDa and high anionic monomer content are taken up in kidney proximal tubule cells up to 1 week after injection, with enhanced accumulation observed in conditions of loss of glomerular filtration barrier integrity. These guidelines may inform the development of improved polymeric materials for a variety of applications. For chemotherapeutics such as cisplatin that inflict serious renal toxicity [62], polymeric drug carriers should potentially avoid high anionic monomer content to mitigate uptake into proximal tubule cells. In kidney diseases such as polycystic kidney disease where tubule cells are principally afflicted [63], anionic polymeric drug carriers may be considered to improve the therapeutic profile of drugs.

5. Concise methods

5.1. Materials

Poly(ethylene glycol) methyl ether methacrylate monomer (average molecular weight = 300 Da, OEGMA), *N*,*N*′-dicyclohexylcarbodiimide (DCC), 2,2′-bipyridyl (BPY), 2-mercaptoethanol, copper (I) bromide, 4-dimethylaminopyridine (DMAP), and *N*,*N*,*N*′,*N*″,*N*″-pentamethyldiethylenetriamine (PMDETA) were purchased from Sigma-Aldrich. 2,2′-dipyridyl disulfide and *tert*-butyl methacrylate monomer (tBuMA) were purchased from TCI America. α-bromoisobutyric acid was purchased from Fluka. OEGMA and tBuMA were passed through a basic alumina column to remove inhibitors before polymerization. Cy3-maleimide was purchased from Lumiprobe.

5.2. Polymer synthesis and characterization

A pyridyl disulfide-terminated ATRP initiator was synthesized as previously described [64]. The initiator was purified by column chromatography, and purity was confirmed by ^{1}H NMR. In a typical polymerization, the ATRP initiator, ligand (PMDETA or BPY), and monomers (OEGMA and tBuMA) were dissolved in solvent and added to a round-bottom flask. The solution was purged with Ar gas for 10 min. After, solid CuBr was rapidly added, and the solution was purged again. The following reaction conditions were carried out for each polymer (mole ratios): (*i*) LMW 1:4 and HMW 1:4, initiator:PMDETA:OEGMA:tBuMA:Cu(I) = 1:1:40:160:1, [monomer] = 3 M, in anisole, 60 °C for 4 or 8 h, respectively; (*ii*) LMW 1:1, initiator:PMDETA:OEGMA:tBuMA:Cu(I) = 1:1:400:400:1, [monomer] = 2 M, in methyl ethyl ketone, room temperature for 2 h; (*iii*) LMW 1:0, initiator:BPY:OEGMA:tBuMA:Cu(I) = 1:1.2:667:0:1, [monomer] = 2 M, in ethanol, 50 °C for 6 h. HMW and LMW 1:4 polymers were precipitated into cold hexanes; LMW 1:1 and LMW PEG polymers were precipitated in cold ether. Polymers were collected by centrifugation and vacuum-dried for at least 24 h, and characterized for molecular weight and dispersity (*Đ*) via gel permeation chromatography (GPC) as previously described [65]. Purity and monomer ratios in the statistical copolymers were assessed with ^{1}H NMR. The integrated signals of the terminal methyl groups of the OEGMA (3 protons) and the *tert*-butyl groups of the tBuMA (9 protons) were compared.

For the synthesis of the HPMA copolymers, the co-monomers *N*-(2-hydroxypropyl) methacrylamide (HPMA) [66], *N*-methacryloylaminopropyl-2-amino-3-(isothiourea-phenyl) propyl-cyclohexane-1,2-diamine-*N,N—N′,N′,N″,N″*-pentaacetic acid (APMA-CHX-A″-DTPA) [67], and 5-[3-(methacryloylaminopropyl) thioureidyl] rhodamine (APMA-rhodamine) were synthesized using established methods. APMA-rhodamine was adapted from the synthesis of APMA-FITC [68], substituting rhodamine-isothiocyanate instead of fluorescein-isothiocyanate. Copolymerization was performed using free radical copolymerization, using azobisisobutyronitrile (AIBN) as an initiator. The reaction was carried out in a nitrogen-purged sealed glass ampule for 24 h and 50 °C. For the control copolymer, the following feed ratio in mole percent was used: HPMA:APMA-CHX-A″-DTPA:APMA-rhodamine (98:0:2). For the DTPA-containing (anionic) copolymer the following ratio was used: HPMA:APMA-CHX-A″-DTPA:APMA-rhodamine (88:10:2). Initiator concentration was 5 mg of initiator per 100 mg total monomers in both syntheses, in 500 μL of MeOH. Copolymers were purified through dialysis against dH_2O and lyophilized. Copolymers were characterized for molecular weight and dispersity using size exclusion chromatography. Co-monomer content was measured using UV—Vis spectroscopy. For the control copolymer, rhodamine fluorescent label content was determined to be 0.156 mmol/g. For the anionic copolymer, rhodamine content was determined to be 0.863 mmol/g and DTPA monomer content was found to be 0.598 mmol/g.

5.3. Polymer deprotection and fluorescent labeling

Polymers containing tBuMA were deprotected in trifluoroacetic acid, to remove the *tert*-butyl groups and reveal carboxylic acids, for 2 h with stirring. After, polymers were precipitated in cold ether, collected by centrifugation, and vacuum-dried overnight. Polymers were then dissolved in molecular-grade H_2O pH 8, dialyzed against dH_2O for 24 h, and lyophilized. The deprotected polymers were prepared for dye conjugation by reducing the disulfide bond present in the initiator. Polymers were dissolved in PBS-EDTA, purged with Ar for 10 min, and a 1000-fold molar-excess of dithiothretriol (DTT) was added. The reaction was left overnight. Polymers were desalted using a PD-10 desalting column (GE), dissolved in a 2:1 PBS-EDTA:DMSO solution, purged, and a 5 × molar-excess of Cy3-maleimide dye (Lumiprobe) dissolved in *N,N*-dimethylformamide was added. After 24 h, labeled polymers were dialyzed against dH_2O for 1.5 wk.

5.4. Polymer biodistribution studies

All animal experiments were executed in compliance with the University of Washington IACUC guidelines. For the initial LMW polymer biodistribution study, polymers (4 nmol) dissolved in PBS were injected in 7-week old mice via retro-orbital route. After 7 d, animals were sacrificed, perfused with PBS, and major organs (heart, lungs, liver, spleen, and kidneys) were harvested. Organ fluorescence was quantified by a Xenogen IVIS using ex/em = 535/580 nm. Regions of interest were drawn across each organ for quantification, and total radiant efficiencies were normalized by organ weight. Statistical analyses were performed using GraphPad Prism and R software. Experimental FSGS was induced in 9-week old male BALB/c mice (Jackson Laboratory) via two intraperitoneal injections (10 mg/20 g mouse) of a cytotoxic anti-podocyte antibody 24 h apart. HMW and LMW polymers (4 nmol) were injected as above on day 7 after disease induction, and animals were sacrificed for organ fluorescence quantification on day 14 as described above.

5.5. Tissue processing and imaging

Kidney tissues were fixed in 4% PFA, washed with PBS, and incubated overnight with 30% sucrose/PBS at 4 °C. Tissues were then embedded in OCT and frozen in an ethanol/dry ice bath. After cryosectioning, tissues were stained with DAPI and mounted with Fluoromount-G (SouthernBiotech). Confocal images were taken as previously reported [37]. Images were captured using a Leica TCS SPE II laser scanning confocal microscope (Solms, Germany) with a HCX PL APO 40 × /1.30 oil objective, at 1024 × 1024 pixel format with 8-bit intensity resolution. Sets of 8 serial images were collected at 2-μm step size. The acquisition wavelengths were: DAPI excitation 405 nm, emission 380—468 nm; Cy3 excitation 561 nm, emission 576—644 nm. Masson's trichrome and silver staining were performed using standard methods. Images were collected at 600 × magnification.

5.6. Urine albumin and creatinine quantification

Spot urines were collected on various days before and throughout experimental FSGS induction. Urine albumin content was quantified by radial immunodiffusion as previously described [69], and creatinine quantified using a creatinine assay kit (Cayman Chemical).

5.7. HK-2 cell culture and polymer characterization

The human proximal tubule cell line HK-2 was cultured in K-SFM (ThermoFisher Scientific) and maintained as described by ATCC. For confocal imaging of polymer uptake, HK-2 cells were seeded on bovine collagen I (Corning)-coated glass coverslips in a 24-well plate at 4×10^4 cells/well. After overnight incubation, media was replaced with fresh media or polymer dissolved in media to 1 μM for 2 h. After, cells were washed three times with PBS, and then fixed and stained with DAPI using standard methods. Confocal images were collected as described above.

For viability studies, HK-2 cells were plated in a 96-well plate at 5×10^3 cells/well. After overnight incubation, media was replaced

with fresh media or polymer dissolved in media to 1 μM. After 1, 3, or 7 d treatment, cells were washed with PBS, and viability was assayed by MTS/PMS (Promega) according to manufacturer instructions.

HK-2 cells were plated in a 24-well plate at 3–4 $\times$ 10^4 cells/well for uptake characterization studies and tested after overnight incubation. To test the effects of temperature on uptake, media was replaced with polymer dissolved in media to 1 μM, and cells were incubated for 1 h at 37 °C or on ice (4 °C). Cells were then washed 3 $\times$ with PBS, lifted with trypsin, resuspended in 1% BSA/PBS, and analyzed by flow cytometry. For competition studies, cells were first incubated with 1 mg/mL dextran sulfate (Sigma-Aldrich) in media for 30 min, and then incubated with 1 μM polymer in the presence of 1 mg/mL dextran sulfate for 2 h. Cells were then processed for flow cytometry as described above. Flow cytometry was performed using an Attune NxT Flow Cytometer (ThermoFisher Scientific). At least 1 $\times$ 10^4 cells were analyzed by FlowJo software, using mean fluorescence intensity as a measure of polymer uptake.

Competing interests

The authors have no competing interests to declare.

Acknowledgments

This work was supported by the Office of the Assistant Secretary of Defense for Health Affairs through the Peer Reviewed medical Research Program under Award Numbers PR151175 and PR151965, National Institutes of Health Grants 1R01DK097598 and R01AG046231, a National Science Foundation Graduate Research Fellowship Program under Grant No. DGE-1256082 to GWL, and a National Cancer Institute NRSA award 1F31CA213901 to NS. Opinions, interpretations, conclusions, and recommendations are those of the authors and are not necessarily endorsed by the Department of Defense, National Institutes of Health, or National Science Foundation. We would like to thank Heather Gustafson, Meilyn Sylvestre, Soren Johnson, Ritika Jain, and George Sun for their help with experiments, and Michele Shaffer for consultation on statistical analysis. We also acknowledge support from the National Institutes of Health (S10 OD016240) to the W.M. Keck Center for Advanced Studies in Neural Signaling and the assistance of Keck Center manager Dr. Nathaniel Peters.

Appendix A. Supplementary data

Supplementary data related to this article can be found at https://doi.org/10.1016/j.biomaterials.2018.06.001.

References

[1] R. Duncan, The dawning era of polymer therapeutics, Nat. Rev. Drug Discov. 2 (2003) 347–360.
[2] N. Larson, H. Ghandehari, Polymeric conjugates for drug delivery, Chem. Mater. 24 (2012) 840–853.
[3] R. Tong, J. Cheng, Anticancer polymeric nanomedicines, Polym. Rev. 47 (2007) 345–381.
[4] D.W. Pack, A.S. Hoffman, S. Pun, P.S. Stayton, Design and development of polymers for gene delivery, Nat. Rev. Drug Discov. 4 (2005) 581–593.
[5] M.E. Davis, Z.G. Chen, D.M. Shin, Nanoparticle therapeutics: an emerging treatment modality for cancer, Nat. Rev. Drug Discov. 7 (2008) 771–782.
[6] F.M. Veronese, et al., PEG-doxorubicin conjugates: influence of polymer structure on drug release, in vitro cytotoxicity, biodistribution, and antitumor activity, Bioconjugate Chem. 16 (2005) 775–784.
[7] F. Alexis, E. Pridgen, L.K. Molnar, O.C. Farokhzad, Factors affecting the clearance and biodistribution of polymeric nanoparticles, Mol. Pharm. 5 (2008) 505–515.
[8] C. He, Y. Hu, L. Yin, C. Tang, C. Yin, Effects of particle size and surface charge on cellular uptake and biodistribution of polymeric nanoparticles, Biomaterials 31 (2010) 3657–3666.
[9] M. Imran ul-haq, B.F. Lai, R. Chapanian, J.N. Kizhakkedathu, Influence of architecture of high molecular weight linear and branched polyglycerols on their biocompatibility and biodistribution, Biomaterials 33 (2012) 9135–9147.
[10] M. Thanou, R. Duncan, Polymer-protein and polymer-drug conjugates in cancer therapy, Curr. Opin. Invest. Drugs 4 (2003) 701–709.
[11] Y. Matsumura, H. Maeda, A new concept for macromolecular therapeutics in cancer chemotherapy: mechanism of tumoritropic accumulation of proteins and the antitumor agent smancs, Canc. Res. 46 (1986) 6387–6392.
[12] M.E. Fox, F.C. Szoka, J.M. Frechet, Soluble polymer carriers for the treatment of cancer: the importance of molecular architecture, Acc. Chem. Res. 42 (2009) 1141–1151.
[13] R.M. Williams, E.A. Jaimes, D.A. Heller, Nanomedicines for kidney diseases, Kidney Int. 90 (2016) 740–745.
[14] N. Kamaly, J.C. He, D.A. Ausiello, O.C. Farokhzad, Nanomedicines for renal disease: current status and future applications, Nat. Rev. Nephrol. 12 (2016) 738–753.
[15] C.H. Choi, J.E. Zuckerman, P. Webster, M.E. Davis, Targeting kidney mesangium by nanoparticles of defined size, Proc. Natl. Acad. Sci. U. S. A. 108 (2011) 6656–6661.
[16] J.E. Zuckerman, C.H. Choi, H. Han, M.E. Davis, Polycation-siRNA nanoparticles can disassemble at the kidney glomerular basement membrane, Proc. Natl. Acad. Sci. U. S. A. 109 (2012) 3137–3142.
[17] H. Kamada, et al., Synthesis of a poly(vinylpyrrolidone-co-dimethyl maleic anhydride) co-polymer and its application for renal drug targeting, Nat. Biotechnol. 21 (2003) 399–404.
[18] M.P. Borgman, et al., Tumor-targeted HPMA copolymer-(RGDfK)-(CHX-A'-DTPA) conjugates show increased kidney accumulation, J. Contr. Release 132 (2008) 193–199.
[19] R. Bruni, et al., Ultrasmall polymeric nanocarriers for drug delivery to podocytes in kidney glomerulus, J. Contr. Release 255 (2017) 94–107.
[20] C.E. Wang, P.S. Stayton, S.H. Pun, A.J. Convertine, Polymer nanostructures synthesized by controlled living polymerization for tumor-targeted drug delivery, J. Contr. Release 219 (2015) 345–354.
[21] D.G. Eng, et al., Glomerular parietal epithelial cells contribute to adult podocyte regeneration in experimental focal segmental glomerulosclerosis, Kidney Int. 88 (2015) 999–1012.
[22] H. Ma, J. Hyun, P. Stiller, A. Chilkoti, Non-fouling" oligo(ethylene glycol)-functionalized polymer brushes synthesized by surface-initiated atom transfer radical polymerization, Adv. Mater. 16 (2004) 338–341.
[23] S. Bhattacharjee, et al., Site-specific zwitterionic polymer conjugates of a protein have long plasma circulation, Chembiochem 16 (2015) 2451–2455.
[24] J.-F. Lutz, Polymerization of oligo(ethylene glycol) (meth)acrylates: toward new generations of smart biocompatible materials, J. Polym. Sci. Polym. Chem. 46 (2008) 3459–3470.
[25] Y. Qi, et al., A brush-polymer conjugate of exendin-4 reduces blood glucose for up to five days and eliminates poly(ethylene glycol) antigenicity, Nat Biomed Eng 1 (2016).
[26] A. Ruggiero, et al., Paradoxical glomerular filtration of carbon nanotubes, Proc. Natl. Acad. Sci. U. S. A. 107 (2010) 12369–12374.
[27] N. Nasongkla, et al., Dependence of pharmacokinetics and biodistribution on polymer architecture: effect of cyclic versus linear polymers, J. Am. Chem. Soc. 131 (2009) 3842–3843.
[28] A. Lewis, Y. Tang, S. Brocchini, J.W. Choi, A. Godwin, Poly(2-methacryloyloxyethyl phosphorylcholine) for protein conjugation, Bioconjugate Chem. 19 (2008) 2144–2155.
[29] M.J. Ryan, et al., HK-2: an immortalized proximal tubule epithelial cell line from normal adult human kidney, Kidney Int. 45 (1994) 48–57.
[30] K.L. Goldenthal, I. Pastan, M.C. Willingham, Initial steps in receptor-mediated endocytosis. The influence of temperature on the shape and distribution of plasma membrane clathrin-coated pits in cultured mammalian cells, Exp. Cell Res. 152 (1984) 558–564.
[31] M.T. Stephan, J.J. Moon, S.H. Um, A. Bershteyn, D.J. Irvine, Therapeutic cell engineering with surface-conjugated synthetic nanoparticles, Nat. Med. 16 (2010) 1035–1041.
[32] R.P. Lyon, D.L. Meyer, J.R. Setter, P.D. Senter, Conjugation of anticancer drugs through endogenous monoclonal antibody cysteine residues, Methods Enzymol. 502 (2012) 123–138.
[33] Y. Liu, Y.-c. Tseng, L. Huang, Biodistribution studies of nanoparticles using fluorescence imaging: a qualitative or quantitative method? Pharmaceut. Res. 29 (2012) 3273–3277.
[34] E. Tasciotti, et al., Near-infrared imaging method for the in vivo assessment of the biodistribution of nanoporous silicon particles, Mol. Imag. 10 (2011), 7290.2011.00011.
[35] H. Lv, S. Zhang, B. Wang, S. Cui, J. Yan, Toxicity of cationic lipids and cationic polymers in gene delivery, J. Contr. Release 114 (2006) 100–109.
[36] J.H. Miner, The glomerular basement membrane, Exp. Cell Res. 318 (2012) 973–978.
[37] D.G. Eng, et al., Detection of renin lineage cell transdifferentiation to podocytes in the kidney glomerulus with dual lineage tracing, Kidney Int. (2018).
[38] N.V. Kaverina, et al., WT1 is necessary for the proliferation and migration of cells of renin lineage following kidney podocyte depletion, Stem Cell Reports 9 (2017) 1152–1166.
[39] N.V. Kaverina, D.G. Eng, R.R. Schneider, J.W. Pippin, S.J. Shankland, Partial podocyte replenishment in experimental FSGS derives from nonpodocyte sources, Am. J. Physiol. Ren. Physiol. 310 (2016) F1397–F1413.

[40] N.V. Kaverina, et al., Tracking the stochastic fate of cells of the renin lineage after podocyte depletion using multicolor reporters and intravital imaging, PLoS One 12 (2017) e0173891.
[41] J. Lichtnekert, et al., Renin-angiotensin-aldosterone system inhibition increases podocyte derivation from cells of renin lineage, J. Am. Soc. Nephrol. 27 (2016) 3611–3627.
[42] T. Ohse, et al., De novo expression of podocyte proteins in parietal epithelial cells during experimental glomerular disease, Am. J. Physiol. Ren. Physiol. 298 (2010) F702–F711.
[43] J.W. Pippin, et al., Cells of renin lineage are adult pluripotent progenitors in experimental glomerular disease, Am. J. Physiol. Ren. Physiol. 309 (2015) F341–F358.
[44] R.R. Schneider, et al., Compound effects of aging and experimental FSGS on glomerular epithelial cells, Aging (Albany NY) 9 (2017) 524–546.
[45] J. Zhang, et al., Podocyte repopulation by renal progenitor cells following glucocorticoids treatment in experimental FSGS, Am. J. Physiol. Ren. Physiol. 304 (2013) F1375–F1389.
[46] J. Zhang, et al., Retinoids augment the expression of podocyte proteins by glomerular parietal epithelial cells in experimental glomerular disease, Nephron Exp. Nephrol. 121 (2012) e23–e37.
[47] S.S. Roeder, et al., Activated ERK1/2 increases CD44 in glomerular parietal epithelial cells leading to matrix expansion, Kidney Int. 91 (2017) 896–913.
[48] J.A. Jefferson, C.E. Alpers, S.J. Shankland, Podocyte biology for the bedside, Am. J. Kidney Dis. 58 (2011) 835–845.
[49] P. Caliceti, F.M. Veronese, Pharmacokinetic and biodistribution properties of poly(ethylene glycol)-protein conjugates, Adv. Drug Deliv. Rev. 55 (2003) 1261–1277.
[50] L.W. Seymour, R. Duncan, J. Strohalm, J. Kopecek, Effect of molecular weight (Mw) of N-(2-hydroxypropyl)methacrylamide copolymers on body distribution and rate of excretion after subcutaneous, intraperitoneal, and intravenous administration to rats, J. Biomed. Mater. Res. 21 (1987) 1341–1358.
[51] H.H. Gustafson, D. Holt-Casper, D.W. Grainger, H. Ghandehari, Nanoparticle uptake: the phagocyte problem, Nano Today 10 (2015) 487–510.
[52] Y. Tsubamoto, et al., Dextran sulfate, a competitive inhibitor for scavenger receptor, prevents the progression of atherosclerosis in Watanabe heritable hyperlipidemic rabbits, Atherosclerosis 106 (1994) 43–50.
[53] E.I. Christensen, H. Birn, Megalin and cubilin: synergistic endocytic receptors in renal proximal tubule, Am. J. Physiol. Ren. Physiol. 280 (2001) F562–F573.
[54] E.I. Christensen, H. Birn, P. Verroust, S.K. Moestrup, Membrane receptors for endocytosis in the renal proximal tubule, Int. Rev. Cytol. 180 (1998) 237–284.
[55] A. Wischnjow, et al., Renal targeting: peptide-based drug delivery to proximal tubule cells, Bioconjugate Chem. 27 (2016) 1050–1057.
[56] X.Y. Zhai, et al., Cubilin- and megalin-mediated uptake of albumin in cultured proximal tubule cells of opossum kidney, Kidney Int. 58 (2000) 1523–1533.
[57] S. Gao, et al., Megalin-mediated specific uptake of chitosan/siRNA nanoparticles in mouse kidney proximal tubule epithelial cells enables AQP1 gene silencing, Theranostics 4 (2014) 1039–1051.
[58] N. Platt, S. Gordon, Scavenger receptors: diverse activities and promiscuous binding of polyanionic ligands, Chem. Biol. 5 (1998) R193–R203.
[59] K. Kawabata, Y. Takakura, M. Hashida, The fate of plasmid DNA after intravenous injection in mice: involvement of scavenger receptors in its hepatic uptake, Pharm. Res. (N. Y.) 12 (1995) 825–830.
[60] M. van Oosten, E. van de Bilt, T.J. van Berkel, J. Kuiper, New scavenger receptor-like receptors for the binding of lipopolysaccharide to liver endothelial and Kupffer cells, Infect. Immun. 66 (1998) 5107–5112.
[61] M. Abbate, C. Zoja, G. Remuzzi, How Does Proteinuria Cause Progressive Renal Damage?, 2006.
[62] R.P. Miller, R.K. Tadagavadi, G. Ramesh, W.B. Reeves, Mechanisms of cisplatin nephrotoxicity, Toxins 2 (2010) 2490–2518.
[63] J.J. Grantham, Polycystic kidney disease: a predominance of giant nephrons, Am. J. Physiol. 244 (1983) F3–F10.
[64] L. Jia, et al., Reduction-responsive cholesterol-based block copolymer vesicles for drug delivery, Biomacromolecules 15 (2014) 2206–2217.
[65] R.J. Lamm, et al., Peptide valency plays an important role in the activity of a synthetic fibrin-crosslinking polymer, Biomaterials 132 (2017) 96–104.
[66] J. Strohalm, J. Kopeček, Poly[N-(2-hydroxypropyl)methacrylamide]. IV. Heterogeneous polymerization, Die Angewandte Makromolekulare Chemie 70 (1978) 109–118.
[67] A. Mitra, A. Nan, J.C. Papadimitriou, H. Ghandehari, B.R. Line, Polymer-peptide conjugates for angiogenesis targeted tumor radiotherapy, Nucl. Med. Biol. 33 (2006) 43–52.
[68] V. Omelyanenko, P. Kopeckova, C. Gentry, J. Kopecek, Targetable HPMA copolymer-adriamycin conjugates. Recognition, internalization, and subcellular fate, J. Contr. Release 53 (1998) 25–37.
[69] C.B. Marshall, R.D. Krofft, J.W. Pippin, S.J. Shankland, CDK inhibitor p21 is prosurvival in adriamycin-induced podocyte injury, in vitro and in vivo, Am. J. Physiol. Ren. Physiol. 298 (2010) F1140–F1151.

HHS Public Access

Author manuscript

ACS Biomater Sci Eng. Author manuscript; available in PMC 2019 December 10.

Published in final edited form as:

ACS Biomater Sci Eng. 2018 December 10; 4(12): 3968–3973. doi:10.1021/acsbiomaterials.8b01163.

Boronic acid copolymers for direct loading and acid-triggered release of Bis-T-23 in cultured podocytes

Yilong Cheng[a,b,†], **Gary W. Liu**[b,†], **Ritika Jain**[b], **Jeffrey W. Pippin**[c], **Stuart J. Shankland**[c], and **Suzie H. Pun**[b,*]

[a]Present address, Department of Applied Chemistry, School of Science and MOE Key Laboratory for Nonequilibrium Synthesis and Modulation of Condensed Matter and State Key Laboratory for Mechanical Behavior of Materials, Xi'an Jiaotong University, No. 28 Xianning West Road, Xi'an, Shaanxi 710049, China

[b]Department of Bioengineering and Molecular Engineering & Sciences Institute University of Washington, 3720 15th Ave NE Seattle, WA 98195, USA

[c]Department of Medicine, Division of Nephrology, School of Medicine, University of Washington, 750 Republican Street, E-179, Seattle, WA 98109, USA

Abstract

We report an acid-reversible linker for triggered release of Bis-T-23, an experimental small molecule drug for kidney disease treatment that restores podocyte morphology during disease. Bis-T-23 contains catechols, which form an acid-reversible, covalent boronate ester bond with boronic acids. We synthesized phenylboronic acid-containing polymers using reversible addition-fragmentation chain transfer polymerization that were able to directly load and solubilize Bis-T-23. Because of the reversibility of the boronic ester bond, drug was released in its native form in a pH-dependent manner. The polymers rapidly trafficked into acidic compartments and did not exhibit cytotoxicity, and polymer-drug conjugates successfully delivered Bis-T-23 into cultured podocytes.

Graphical Abstract

*To whom correspondence should be addressed, spun@uw.edu.
†These authors contributed equally to the work

SUPPORTING INFORMATION

Experimental methods, additional figures, and calculations may be found in supporting information.

CONFLICTS OF INTEREST

The authors declare no competing financial interest.

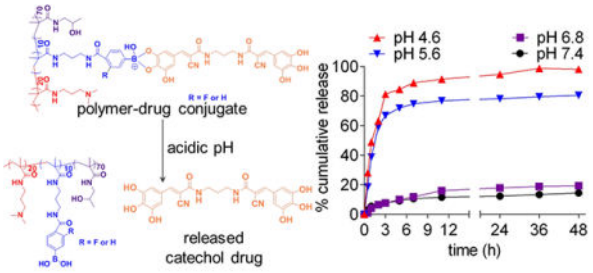

Keywords

Bis-T-23; boronic acid; drug delivery; polymers; triggered release

More than 850 million people worldwide are afflicted with kidney disease.[1] Because of limited therapies to halt disease advancement, many patients progress to chronic kidney failure and ultimately require dialysis or kidney transplantation. However, kidney disease patients continue to face high morbidity and poor five-year survival rates.[2] Human and experimental studies have shown that loss and dysfunction of podocytes, highly specialized and terminally differentiated epithelial cells within the kidney glomerulus essential to filtration, directly underlies scarring of kidney filtration units that leads to deteriorating kidney function and proteinuria.[3] However, current therapies do not specifically modulate podocyte dysfunction, and burden the patient with significant side effects that further complicate the disease.[4–6]

A common response to injury in podocytes is actin cytoskeleton derangement, which precedes morphological changes that lead to disruption of the filtration barrier.[7] Therefore, drugs that modulate the actin cytoskeleton could have widespread clinical impact in treating chronic kidney disease. Schiffer *et al.* recently reported on the therapeutic efficacy of a small molecule, Bis-T-23, which promotes actin polymerization via dynamin oligomerization.[7] In various rodent models of podocyte injury, Bis-T-23 restored overall podocyte morphology and reduced proteinuria, a clinical signature of podocyte injury. However, low drug solubility and the ubiquitous expression of dynamin preclude systemic administration of Bis-T-23 in the clinic due to off-target toxicity.[8, 9] Therefore, targeted Bis-T-23 delivery to glomerular podocytes could significantly expedite clinical translation of this experimental drug.

A critical component of targeted drug delivery is spatiotemporal control of drug release. Ideally, drugs are conjugated or loaded onto carriers in a manner that minimizes drug release during circulation to mitigate drug loss and reduce side effects, and releases drug after target cell binding and uptake. Drug linkers have been engineered to be sensitive to a variety of local cues (pH, enzymes, or reduction/oxidation) for programmed drug release within the target tissue or cell.[10, 11] For example, the antibody-drug conjugate Adcetris contains cathepsin-sensitive linkers for drug release after cellular internalization and trafficking into lysosomes,[12] enabling targeted delivery of the highly potent drug monomethyl auristatin E. These advances in linker chemistry have subsequently improved the safety and efficacy of

chemotherapeutics, and similar technologies could improve the standard of treatment for kidney diseases.

Here, we report an acid-labile, boronate ester linkage for programmed release of Bis-T-23. We exploited the fact that Bis-T-23 contains catechol groups, which bind tightly to boronic acids to form a reversible covalent boronate ester bond.[13] Importantly, no drug modification is required for conjugation to boronic acid-functionalized carriers, and drugs are released in original form. Boronic acids bind tightly to diols, and reactions with catechols such as Bis-T-23 are especially favored because of the aromatic hydroxyl groups (association constant K_a ~830 M^{-1} and 4.6 M^{-1} for catechols and D-glucose, respectively).[13] The conjugated Bis-T-23 can be released by bond-breaking triggered by acidic pH conditions.[14, 15] Therefore, the drug remains in a pro-drug form during circulation, but is released in active form after cellular binding and internalization into acidic, intracellular vesicles (Figure 1). In this work, we developed boronic acid-containing copolymers for loading and pH-sensitive release of the catechol-containing drug Bis-T-23. We characterize these materials for drug loading, release kinetics, cellular trafficking, and cytotoxicity, and demonstrate polymer-drug conjugate delivery in cultured podocytes. Moreover, we report a new method of evaluating Bis-T-23 delivery to podocytes.

Phenylboronic acid-grafted copolymers (PBA copolymers) were synthesized by reversible addition-fragmentation chain transfer (RAFT) polymerization (Scheme S1) of the monomers *N*-(2-hydroxypropyl) methacrylamide (HPMA), *N*-[3-(dimethylamino)propyl]methacrylamide (DMAPMA), and *N*-(3-aminopropyl)methacrylamide (APMA). HPMA was selected due to its biocompatibility and water solubility;[16] DMAPMA, which contains a tertiary amine and is positively charged at physiologic pH, was selected to facilitate cellular internalization in lieu of a targeting ligand;[17] and APMA was selected for facile functionalization with 4-carboxyphenylboronic acid by EDC/NHS conjugation post-polymerization. Notably, cationic polymers containing similar tertiary amines were observed to be rapidly internalized and trafficked into acidic endosomes and lysosomes.[18, 19] This internalization route is an important requirement for the polymers studied here to reverse the boronate ester bond and trigger intracellular drug release.

Monomer conversion and copolymer composition was monitored by ^{1}H NMR during polymerization. Monomer conversion was nearly 100% after 18 h, and polymer composition was determined to be 70:20:10 for HPMA:DMAPMA:APMA (Figure S1). The copolymers exhibited a number average molecular weight (M_n) of 22 kDa and low dispersity ($Đ$ = 1.05) by GPC analysis, indicating good control of polymerization (Figure S2 and Table 1). Functionalization of the copolymers with 4-carboxyphenylboronic acid was confirmed by ^{1}H NMR via emergence of new peaks at 7.9 and 7.6 ppm, indicating successful and complete reaction of primary amine side chains with PBA (Figure S1). Comparison of the integrals of the protons in PBA at 7.6 and 7.9 ppm with that of the protons in HPMA at 3.8 ppm confirmed that the final PBA copolymer was p(HPMA$_{70}$-*co*-DMAPMA$_{20}$-*co*-(APMA-*g*-PBA)$_{10}$).

When conjugated to PBA copolymers, Bis-T-23 gained a new absorbance at λ = 410 nm, which was used to monitor polymer drug loading. In the absence of polymer, Bis-T-23

exhibited low water solubility and formed a yellow precipitate in aqueous solutions (Figure 2A). At increasing polymer:drug mass ratios, precipitation decreased, and drug absorbance increased until at 14:1 ratio, after which the observed drug absorbance plateaued (Figure 2A and 2B). Therefore, a polymer:drug ratio of 14:1 was used for subsequent drug loading and studies. In these conditions, 24.2% of the available PBA are loaded with drug (see Supporting Information for calculations). Dynamic light scattering analysis was also performed to test if aggregation occurred during drug loading, as Bis-T-23 is symmetrical and may crosslink polymers. No differences in size distribution were observed between polymer only and polymer-drug conjugates, suggesting that these loading conditions do not result in cross-linking and aggregation (Figure S3). This may be due to steric hindrance of the benzyl in both the polymer and Bis-T-23.

Polymer-drug conjugates were then tested for pH-dependent drug release in buffers at pH 7.4, 6.8, 5.6, and 4.6, with the latter two values within the late endosomal and lysosomal pH spanning 6.5–4.5.[20, 21] While polymer-conjugates at pH 4.6 and 5.6 exhibited rapid and nearly complete drug release, conjugates at pH 6.8 and 7.4 exhibited minimal drug release within the same time frame (Figure 2C). After 48 h, PBA copolymers exhibited 14.5%, 19.3%, 80.4%, and 98.1% cumulative Bis-T-23 release in pH 7.4, 6.8, 5.6, and 4.6, respectively. These observations demonstrate that the copolymers exhibit pH-sensitive drug release, and that the PBA copolymers could release Bis-T-23 in pH ranges relevant to acidic endosomes and lysosomes.

Despite the pK_a of the PBA studied here being greater than 8.0,[22, 23] Bis-T-23 was retained on the PBA copolymer at pH 7.4, likely due to the high binding affinity between PBA and catechols. As the pK_a of the boronic acid may affect drug loading and release, polymers containing fluoroPBA (FPBA), which exhibits a lower pK_a around 7.2–7.8 due to an electronegative fluorine,[24, 25] were similarly synthesized and characterized (Figure S1). FPBA copolymers exhibited optimal drug loading at polymer:drug ratio 12:1 with similar trends of pH-dependent drug release as PBA copolymers (Figure S4). As no major differences in drug loading and release were observed between PBA and FPBA copolymers, PBA copolymers were selected for further study due to greater aqueous solubility. Therefore, polymer-drug conjugates may be formed at pH 7 without the need to modulate the pK_a of the phenylboronic acid.

Drug release was also tested in the presence of glucose, as vicinal diols might prematurely displace conjugated Bis-T-23. Physiologically, blood glucose concentrations range from 0.63 to 0.99 mg/mL in normal children and adults.[26] Glucose at concentrations up to 1.5 mg/mL did not cause significant drug release from the PBA copolymers (Figure S5). Moreover, mannitol, which contains multiple hydroxyls and exhibits a higher K_a with boronic acid than glucose (K_a = 120 M^{-1} and 4.6 M^{-1}, respectively),[13] did not cause any significant Bis-T-23 release at the same concentration (Figure S5). The stability of the boronate ester is likely due to the 180-fold higher K_a of catechols and boronic acids compared to diols. Therefore, diols at physiological concentrations do not displace Bis-T-23, indicating that boronate ester reversal is more sensitive to pH than diols (Figure S5).

Bis-T-23-loaded polymers were then tested for drug delivery in cultured podocytes. First, the trafficking of PBA copolymers in podocytes was examined by flow cytometry and confocal microscopy. As early as 20–30 min, fluorescently labeled PBA copolymers were mostly internalized (Figure 3A) and colocalized with LysoTracker, a marker of lysosomes (Figure 3B). This is consistent with other studies reporting that polycationic materials rapidly traffic into acidic compartments as early as 5 min, with greater trafficking into more acidic late endosomes and lysosomes observed 10–20 min later.[27, 28] Bis-T-23 promotes dynamin oligomerization, which causes actin polymerization and crosslinking and focal adhesion maturation.[7, 29–31] By image analysis, while Bis-T-23 significantly increased F-actin content in cultured podocytes, polymer-drug conjugates did not (Figure S6), likely due to the low dynamic range of this method. Therefore, we sought to develop a more high-throughput method of evaluating Bis-T-23 delivery in cultured podocytes. Given that podocytes endocytose albumin[32] and the importance of dynamin in this process,[33] we hypothesized that Bis-T-23 would modulate uptake of albumin. Indeed, in initial studies, Bis-T-23 inhibited albumin uptake up to 27% (Figure S7). Therefore, flow cytometry analysis of fluorescein-albumin uptake was used to quantify polymer-drug delivery. In podocytes, free Bis-T-23 and polymer-Bis-T-23 significantly inhibited albumin uptake (Figure 4A). Notably, cells were incubated with treatments for 20 min in PBS; due to minimal drug release within this time in pH 7.4 (<5%), polymer-Bis-T-23 effects was more likely due to acid-triggered release rather than basal release. Additionally, free Bis-T-23 and polymer-Bis-T-23 significantly inhibited transferrin uptake in a human T cell line (Figure 4B), consistent with previous studies showing Bis-T-23 inhibition of transferrin uptake,[34] and did not exhibit significant toxicity towards cultured podocytes (Figure 4C). These findings indicate that polymer-Bis-T-23 conjugates are internalized into acidic compartments, Bis-T-23 is being released intracellularly, and the polymers are not significantly toxic in the conditions tested.

While recent high-throughput screening campaigns have identified new small molecule drug candidates for treating kidney disease,[35, 36] solubility and off-target side effects remain major obstacles to clinical translation of experimental drugs such as Bis-T-23. Polymeric drug carriers have emerged as an answer to some of these challenges by altering drug properties and pharmacokinetics. An important aspect of these carriers is the drug linker that controls drug release under specific conditions. Phenylboronic acid-containing polymers have been recently reported in applications in drug delivery due to their various stimuli-sensitive properties.[14, 15, 37] In this work, we developed PBA copolymers for acid-triggered release of the catechol-containing drug Bis-T-23, taking advantage of the fact that catechols form an acid-reversible boronate ester with boronic acids. This chemistry has been utilized in a number of drug delivery applications for stimulus-triggered drug release from polymer systems. Su *et al* reported on polymer-drug conjugates comprising the boronic acid-containing chemotherapeutic, bortezomib, and catechol-containing polymers.[15] The materials exhibited acidic pH-selective drug release and maintained *in vitro* cancer cell killing. Aguirre-Chagala *et* al and Ma *et al* reported on boronic acid-containing polymers for loading the diol-containing chemotherapeutic, capecitabine. These materials self-assembled into micelles and exhibited pH-sensitive drug release.[38, 39] Li *et al* developed drug-loaded, polymeric micelles through crosslinking of adjacent boronic acid- and catechol-containing polymers. These micelles also exhibited acidic pH- and mannitol-triggered drug release, as

well as improved particle stability *in vivo*.[14] Moreover, boronate esters have broad utility in other applications, including isolation of catechol-containing compounds from plasma for quantification,[40] and saccharide-triggered release of catechol-containing model drugs from boronic acid-functionalized nanoparticles.[41]

This work reports PBA copolymers that reversibly load the catechol-containing drug Bis-T-23 without any further drug modification and release active drug after cell internalization. Polymer-drug conjugates were stable at physiological pH and in the presence of sugars, indicating potential stability of the conjugates during circulation *in vivo*. *In vitro*, PBA copolymers distributed into acidic endosomes, and through a flow cytometry assay to evaluate Bis-T-23 delivery, polymer-drug conjugates were able to deliver drug intracellularly. Collectively, these findings suggest that boronate ester chemistry may be an attractive strategy for releasing Bis-T-23 after cellular uptake. The copolymers reported here included the tertiary amine-containing monomer DMAPMA, which mediates cellular internalization for proof-of-concept *in vitro* studies. Future work includes functionalizing uncharged versions of these polymers for targeted podocyte delivery of Bis-T-23 in the kidney. This strategy could also be readily applied to other catechol-containing drugs such as quercetin or EGCG.[42, 43]

Supplementary Material

Refer to Web version on PubMed Central for supplementary material.

ACKNOWLEDGMENTS

This work was supported by the Office of the Assistant Secretary of Defense for Health Affairs through the Peer Reviewed Medical Research Program under Award No. W81XWH-16-1-0167 and by the National Science Foundation Graduate Research Fellowship Program under Grant No. DGE-1256082 to G. W. L. Y.L.C. gratefully acknowledges support from the “Young Talent Support Plan” of Xi’an Jiaotong University and the Fundamental Research Funds for the Central Universities. S. J. S. and J. W. P. were supported by the NIDDK (R01 DK09759801A1 and UH2 DK107343–01) and the NIA (R01 AG046231–01A1). We thank Changkyu Gu and Sanja Sever for important discussion about Bis-T-23. Opinions, interpretations, conclusions, and recommendations are those of the authors and are not necessarily endorsed by the Department of Defense or the National Science Foundation. We also acknowledge support from the NIH (S10 OD016240) to the W. M. Keck Center for Advanced Studies in Neural Signaling and the assistance of Keck Center manager Dr. Nathaniel Peters, as well as thank Shijie Cao for his expertise and guidance on dynamic light scattering experiments.

REFERENCES

(1). Hill NR; Fatoba ST; Oke JL; Hirst JA; O’Callaghan CA; Lasserson DS; Hobbs FD, Global Prevalence of Chronic Kidney Disease - A Systematic Review and Meta-Analysis. PLoS One 2016, 11 (7), e0158765 DOI: 10.1371/journal.pone.0158765. [PubMed: 27383068]

(2). Collins AJ; Foley RN; Gilbertson DT; Chen SC, The state of chronic kidney disease, ESRD, and morbidity and mortality in the first year of dialysis. Clin. J. Am. Soc. Nephrol 2009, 4 Suppl 1, S5–11. DOI: 10.2215/CJN.05980809.

(3). Kriz W; Lemley KV, A potential role for mechanical forces in the detachment of podocytes and the progression of CKD. J. Am. Soc. Nephrol 2015, 26 (2), 258–69. DOI: 10.1681/ASN.2014030278. [PubMed: 25060060]

(4). Ruggenenti P; Ruggiero B; Cravedi P; Vivarelli M; Massella L; Marasa M; Chianca A; Rubis N; Ene-Iordache B; Rudnicki M; Pollastro RM; Capasso G; Pisani A; Pennesi M; Emma F; Remuzzi G, Rituximab in steroid-dependent or frequently relapsing idiopathic nephrotic syndrome. J. Am. Soc. Nephrol 2014, 25 (4), 850–63. DOI: 10.1681/ASN.2013030251. [PubMed: 24480824]

(5). Greenbaum LA; Benndorf R; Smoyer WE, Childhood nephrotic syndrome--current and future therapies. Nat. Rev. Nephrol 2012, 8 (8), 445–58. DOI: 10.1038/nrneph.2012.115. [PubMed: 22688744]

(6). Gipson DS; Massengill SF; Yao L; Nagaraj S; Smoyer WE; Mahan JD; Wigfall D; Miles P; Powell L; Lin JJ; Trachtman H; Greenbaum LA, Management of childhood onset nephrotic syndrome. Pediatrics 2009, 124 (2), 747–57. DOI: 10.1542/peds.2008-1559. [PubMed: 19651590]

(7). Schiffer M; Teng B; Gu C; Shchedrina VA; Kasaikina M; Pham VA; Hanke N; Rong S; Gueler F; Schroder P; Tossidou I; Park JK; Staggs L; Haller H; Erschow S; Hilfiker-Kleiner D; Wei C; Chen C; Tardi N; Hakroush S; Selig MK; Vasilyev A; Merscher S; Reiser J; Sever S, Pharmacological targeting of actin-dependent dynamin oligomerization ameliorates chronic kidney disease in diverse animal models. Nat. Med 2015, 21 (6), 601–609. DOI: 10.1038/nm.3843. [PubMed: 25962121]

(8). Sontag JM; Fykse EM; Ushkaryov Y; Liu JP; Robinson PJ; Sudhof TC, Differential expression and regulation of multiple dynamins. J. Biol. Chem 1994, 269 (6), 4547–54. [PubMed: 8308025]

(9). Allison SJ, Chronic kidney disease: Actin cytoskeleton alterations in podocytes: a therapeutic target for chronic kidney disease. Nat. Rev. Nephrol 2015, 11 (7), 385 DOI: 10.1038/nrneph.2015.79. [PubMed: 25963588]

(10). Chu DS; Sellers DL; Bocek MJ; Fischedick AE; Horner PJ; Pun SH, MMP9-sensitive polymers mediate environmentally-responsive bivalirudin release and thrombin inhibition. Biomater. Sci 2015, 3 (1), 41–45. DOI: 10.1039/C4BM00259H. [PubMed: 25589953]

(11). Aryal S; Hu CM; Zhang L, Polymer--cisplatin conjugate nanoparticles for acid-responsive drug delivery. ACS Nano 2010, 4 (1), 251–8. DOI: 10.1021/nn9014032. [PubMed: 20039697]

(12). Vaklavas C; Forero-Torres A, Safety and efficacy of brentuximab vedotin in patients with Hodgkin lymphoma or systemic anaplastic large cell lymphoma. Ther. Adv. Hematol 2012, 3 (4), 209–25. DOI: 10.1177/2040620712443076. [PubMed: 23606932]

(13). Springsteen G; Wang B, A detailed examination of boronic acid–diol complexation. Tetrahedron 2002, 58 (26), 5291–5300. DOI: 10.1016/S0040-4020(02)00489-1.

(14). Li Y; Xiao W; Xiao K; Berti L; Luo J; Tseng HP; Fung G; Lam KS, Well-defined, reversible boronate crosslinked nanocarriers for targeted drug delivery in response to acidic pH values and cis-diols. Angew. Chem. Int. Ed. Engl 2012, 51 (12), 2864–9. DOI: 10.1002/anie.201107144. [PubMed: 22253091]

(15). Su J; Chen F; Cryns VL; Messersmith PB, Catechol polymers for pH-responsive, targeted drug delivery to cancer cells. J. Am. Chem. Soc 2011, 133 (31), 11850–3. DOI: 10.1021/ja203077x. [PubMed: 21751810]

(16). Kopecek J; Kopeckova P, HPMA copolymers: origins, early developments, present, and future. Adv. Drug. Deliv. Rev 2010, 62 (2), 122–49. DOI: 10.1016/j.addr.2009.10.004. [PubMed: 19919846]

(17). Agarwal S; Zhang Y; Maji S; Greiner A, PDMAEMA based gene delivery materials. Materials Today 2012, 15 (9), 388–393. DOI: 10.1016/S1369-7021(12)70165-7.

(18). Cheng Y; Yumul RC; Pun SH, Virus-Inspired Polymer for Efficient In Vitro and In Vivo Gene Delivery. Angew. Chem. Int. Ed. Engl 2016, 55 (39), 12013–7. DOI: 10.1002/anie.201605958. [PubMed: 27538359]

(19). Jones RA; Poniris MH; Wilson MR, pDMAEMA is internalised by endocytosis but does not physically disrupt endosomes. J. Control. Release 2004, 96 (3), 379–391. DOI: 10.1016/j.jconrel.2004.02.011. [PubMed: 15120895]

(20). Hu YB; Dammer EB; Ren RJ; Wang G, The endosomal-lysosomal system: from acidification and cargo sorting to neurodegeneration. Transl. Neurodegener 2015, 4, 18 DOI: 10.1186/s40035-015-0041-1. [PubMed: 26448863]

(21). Huotari J; Helenius A, Endosome maturation. EMBO J. 2011, 30 (17), 3481–500. DOI: 10.1038/emboj.2011.286. [PubMed: 21878991]

(22). Kubo Y; Nishiyabu R; James TD, Hierarchical supramolecules and organization using boronic acid building blocks. Chem. Commun (Camb.) 2015, 51 (11), 2005–20. DOI: 10.1039/c4cc07712a. [PubMed: 25465854]

(23). Roy D; Sumerlin BS, Glucose-Sensitivity of Boronic Acid Block Copolymers at Physiological pH. ACS Macro Letters 2012, 1 (5), 529–532. DOI: 10.1021/mz300047c.

(24). Matsumoto A; Ishii T; Nishida J; Matsumoto H; Kataoka K; Miyahara Y, A synthetic approach toward a self-regulated insulin delivery system. Angew. Chem. Int. Ed. Engl 2012, 51 (9), 2124–8. DOI: 10.1002/anie.201106252. [PubMed: 22162189]

(25). Sharma B; Bugga P; Madison LR; Henry AI; Blaber MG; Greeneltch NG; Chiang N; Mrksich M; Schatz GC; Van Duyne RP, Bisboronic Acids for Selective, Physiologically Relevant Direct Glucose Sensing with Surface-Enhanced Raman Spectroscopy. J. Am. Chem. Soc 2016 DOI: 10.1021/jacs.6b07331.

(26). Güemes M; Rahman SA; Hussain K, What is a normal blood glucose? Arch. Dis. Child 2016, 101 (6), 569–574. DOI: 10.1136/archdischild-2015-308336. [PubMed: 26369574]

(27). Lazebnik M; Pack DW, Rapid and facile quantitation of polyplex endocytic trafficking. J. Control. Release 2017, 247, 19–27. DOI: 10.1016/j.jconrel.2016.12.035. [PubMed: 28043862]

(28). Canton I; Battaglia G, Endocytosis at the nanoscale. Chem. Soc. Rev 2012, 41 (7), 2718–2739. DOI: 10.1039/c2cs15309b. [PubMed: 22389111]

(29). Sever S; Schiffer M, Actin dynamics at focal adhesions: a common endpoint and putative therapeutic target for proteinuric kidney diseases. Kidney Int. 2018, 93 (6), 1298–1307. DOI: 10.1016/j.kint.2017.12.028. [PubMed: 29678354]

(30). Gu C; Chang J; Shchedrina VA; Pham VA; Hartwig JH; Suphamungmee W; Lehman W; Hyman BT; Bacskai BJ; Sever S, Regulation of dynamin oligomerization in cells: the role of dynamin-actin interactions and its GTPase activity. Traffic 2014, 15 (8), 819–38. DOI: 10.1111/tra.12178. [PubMed: 24891099]

(31). Gu C; Lee HW; Garborcauskas G; Reiser J; Gupta V; Sever S, Dynamin Autonomously Regulates Podocyte Focal Adhesion Maturation. J. Am. Soc. Nephrol 2017, 28 (2), 446–451. DOI: 10.1681/ASN.2016010008 [PubMed: 27432739]

(32). Dobrinskikh E; Okamura K; Kopp JB; Doctor RB; Blaine J, Human podocytes perform polarized, caveolae-dependent albumin endocytosis. Am. J. Physiol. Renal. Physiol 2014, 306 (9), F941–51. DOI: 10.1152/ajprenal.00532.2013. [PubMed: 24573386]

(33). Inoue K; Ishibe S, Podocyte endocytosis in the regulation of the glomerular filtration barrier. Am. J. Physiol. Renal. Physiol 2015, 309 (5), F398–405. DOI: 10.1152/ajprenal.00136.2015. [PubMed: 26084928]

(34). Sandgren KJ; Wilkinson J; Miranda-Saksena M; McInerney GM; Byth-Wilson K; Robinson PJ; Cunningham AL, A differential role for macropinocytosis in mediating entry of the two forms of vaccinia virus into dendritic cells. PLoS Pathog. 2010, 6 (4), e1000866 DOI: 10.1371/journal.ppat.1000866. [PubMed: 20421949]

(35). Sieber J; Wieder N; Clark A; Reitberger M; Matan S; Schoenfelder J; Zhang J; Mandinova A; Bittker JA; Gutierrez J; Aygun O; Udeshi N; Carr S; Mundel P; Jehle AW; Greka A, GDC-0879, a BRAF(V600E) Inhibitor, Protects Kidney Podocytes from Death. Cell. Chem. Biol. 2018, 25 (2), 175–184 e4. DOI: 10.1016/j.chembiol.2017.11.006. [PubMed: 29249695]

(36). Lee HW; Khan SQ; Faridi MH; Wei C; Tardi NJ; Altintas MM; Elshabrawy HA; Mangos S; Quick KL; Sever S; Reiser J; Gupta V, A Podocyte-Based Automated Screening Assay Identifies Protective Small Molecules. J. Am. Soc. Nephrol 2015 DOI: 10.1681/ASN.2014090859.

(37). Lv S; Wu Y; Cai K; He H; Li Y; Lan M; Chen X; Cheng J; Yin L, High Drug Loading and Sub-Quantitative Loading Efficiency of Polymeric Micelles Driven by Donor-Receptor Coordination Interactions. J. Am. Chem. Soc 2018, 140 (4), 1235–1238. DOI: 10.1021/jacs.7b12776. [PubMed: 29332390]

(38). Aguirre-Chagala YE; Santos JL; Huang Y; Herrera-Alonso M, Phenylboronic Acid-Installed Polycarbonates for the pH-Dependent Release of Diol-Containing Molecules. ACS Macro Letters 2014, 3 (12), 1249–1253. DOI: 10.1021/mz500594m.

(39). Ma R; Zhang C; Liu Y; Li C; Xu Y; Li B; Zhang Y; An Y; Shi L, Iminoboronate-based dual-responsive micelles via subcomponent self-assembly for hydrophilic 1,2-diol-containing drug delivery. RSC Advances 2017, 7 (34), 21328–21335. DOI: 10.1039/c7ra01742a.

(40). Huang T; Xiong Y; Chen N; Wang D; Lai Y; Deng C, Highly selective enrichment of baicalin in rat plasma by boronic acid-functionalized core-shell magnetic microspheres: Validation and

application to a pharmacokinetic study. Talanta 2016, 147, 501–9. DOI: 10.1016/j.talanta.2015.10.042. [PubMed: 26592639]

(41). Liu H-B; Yan Q; Wang C; Liu X; Wang C; Zhou X-H; Xiao S-J, Saccharide- and temperature-responsive polymer brushes grown on gold nanoshells for controlled release of diols. Colloids Surf. A 2011, 386 (1), 131–134. DOI: 10.1016/j.colsurfa.2011.07.022.

(42). Jung JH; Lee JO; Kim JH; Lee SK; You GY; Park SH; Park JM; Kim EK; Suh PG; An JK; Kim HS, Quercetin suppresses HeLa cell viability via AMPK-induced HSP70 and EGFR down-regulation. J. Cell. Physiol 2010, 223 (2), 408–14. DOI: 10.1002/jcp.22049. [PubMed: 20082303]

(43). Chakrabarty S; Ganguli A; Das A; Nag D; Chakrabarti G, Epigallocatechin-3-gallate shows anti-proliferative activity in HeLa cells targeting tubulin-microtubule equilibrium. Chem.-Biol. Interact 2015, 242, 380–389. DOI: 10.1016/j.cbi.2015.11.004. [PubMed: 26554336]

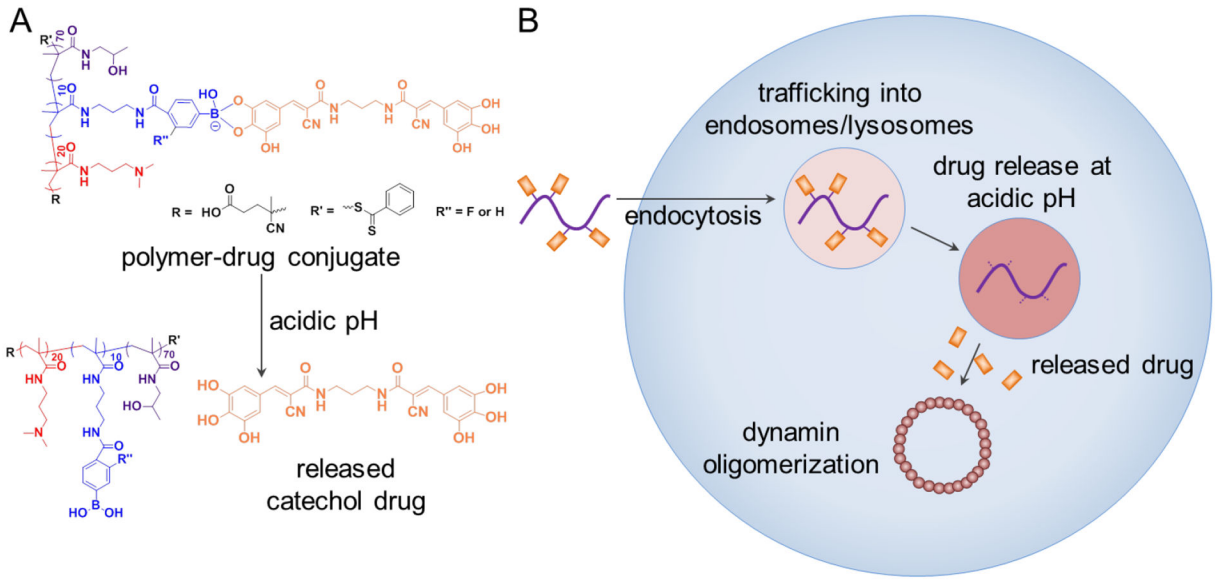

Figure 1.

Schematic of polymer-drug conjugates and release mechanism. **A**. Phenylboronic acid (PBA) copolymers load Bis-T-23 through boronate ester formation between boronic acids on copolymer side chains and catechols on Bis-T-23. At acidic pH conditions, the boronate ester bond reverses, and Bis-T-23 is released in its native form. **B**. Copolymers are rapidly endocytosed due to cationic side chains and are trafficked into acidic endosomes and lysosomes, which trigger bond reversal. Bis-T-23 is then released, catalyzing dynamin oligomerization.

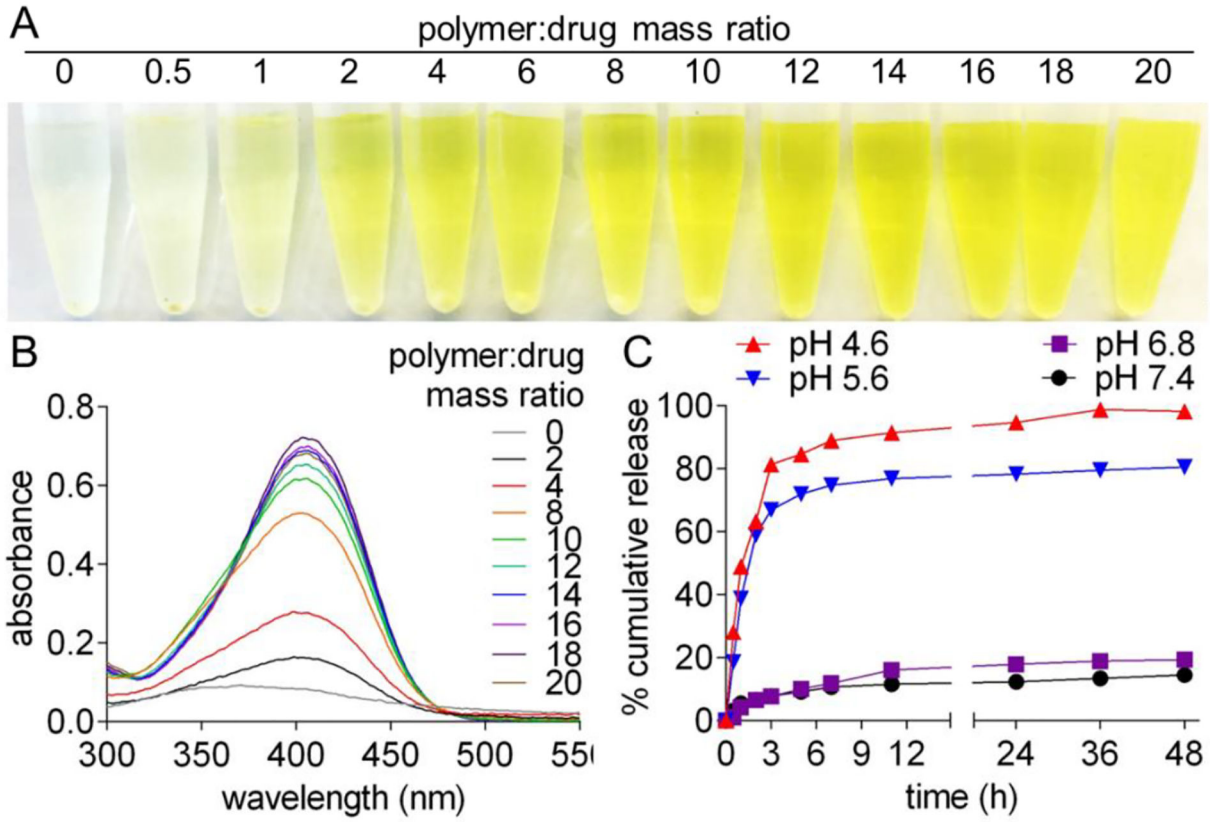

Figure 2.

Characterization of PBA copolymer behavior. **A**. Image of polymer-drug conjugates loaded at increasing polymer:drug mass ratios. **B**. Absorbance quantification of polymer-drug conjugates. When loaded onto PBA copolymers, Bis-T-23 exhibits a new absorbance at λ = 410 nm. **C**. Bis-T-23 release from polymer-drug conjugates at various pH.

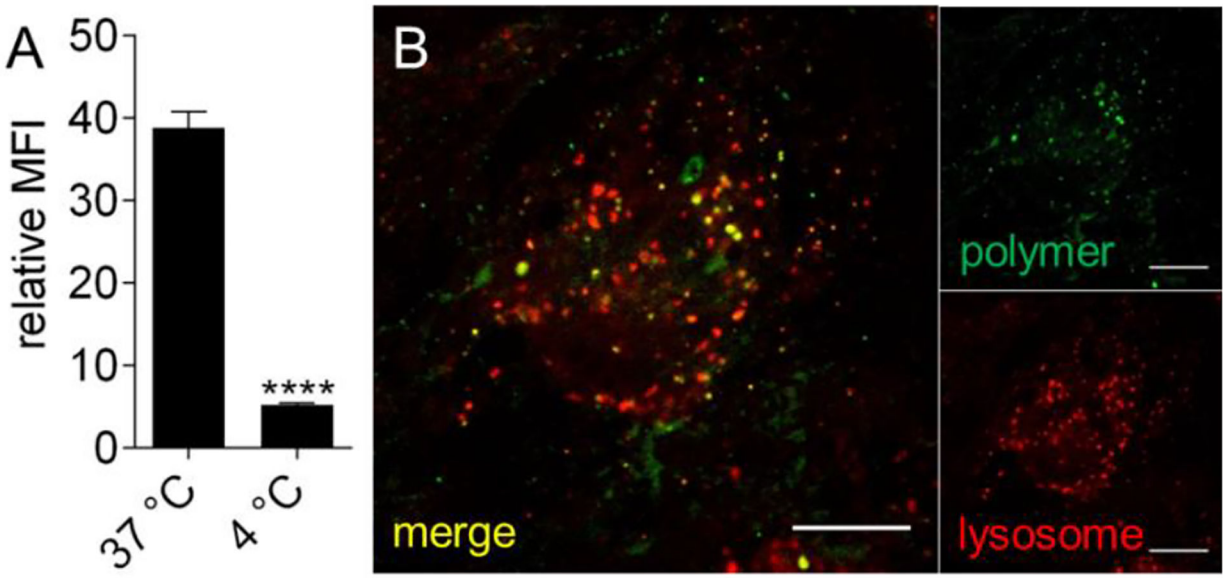

Figure 3.

In vitro polymer uptake. **A**. Polymer uptake by podocytes, measured by mean fluorescence intensity (MFI), after 20 min incubation at 37 or 4 °C. **B**. Fluorescent images of podocytes treated with fluorescein-PBA copolymers obtained by confocal microscopy. Green, polymer; red, lysosomes; yellow, merge. Pearson's correlation coefficient = 0.5. Scale bars, 10 μm.

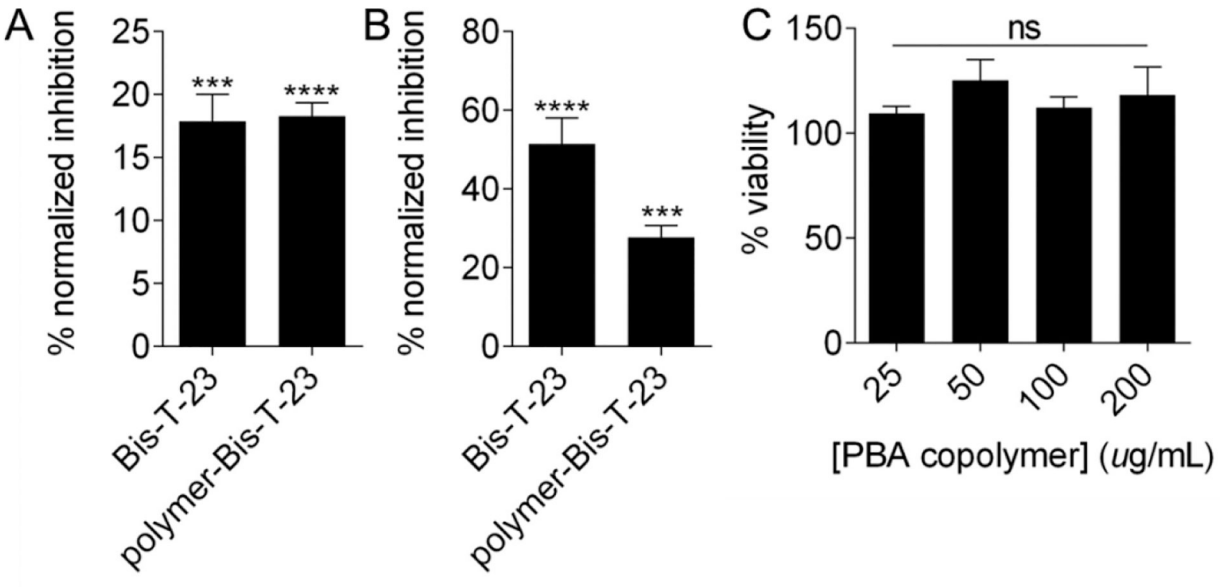

Figure 4.

In vitro drug delivery and cytotoxicity of polymer-drug conjugates. **A**. Normalized inhibition of fluorescein-BSA uptake in podocytes. **B**. Normalized inhibition of fluorescein-transferrin in Jurkat cells. Treatments were normalized by respective vehicle (DMSO or polymer) controls. **C**. Percent viability of treatments relative to untreated podocytes. Bars represent means ± SEM. ****p*-value < 0.001; *****p*-value < 0.0001; ns, not significant.

Table 1

Summary of p(HPMA-*co*-DMAPMA-*co*-APMA) copolymers

Polymer	M_n [a] (Da)	M_n [b] (Da)	$Đ$
p($HPMA_{70}$-*co*-$DMAPMA_{20}$-*co*-$APMA_{10}$)	15,200	22,000	1.05
p($HPMA_{70}$-*co*-$DMAPMA_{20}$-*co*-(APMA-*g*-$PBA)_{10}$)	16,300	N/A	N/A

[a] ^{1}H NMR,

[b] GPC